ÇUKUROVA UNIVERSITY
INSTITUTE OF NATURAL AND APPLIED SCIENCES

PhD THESIS

Barış ATA

DECOUPLED BACKSTEPPING SLIDING MODE CONTROL OF UNDERACTUATED SYSTEMS WITH UNCERTAINTY

DEPARTMENT OF COMPUTER ENGINEERING

ADANA-2019

ÇUKUROVA UNIVERSITY
INSTITUTE OF NATURAL AND APPLIED SCIENCES

DECOUPLED BACKSTEPPING SLIDING MODE CONTROL OF UNDERACTUATED SYSTEMS WITH UNCERTAINTY

Barış ATA

PhD THESIS

DEPARTMENT OF COMPUTER ENGINEERING

We certify that the thesis titled above was reviewed and approved for the award of degree of the Doctor of Philosophy by the board of jury on 30/05/2019.

……..…....	……..…….	…….……...…
Prof. Dr. Ramazan ÇOBAN	Prof. Dr. İlyas EKER	Assoc. Prof. Dr. M. Fatih AKAY
SUPERVISOR	MEMBER	MEMBER
……...…	…..……..……..……..….....	
Asst. Prof. Dr. Çiğdem ACI	Asst. Prof. Dr. Esra SARAÇ EŞSİZ	
MEMBER	MEMBER	

This PhD Thesis is written at the Computer Engineering Department of Institute of Natural and Applied Sciences of Çukurova University.
Registration Number:

Prof. Dr. Mustafa GÖK
Director
Institute of Natural and Applied Science

ABSTRACT

PhD THESIS

DECOUPLED BACKSTEPPING SLIDING MODE CONTROL OF UNDERACTUATED SYSTEMS WITH UNCERTAINTY

Barış ATA

ÇUKUROVA UNIVERSITY
INSTITUTE OF NATURAL AND APPLIED SCIENCES
DEPARTMENT OF COMPUTER ENGINEERING

Supervisor : Prof. Dr. Ramazan ÇOBAN
Year: 2019, Pages: 99
Juries : Prof. Dr. Ramazan ÇOBAN
: Prof. Dr. İlyas EKER
: Assoc. Prof. Dr. M. Fatih AKAY
: Asst. Prof. Dr. Çiğdem ACI
: Asst. Prof. Dr. Esra SARAÇ EŞSİZ

The purpose of this thesis is to design a decoupled backstepping sliding mode control method for underactuated systems under uncertainties and disturbances. The sliding mode control technique is an effective robust control approach to overcome model uncertainties and external disturbances. However, the sliding mode control method can manage parametric uncertainties only in combination with other methods such as backstepping control. The backstepping control design is mainly used to deal with the control of the nonlinear systems with parametric uncertainties. In the present thesis, the sliding mode control technique and the backstepping control technique are combined owing to their merits using a decoupling algorithm to control underactuated systems. Since the design methodology is based on the Lyapunov theorem, the stability of the system is guaranteed. The effectiveness of the proposed method is verified by the experimental results of the controller which is applied to an inverted pendulum on a cart system as an example of underactuated systems. The simulations and the experimental results show that the decoupled backstepping sliding mode control achieves a satisfactory control performance and the proposed method provides a robust performance to overcome parametric uncertainties where the decoupled sliding mode control fails.

Keywords: Backstepping control, sliding mode control, underactuated systems

ÖZ

DOKTORA TEZİ

BELİRSİZLİK ALTINDAKİ EKSİK EYLEYİCİLİ SİSTEMLERİN AYRIKLAŞTIRILMIŞ GERİ ADIMLAMALI KAYAN KİPLİ KONTROL METODU İLE KONTROLÜ

Barış ATA

ÇUKUROVA ÜNİVERSİTESİ
FEN BİLİMLERİ ENSTİTÜSÜ
BİLGİSAYAR MÜHENDİSLİĞİ ANABİLİM DALI

Danışman : Prof. Dr. Ramazan ÇOBAN
Yıl: 2019, Sayfa: 99
Jüri : Prof. Dr. Ramazan ÇOBAN
: Prof. Dr. İlyas EKER
: Doç. Dr. M. Fatih AKAY
: Dr. Öğr. Üyesi Çiğdem ACI
: Dr. Öğr. Üyesi Esra SARAÇ EŞSİZ

Bu tezin amacı belirsizlik ve bozucular altındaki eksik eyleyicili sistemler için bir ayrıklaştırılmış geri adımlamalı kayan kipli kontrol yönteminin tasarlanmasıdır. Kayan kipli kontrol, model belirsizlikleri ve dış bozuculara karşı etkili bir gürbüz kontrol yaklaşımıdır. Ancak kayan kipli kontrol metodu sadece geri adımlamalı kontrol gibi başka yöntemlerle birlikte kullanıldığında parametrik belirsizliklerle başa çıkabilir. Geri adımlamalı kontrol yönteminin başlıca kullanım alanı parametrik belirsizlikler içeren doğrusal olmayan sistemlerin gürbüz kontrolüdür. Bu tez çalışmasında her iki yöntemin de başarılı yönlerinden faydalanmak için kayan kipli kontrol ve geri adımlamalı kontrol yöntemleri bir ayrıklaştırma algoritması kullanarak birleştirilmiştir. Kontrolörün tasarım yöntemi Lyapunov teoremine dayandığı için sistemin kararlılığı garanti altına alınmıştır. Önerilen yöntemin başarımı, kontrolörün eksik eyleyicili sistemlerin bir örneği olan arabalı ters sarkaç sistemine uygunlaması ile doğrulanmıştır. Benzetim sonuçları ve deneysel sonuçlar önerilen ayrıklaştırılımış geri adımlamalı kayan kipli kontrol yönteminin tatmin edici bir kontrol performanı sağladığını göstermiştir. Ayrıca, ayrıklaştırılmış kayan kipli kontrol yönteminin başarısız olduğu parametrik belirsizliklerin üstesinden gelmede önerilen metod gürbüz bir kontrol performansı sağlamıştır.

Anahtar kelimeler: Geri adımlamalı kontrol, kayan kipli kontrol, eksik eyleyicili sistemler

EXTENDED ABSTRACT

In this thesis, a decoupled backstepping sliding mode control method proposed to control underactuated systems under uncertainties and disturbances. Underactuated systems are mechanical systems with less number of actuators than their degrees of freedom. Control of the underactuated mechanical systems have seen an enormous interest in the control engineering field because of their advantages such as having low complexity and cost due to fewer actuators used in the system.

The inverted pendulum on a cart system is a benchmark tool used in control laboratories since the 1950s. Also, the inverted pendulum on a cart system is an example of the underactuated systems which the position of the cart and the angle of the pendulum are controlled by just one actuator.

In this study, the sliding mode control method and backstepping control method is combined owing to their merits. The sliding mode control technique has been recognized as an effective control method against the model uncertainties and external disturbances and the backstepping control method can deal with the parametric uncertainties on the control of the nonlinear systems. Therefore, combining the sliding mode control and backstepping methods will lead a design which is immune to model uncertainties, parametric uncertainties, and external disturbances.

One of the main drawbacks of the sliding mode control method on the control of the underactuated system is that the conventional sliding mode control cannot be applied to underactuated systems directly because of their highly coupled dynamics. Researchers proposed partial linearization methods to model regular form of the inverted pendulum on a cart system in the literature to overcome this drawback. Some parameters of the system are neglected in these methods due to the complex nature of the inverted pendulum on a cart system. However, a more realistic model of the system is needed for experimental studies. Therefore, instead

of partial linearization of the system, a decoupling algorithm for sliding mode control proposed in the literature is used in this study to design a backstepping sliding mode controller.

In this thesis, stabilizing the pendulum at the upright position while bringing the cart a desired position is selected as the main control object. To this end, the complete mathematical model of the inverted pendulum on a cart system is derived and the DC motor characteristics are added to the mathematical model of the inverted pendulum on a cart system to create a more realistic model. After that, a decoupled sliding mode controller and a decoupled backstepping sliding mode controller are designed to accomplish the control objective.

The decoupled sliding mode control and the proposed decoupled backstepping sliding mode control are tested on simulation using the derived mathematical model of the inverted pendulum on a cart model. The simulation results prove the stability and the effectiveness of both methods. The decoupled sliding mode control and the proposed decoupled backstepping sliding mode control methods are compared in two simulation tests for different initial conditions to investigate their performance on the inverted pendulum on a cart system without parametric uncertainties. These simulations are repeated with parametric uncertainties. Comparison results are presented by figures and error based performance indices.

Overall, the simulation results have shown that the proposed decoupled backstepping sliding mode control method is more efficient than the conventional decoupled sliding mode control method.

After obtaining satisfactory performance on the simulation tests, the decoupled sliding mode control and the proposed decoupled backstepping sliding mode control methods are applied to a real plant. Experiments have performed on Feedback's 33-200 digital pendulum mechanical unit. The simulation tests are recreated on the experimental setup to provide a clearer view about the performance of the proposed method. The decoupled sliding mode control and the

proposed decoupled backstepping sliding mode control methods are compared in two experimental tests for different initial conditions to investigate their performance on the real system without parametric uncertainties. These two experiments are repeated with parametric uncertainties. Experimental comparison results are presented by figures and error based performance indices.

These experiments show that the proposed decoupled backstepping sliding mode control method manages to handle parametric uncertainty and control the cart position successfully where the decoupled sliding mode control fails. Overall, the experimental results have shown that the proposed decoupled backstepping sliding mode control method is more efficient than the conventional decoupled sliding mode control method.

GENİŞLETİLMİŞ ÖZET

Bu tezde, belirsizlik ve bozucular altındaki eksik eyleyicili sistemlerin kontrolü için bir ayrıklaştırılmış geri adımlamalı kayan kipli kontrol yöntemi önerilmiştir. Serbestlik derecesinden daha az sayıda eyleyiciye sahip mekanik sistemler eksik eyleyicili sistemler olarak adlandırılmaktadır. Daha az eyleyiciye sahip olmaları nedeniyle düşük karmaşıklık ve maliyet gibi avantajlara sahip olan eksik eyleyicili mekanik sistemlerin kontrolü, kontrol mühendisliği alanında geniş bir ilgi görmektedir.

Arabalı ters sarkaç sistemi 1950'lerden beri kontrol laboratuvarlarında bir karşılaştırma aracı olarak kullanılmaktadır. Ayrıca arabanın pozisyonu ve sarkacın açısının tek bir eyleyiciyle kontrol edilmesi nedeniyle arabalı ters sarkaç sistemi eksik eyleyicili sistemlere bir örnek oluşturmaktadır.

Bu çalışmada, kayan kipli kontrol ve geri adımlamalı kontrol yöntemleri sağladıkları faydalar nedeniyle bir arada kullanılmıştır. Kayan kipli kontrol yöntemi model belirsizliklerine ve dış bozuculara karşı etkili bir kontrol yöntemi olarak bilinmektedir. Geri adımlamalı kontrol yöntemi ise doğrusal olmayan sistemlerin kontrolünde parametrik belirsizlikler ile başa çıkabilmektedir. Bu nedenle, kayan kipli kontrol ve geri adımlamalı kontrol yöntemlerinin birleştirilmesi model belirsizliklerine, parametrik belirsizliklere ve dış bozuculara bağışık bir tasarıma yol açacaktır.

Kayan kipli kontrol yönteminin en önemli dezavantajlarından biri klasik kayan kipli kontrol yönteminin yüksek bağlaşık yapıları nedeniyle eksik eyleyicili sistemlere doğrudan uygulanamamasıdır. Literatürde araştırmacılar bu sorunu aşmak için arabalı ters sarkacı düzenli formda modellenmesine yardımcı olan kısmi doğrusallaştırma metodları önermişlerdir. Bu yöntemlerde arabalı ters sarkaç sisteminin karmaşık doğası nedeniyle sistemin kimi parametreleri göz ardı edilmiştir. Ancak deneysel çalışmalar için daha gerçekçi modellere ihtiyaç duyulmaktadır. Bu nedenle, bu çalışmada bir geri adımlamalı kayan kipli kontrolör

tasarlamak için kısmi doğrusallaştırma yöntemleri yerine yine literatürde yer alan bir ayrıklaştırma algoritması kullanılmıştır.

Bu tezde, arabayı başlangıç konumundan istenen bir konuma hareket ettirirken sarkacı dik pozisyonda dengede tutmak temel kontrol hedefi olarak belirlenmiştir. Bu amaçla arabalı ters sarkaç sisteminin tam matematiksel modeli elde edilmş ve daha gerçekçi bir model yaratabilmek için DC motor karakteristikleri de bu modele dahil edilmiştir. Ardından kontrol hedefine ulaşabilmek için bir ayrıklaştırılmış kayan kipli kontrolör ve bir ayrıklaştırılmış geri adımlamalı kayan kipli kontrolör tasarlanmıştır.

Elde edilen arabalı ters sarkaç sisteminin tam matematiksel modeli kullanılarak ayrıklaştırılmış kayan kipli kontrol yöntemi ve önerilen ayrıklaştırılmış geri adımlamalı kayan kipli kontrol yöntemi benzetim modelleri ile test edilmiştir. Ayrıklaştırılmış kayan kipli kontrol yöntemi ve önerilen ayrıklaştırılmış geri adımlamalı kayan kipli kontrol yöntemi performanslarının incelenmesi için parametrik belirsizlik içermeyen iki ayrı benzetim testinde farklı başlangıç koşulları için karşılaştırılmıştır. Ardından bu testler parametrik belirsizlik altında tekrar edilmiştir. Karşılaştırma sonuçları grafikler ve hata tabanlı performans indisleri yardımıyla sunulmuştur.

Sonuç olarak benzetim sonuçları önerilen ayrıklaştırılmış geri adımlamalı kayan kipli kontrol yönteminin ayrıklaştırılmış kayan kipli kontrol yöntemine göre daha etkili olduğunu gstermiştir.

Benzetim testlerinden elde edilen tatmin edici sonuçların ardından ayrıklaştırılmış kayan kipli kontrol ve önerilen ayrıklaştırılmış geri adımlamalı kayan kipli kontrol yöntemleri gerçek bir sisteme uygulanmıştır. Deneyler Feedbak firmasının 33-200 dijital sarkaç mekanik ünitesi üzerinde gerçekleştirilmiştir. Önerilen yöntemin performansı hakkında daha net bir bakış açısı elde edebilmek için benzetim testleri deney düzeneği üzerinde yeniden gerçekleştirilmiştir. Ayrıklaştırılmış kayan kipli kontrol yöntemi ve önerilen ayrıklaştırılmış geri adımlamalı kayan kipli kontrol yöntemi gerçek sistem üzerindeki

performanslarının incelenmesi için parametrik belirsizlik içermeyen iki ayrı deneysel testte farklı başlangıç koşulları için karşılaştırılmıştır. Ardından bu testler parametrik belirsizlik altında tekrar edilmiştir. Deneysel karşılaştırma sonuçları grafikler ve hata tabanlı performans indisleri yardımıyla sunulmuştur.

Deneysel sonuçlar önerilen ayrıklaştırılımış geri adımlamalı kayan kipli kontrol yönteminin, ayrıklaştırılmış kayan kipli kontrol yönteminin başarısız olduğu parametrik belirsizliklerle başa çıkarak arabanın pozisyonunu başarılı bir şekilde kontrol edebildiğini göstermiştir. Sonuç olarak deneysel sonuçlar önerilen ayrıklaştırılmış geri adımlamalı kayan kipli kontrol yönteminin ayrıklaştırılmış kayan kipli kontrol yöntemine göre daha etkili sonuçlar ortaya koyduğunu göstermiştir.

ACKNOWLEDGEMENT

I would like to present my gratitude to my supervisors Assoc. Prof. Dr. Ramazan ÇOBAN for his endless support, patience, guidance, and motivation for the successful completion of this thesis.

I wish to express my special thanks to Prof. Dr. İlyas EKER and Assoc. Prof. Dr. M. Fatih AKAY for their suggestions, corrections and their valuable help. I would like to thank members of the PhD thesis jury Asst. Prof. Dr. Çiğdem ACI and Asst. Prof. Dr. Esra SARAÇ EŞSİZ for their constructive suggestions and corrections.

Special thanks to my beloved wife Işıl for her limitless support and patience.

CONTENTS **PAGE**

LIST OF TABLES **PAGE**

LIST OF FIGURES **PAGE**

LIST OF ABBREVIATIONS

IFAC	: International Federation of Automatic Control
DC	: Direct current
PID	: Proportional–integral–derivative
SMC	: Sliding mode control
DSMC	: Decoupled sliding mode control
DBSMC	: Decoupled backstepping sliding mode control
VSC	: Variable structure control
BSMC	: Backstepping sliding mode control
IAE	: Integral absolute error
ISE	: Integral squared error
ITAE	: Integral time absolute error
ITSE	: Integral time squared error
PC	: Personal computer
PCI	: Peripheral component interconnect
DPC	: Digital pendulum controller

1. INTRODUCTION

Underactuated systems are mechanical systems with less number of actuators than their degrees of freedom. Underactuated systems are widely used in real-time applications such as underwater vehicles (Woods et al., 2012), robotics (Oryschuk et al., 2009; Zeng-Guang Hou et al., 2009) and aerospace (Olfati-Saber, 2001). Underactuated systems can be classified by the reason of underactutaion (Olfati-Saber, 2001). A system can become underactuated by the dynamics of the system by nature (Hussein and Bloch, 2008), by design to reduce the cost (Walsh et al., 1994; Spong, 1995), by artificially induced for a research purpose (Spong, 1987) or by actuator failure.

Consequently, underactuated systems have at least one unactuated degree of freedom; hence, they consume less energy and their cost and complexity are low due to fewer actuators used in the systems. Because of these advantages, the control and analysis of underactuated mechanical systems have seen an enormous interest and active research since the 1990s (Spong, 1998; Yu and Liu, 2013; Huang et al., 2018). However, controlling an underactuated mechanical system presents a challenging problem than fully actuated systems. Hereby, a wide range of underactuated systems is used as benchmark tools to design and compare different control techniques, such as the beam and ball system, the translational oscillator with rotational actuator system and the inverted pendulum on a cart system (She et al., 2012; Zhang et al., 2017; Shah and Rehman, 2018)

The inverted pendulum on a cart system is an example of the underactuated system in which both the angle of the rod and the position of the cart are controlled by only one actuator. Also, other characteristics of the system such as nonlinearity and instability turn inverted pendulum on a cart system into a challenging problem in the field of control engineering. The control of inverted pendulum on a cart is a classical example to verify the effectiveness and performance of control techniques. As a consequence inverted pendulums have been classic tools in the

control laboratories since the 1950s (Åström and Furuta, 2000). Also, the control of the inverted pendulum on a cart system has been determined as a benchmark control problem by the International Federation of Automatic Control (Davison, 1990). Moreover, the dynamics of the inverted pendulum on a cart system are fundamental to maintenance balance problem and resembles many real systems such as two-wheeled robots (Jeong and Takahashi, 2007), bipedal walking (Kuo, 2007), humanoid robots (Elhasairi and Pechev, 2015) and rocket thrusters (Anderson, 1988).

The inverted pendulum on a cart system consists of a cart moving along a rail and a rod which is hinged to cart. The cart is moved by a DC motor. The DC motor supplies some force needed for the motion of the cart via a pulley-belt mechanism. It is well known that the inverted pendulum on a cart system has two equilibrium point: One of them is stable and it corresponds to the downward position of the pendulum, and the other one is unstable and corresponds to the upright position of the pendulum. Therefore, moving the cart while maintaining the pendulum in the upright position using an appropriate continuous feedback signal can be considered as the main control problem (Ata and Coban, 2015). Various control techniques have been proposed to control an inverted pendulum on a cart system, such as energy-based control (Spong, 1996; Åström and Furuta, 2000; Siuka and Schöberl, 2009), PID control (Chang et al., 2002; Subudhi et al., 2012), linear quadratic regulator (Kumar and Jerome, 2013; Ata and Coban, 2017), fuzzy control (Zhang et al., 2011; Nejadfard et al., 2013) and sliding mode control (SMC) (Lo and Kuo, 1998; Adhikary and Mahanta, 2013; Mahjoub et al., 2015; Ata and Coban, 2019).

The SMC technique is a particular type of variable structure control (VSC) method and it has been recognized as an effective robust control approach to model uncertainties and external disturbances (Utkin, 1977; Utkin, 1992). The conventional SMC occurs in two phases; reaching phase and sliding phase. In the reaching phase, the system states are forced from an initial condition to a pre-

defined sliding surface. The system can handle matched uncertainties and certain disturbances when the states reach the sliding surface. The reaching phase is followed by the sliding phase where the system states are restricted to stay on the sliding surface and slides on the surface to an equilibrium (Utkin, 1992). Although the SMC technique is a robust method and it has a straight forward design procedure, it has a drawback called the chattering phenomenon (Utkin and Lee, 2006). The chattering effect can be caused by unmodeled dynamics or the finite sampling rate of digital controllers (Utkin and Lee, 2006) and extensive research is counting for chattering removal (Levant, 1993; Levant, 2003; Lee and Utkin, 2007; Wang and Adeli, 2012; Furat and Eker, 2014). Besides, the conventional SMC cannot be used directly on underactuated systems due to their coupled dynamics, the decoupled sliding mode control (DSMC) technique can be used to overcome this drawback (Lo and Kuo, 1998). The DSMC technique provides a method to decouple a nonlinear system into two subsystems which have different control objectives. Using the DSMC method, the second subsystem can be incorporated into the first subsystem (Lo and Kuo, 1998). Moreover, the SMC can manage parametric uncertainties in combination with other methods such as backstepping control (Coban, 2017a).

The backstepping technique is a nonlinear control method based on the Lyapunov theorem and also known as adding an integrator (Freeman and Kokotović, 1996). In the backstepping control, some of the states are used as virtual control signals in control law design, and the virtual signals satisfy the selected Lyapunov function in each step of the design process. Hence, the stability of the overall system can be guaranteed. The backstepping control design is mainly used to deal with the robust control of the nonlinear systems with parametric uncertainties (Wang and Stengel, 2002).

Hereby, the SMC and the backstepping techniques can be combined to design a robust controller to uncertainties and disturbances (Lu et al., 2011; Adhikary and Mahanta, 2013; Coban, 2017a). The backstepping sliding mode

control offers an improvement in steady-state error compared to the backstepping control and the SMC; also, it rejects disturbance and improves robustness against the parametric uncertainty (Coban, 2017b).

Research interest in controlling the inverted pendulum on a cart system (Lo and Kuo, 1998; Adhikary and Mahanta, 2013; Mahjoub et al., 2015) using the SMC continues in recent years. Mahjoub et al. proposed first-order and second-order sliding mode controllers for underactuated systems considering inverted pendulum on a cart system (Mahjoub et al., 2015). They used a stabilization method (Voytsekhovsky and Hirschorn, 2008) to approximate the inverted pendulum on a cart system with an input-output linearizable control system and presented the results using simulation tests. Adhikary and Mahanta combined backstepping and SMC methods and proposed an integral backstepping sliding mode controller for stabilization of the inverted pendulum on a cart system (Adhikary and Mahanta, 2013). They used Man and Lin's approach (Man and Lin, 2010) to partially linearize the inverted pendulum on a cart system and presented the results using simulation tests. Coban and Ata presented a decoupled sliding mode controller for inverted pendulum on a cart system (Coban and Ata, 2017). They used the decoupling algorithm proposed by Lo and Kuo (Lo and Kuo, 1998) to apply the SMC to an inverted pendulum on a cart system and presented the results using experimental tests.

Young et al. specified that the real test for the sliding mode research community will be the willingness of control engineers to experiment with the SMC method in their professional practice (Young et al., 1999). Although the SMC technique has been widely used, researchers have generally preferred simulations rather than the real systems; especially in the control of the inverted pendulum on a cart system (Lo and Kuo, 1998; Lin and Mon, 2005; Park and Chwa, 2009; Adhikary and Mahanta, 2013; Mahjoub et al., 2015). Complex nature of the inverted pendulum on a cart system leads to neglect some parameters of the system in these simulations such as cart friction coefficient and pendulum damping

coefficient. Also, the effect of the actuator to the inverted pendulum on a cart system has neglected in simulations (Lo and Kuo, 1998; Adhikary and Mahanta, 2013; Mahjoub et al., 2015).

The aim of this thesis is to propose a decoupled backstepping sliding mode control (DBSMC) method for underactuated systems with uncertainty. An inverted pendulum on a cart system is selected as a benchmark example for underactuated systems to examine the effectiveness of the proposed method. Stabilizing the pendulum at the upright position while bringing the cart a desired position is selected as the main control object. The complete mathematical model of the inverted pendulum on a cart system is derived according to its movement characteristics. The DC motor characteristics are added to the mathematical model of the inverted pendulum on a cart system to create a more realistic mathematical model. A decoupled sliding mode controller and a decoupled backstepping sliding mode controller are designed to control an inverted pendulum on a cart system. Since the design methodology of both controllers is based on the Lyapunov theorem, the stability of the system is guaranteed. The DSMC and the proposed DBSMC are simulated using the complete mathematical model of the inverted pendulum on a cart with DC motor system to investigate the stability of the controllers. The DSMC and the proposed DBSMC methods compared in simulation tests to investigate their performance on the inverted pendulum on a cart system with and without parametric uncertainties. After simulation tests, The DSMC and the proposed DBSMC methods experimentally applied an inverted pendulum on a cart system. Several simulation and experimental results are presented to show the effectiveness of the proposed algorithm. The results confirm the fact that the proposed DBSMC is more effective compared to the DSMC and the DBSMC provides a robust control on the systems with parametric uncertainties where the DSMC fails.

The rest of the thesis is organized as follows: In Chapter 2, a complete mathematical model of the inverted pendulum with DC motor is derived. In

Chapter 3, theoretical backgrounds of the SMC and the backstepping approach are explained. The basic principles of the DSMC and the DBSMC designs are presented. In Chapter 4, the DSMC and the DBSMC designs for the inverted pendulum on a cart system are presented. Simulation and experimental results are presented with not only graphical results but also various statistical analyses. Conclusions are drawn in Chapter 5.

2. INVERTED PENDULUM ON A CART

The inverted pendulum on a cart system consists of a cart moving along a rail and a rod which is hinged to the cart. The cart is moved by a DC motor. The DC motor supplies some force needed for the motion of the cart via a pulley-belt mechanism. Dynamics of the inverted pendulum system can be represented as a set of equations which is called mathematical model. Either this model can be represented in transfer function form or state space form. In this section, the complete mathematical model of the inverted pendulum on a cart system has been derived.

2.1. Dynamics of the Inverted Pendulum on a Cart System

The parametric representation of the inverted pendulum system is shown in Figure 2.1. Let x be the displacement of the cart from the initial position and θ is the angle in the vertical direction. m and l are the mass and the length of the pendulum, respectively; M is the mass of the cart; g is the acceleration due to gravity; and F is the force applied to the cart. Besides these parameters, J_p is the moment of inertia; d is the pendulum damping coefficient, and b is the cart friction coefficient which are not shown in Figure 2.1. The inverted pendulum on a cart system parameters are presented in Table 1.

The complete mathematical model of the inverted pendulum on a cart system can be derived from the Newton's laws of motion according to its movement characteristics. The motion of the inverted pendulum on a cart system consists of the linear motion of the motor driven cart in the X-axis and the rotational motion of the pendulum in the X-Y plane. Hence there will be two dynamic equations.

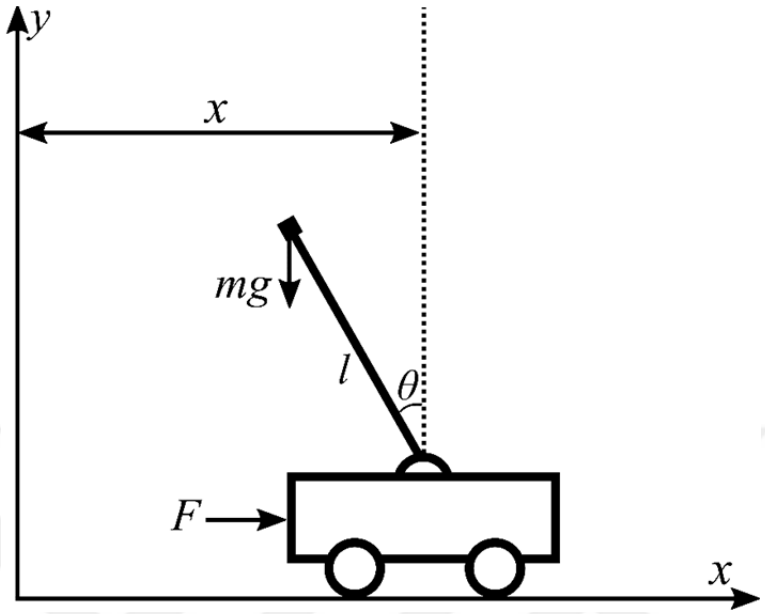

Figure 2.1. Parametric representation of the inverted pendulum on a cart system

Table 2.1. Inverted pendulum on a cart system parameters

Parameter	Meaning	Unit
x	Displacement of cart	m
θ	Pendulum angle	rad
m	Mass of pendulum	kg
l	Length of pendulum	m
M	Mass of cart	M
g	Acceleration of gravity	m/s^2
F	Force applied to the cart	N
J_p	Moment of inertia	kgm^2
b	Friction coefficient	Ns/m
d	Damping coefficient	Nms/rad

Let P and N be vertical and horizontal components of the force applied on the cart as shown in Figure 2.2. Considering Figure 2.1, x_G and y_G, coordinates of center of gravity of the mass can be defined as follows:

$$x_G = x - l\sin\left(\theta(t)\right) \tag{2.1}$$

$$y_G = l\cos\left(\theta(t)\right). \tag{2.2}$$

$\theta(t)$ will be presented as θ in the rest of the study for simplification.

Noting that

$$\frac{d}{dt}\left(\sin(\theta)\right) = \cos(\theta)\dot{\theta}$$

and

$$\frac{d^2}{dt^2}\left(\sin(\theta)\right) = -\sin(\theta)\dot{\theta}^2 + \cos(\theta)\ddot{\theta},$$

the horizontal reaction force N can be written as

$$N = m\left(\ddot{x} + \dot{\theta}^2 l\sin(\theta) - \ddot{\theta} l\cos(\theta)\right). \tag{2.3}$$

The force F applied on the cart is equal to the sum of the forces due to acceleration, friction component of force that opposes the linear motion of the cart, and the horizontal reaction:

$$F = M\ddot{x} + b\dot{x} + N. \tag{2.4}$$

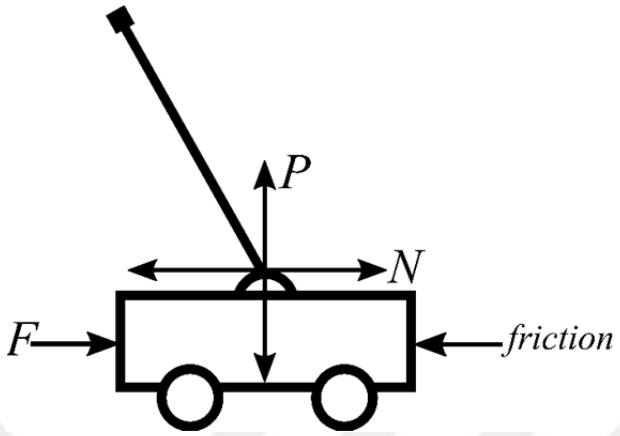

Figure 2.2. Free body diagram of the inverted pendulum on a cart system

Substituting Equation (2.3) into Equation (2.4), one has

$$F = M\ddot{x} + b\dot{x} + m\left(\ddot{x} - \ddot{\theta}l\cos(\theta) + \dot{\theta}^2 l\sin(\theta)\right). \tag{2.5}$$

Rearranging Equation (2.5) gives the first equation of motion for the inverted pendulum on a cart system as follows:

$$F = (M+m)\ddot{x} + b\dot{x} + ml\dot{\theta}^2\sin(\theta) - ml\ddot{\theta}\cos(\theta). \tag{2.6}$$

The forces perpendicular to the pendulum should be added up to obtain the second equation of motion for the inverted pendulum on a cart system. Considering Figure (2.2), the vertical force *P* can be calculated via the weight of the pendulum. Let y_G be the displacement of pendulum from the pivot. Hence, *P* can be defined as

$$P - mg = m\frac{d^2}{dt^2}\left(l\cos(\theta)\right). \tag{2.7}$$

Noting that

$$\frac{d}{dt}\left(\cos(\theta)\right) = -\sin(\theta)\dot{\theta}$$

and

$$\frac{d^2}{dt^2}\left(\cos(\theta)\right) = -\cos(\theta)\dot{\theta}^2 - \sin(\theta)\ddot{\theta},$$

Equation (2.7) can be rewritten as

$$P = mg - ml\dot{\theta}^2\cos(\theta) - ml\ddot{\theta}\sin(\theta). \tag{2.8}$$

Noting that the torque equation $\vec{\tau} = \vec{l} \otimes \vec{F}$ where the notation $\otimes$ indicates vector product, the torque equation can be written as

$$\begin{aligned}\vec{\tau} &= \begin{bmatrix} \vec{x} & \vec{y} & \vec{z} \\ -l\sin(\theta) & l\cos(\theta) & 0 \\ -N & -P & 0 \end{bmatrix} \\ &= (-1)^{1+3}\vec{z}\left[(-P)\left(-l\sin(\theta)\right) - \left(-Nl\cos(\theta)\right)\right].\end{aligned} \tag{2.9}$$

Equation (2.9) can be rearranged as

$$\tau = Pl\sin(\theta) + Nl\cos(\theta). \tag{2.10}$$

Also, the torque τ can be defined as follows:

$$\tau = J_p\ddot{\theta} + d\dot{\theta}. \tag{2.11}$$

Equating Equation (2.10) and Equation (2.11) yields

$$Pl\sin(\theta) + Nl\cos(\theta) = J_p\ddot{\theta} + d\dot{\theta}. \tag{2.12}$$

Substituting Equation (2.3) and Equation (2.8) into Equation (2.12), one has

$$\begin{aligned} J_p\ddot{\theta} + d\dot{\theta} = &-ml^2\ddot{\theta}\sin^2(\theta) - ml^2\dot{\theta}^2\cos(\theta)\sin(\theta) + mgl\sin(\theta) \\ &+ml\ddot{x}\cos(\theta) - ml^2\ddot{\theta}\cos^2(\theta) + ml^2\dot{\theta}^2\sin(\theta)\cos(\theta). \end{aligned} \tag{2.13}$$

Rearranging Equation (2.13) yields

$$J_p\ddot{\theta} + d\dot{\theta} = mgl\sin(\theta) + ml\ddot{x}\cos(\theta) - ml^2\ddot{\theta}\left(\cos^2(\theta) + \sin^2(\theta)\right). \tag{2.14}$$

Using the well-known trigonometric equation $\cos^2(\theta) + \sin^2(\theta) = 1$, Equation (2.14) can be rewritten as follows:

$$\left(J_p + ml^2\right)\ddot{\theta} - mglsin(\theta) - ml\ddot{x}cos(\theta) + d\dot{\theta} = 0. \tag{2.15}$$

Consequently, Equation (2.6) and Equation (2.15) are the equations of motion for the inverted pendulum on a cart system that describe the translational motion and the rotational motion respectively.

2.2. Nonlinear Model of the Inverted Pendulum on a Cart System

The equations of motion for inverted pendulum on a cart from above can also be rearranged into series of differential equations. From Equation (2.6) and Equation (2.15) $\ddot{x}$ and $\ddot{\theta}$ can be shown as, respectively,

$$\ddot{x} = \frac{-b\dot{x} + ml\ddot{\theta}\cos(\theta) - ml\dot{\theta}^2\sin(\theta) + F}{M+m} \tag{2.16}$$

$$\ddot{\theta} = \frac{mgl\sin(\theta) + ml\ddot{x}\cos(\theta) - d\dot{\theta}}{J_p + ml^2}. \tag{2.17}$$

Substituting Equation (2.17) into Equation (2.6), one has

$$F = (M+m)\ddot{x} + b\dot{x} - ml\cos(\theta)\left(\frac{mgl\sin(\theta) + ml\ddot{x}\cos(\theta) - d\dot{\theta}}{J_p + ml^2}\right) + ml\dot{\theta}^2\sin(\theta). \tag{2.18}$$

Rearranging Equation (2.18) yields

$$\begin{aligned} F\left(J_p + ml^2\right) = {} & \left(J_p + ml^2\right)(M+m)\ddot{x} + \left(J_p + ml^2\right)b\dot{x} \\ & - m^2l^2g\sin(\theta)\cos(\theta) - m^2l^2\cos^2(\theta)\ddot{x} \\ & + mld\dot{\theta}\cos(\theta) + \left(J_p + ml^2\right)ml\dot{\theta}^2\sin(\theta). \end{aligned} \tag{2.19}$$

Collecting $\ddot{x}$ terms on the left-hand-side in Equation (2.19) yields

$$\begin{aligned}\left(J_p+ml^2\right)(M+m)\ddot{x}-m^2l^2\cos^2(\theta)\ddot{x} = &-\left(J_p+ml^2\right)b\dot{x}\\ &+m^2l^2g\cos(\theta)\sin(\theta)\\ &-mld\dot{\theta}\cos(\theta)\\ &-\left(J_p+ml^2\right)ml\dot{\theta}^2\sin(\theta)\\ &+F\left(J_p+ml^2\right).\end{aligned} \tag{2.20}$$

Equation (2.20) can be rewritten as

$$\begin{aligned}\ddot{x} = &\frac{-\left(J_p+ml^2\right)b\dot{x}+m^2l^2g\cos(\theta)\sin(\theta)-mld\dot{\theta}\cos(\theta)}{\left(J_p+ml^2\right)(M+m)-m^2l^2\cos^2(\theta)}\\ &+\frac{-\left(J_p+ml^2\right)\mathrm{m}l\dot{\theta}^2\sin(\theta)+\left(J_p+ml^2\right)F}{\left(J_p+ml^2\right)(M+m)-m^2l^2\cos^2(\theta)}.\end{aligned} \tag{2.21}$$

Similarly substituting Equation (2.16) into Equation (2.15), one has

$$\begin{aligned}&\left(J_p+ml^2\right)\ddot{\theta}-mgl\sin(\theta)\\ &-ml\cos(\theta)\left(\frac{-b\dot{x}+ml\ddot{\theta}\cos(\theta)-ml\dot{\theta}^2\sin(\theta)+F}{M+m}\right)+d\dot{\theta}=0.\end{aligned} \tag{2.22}$$

Rearranging Equation (2.22) yields

$$\begin{aligned}&\left(J_p+ml^2\right)(M+m)\ddot{\theta}-(M+m)mgl\sin(\theta)\\ &+ml\cos(\theta)b\dot{x}-m^2l^2\cos^2(\theta)\ddot{\theta}+m^2l^2\cos(\theta)\sin(\theta)\dot{\theta}^2\\ &-ml\cos(\theta)F+(M+m)d\dot{\theta}=0.\end{aligned} \tag{2.23}$$

Collecting $\ddot{\theta}$ terms on the left-hand-side in Equation (2.23) yields

$$\begin{aligned}\left(J_p+ml^2\right)(M+m)\ddot{\theta}-m^2l^2\cos^2(\theta)\ddot{\theta}=&(M+m)mgl\sin(\theta)\\&-ml\cos(\theta)b\dot{x}\\&-m^2l^2\cos(\theta)\sin(\theta)\dot{\theta}^2\\&-(M+m)d\dot{\theta}+ml\cos(\theta)F.\end{aligned}\tag{2.24}$$

Equation (2.24) can be arranged as follows:

$$\begin{aligned}\ddot{\theta}=&\frac{(M+m)mgl\sin(\theta)-mlb\cos(\theta)\dot{x}-m^2l^2\cos(\theta)\sin(\theta)\dot{\theta}^2}{\left(J_p+ml^2\right)(M+m)-m^2l^2\cos^2(\theta)}\\&+\frac{-(M+m)d\dot{\theta}+ml\cos(\theta)F}{\left(J_p+ml^2\right)(M+m)-m^2l^2\cos^2(\theta)}.\end{aligned}\tag{2.25}$$

Let the states be x, $\dot{x}$, θ, and $\dot{\theta}$:

$$\begin{bmatrix}x_1\\x_2\\x_3\\x_4\end{bmatrix}=\begin{bmatrix}x\\\dot{x}\\\theta\\\dot{\theta}\end{bmatrix},$$

state equations of the inverted pendulum on a cart system can be shown as

$$\dot{x}_1=x_2\tag{2.26}$$

$$\begin{aligned}\dot{x}_2=&\frac{-\left(J_p+ml^2\right)bx_2+m^2l^2g\cos(x_3)\sin(x_3)-mldx_4\cos(x_3)}{\left(J_p+ml^2\right)(M+m)-m^2l^2\cos^2(x_3)}\\&+\frac{-\left(J_p+ml^2\right)\mathrm{m}l{x_4}^2\sin(x_3)+\left(J_p+ml^2\right)F}{\left(J_p+ml^2\right)(M+m)-m^2l^2\cos^2(x_3)}\end{aligned}\tag{2.27}$$

$$\dot{x}_3=x_4\tag{2.28}$$

$$\dot{x}_4 = \frac{(M+m)mgl\sin x_3 - mlb\cos(x_3)x_2 - m^2l^2\cos(x_3)\sin(x_3)x_4^{\,2}}{(J_p+ml^2)(M+m)-m^2l^2\cos^2(x_3)} + \frac{-(M+m)dx_4 + ml\cos(x_3)F}{(J_p+ml^2)(M+m)-m^2l^2\cos^2(x_3)}. \tag{2.29}$$

2.3. DC Motor Model

In the inverted pendulum on a cart system, the cart is driven by a DC motor. To create a more realistic model, the motor characteristics should be added to the mathematical model of the inverted pendulum on a cart system (Ata and Coban, 2017).

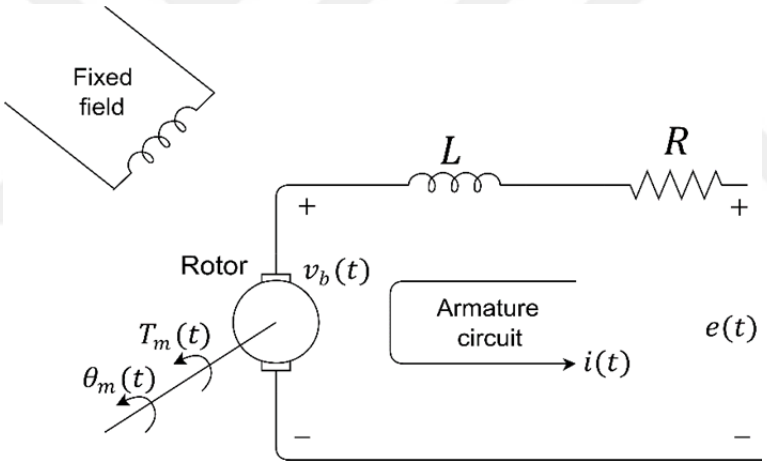

Figure 2.3. DC Motor schematics

A motor is an electromechanical component that gives a movement output for a voltage input. That is a mechanical output generated by an electrical input (Nise, 2010). In this section, the transfer function is derived for a particular kind of electromechanical system called armature-controlled DC servomotor (Mablekos, 1980). The motor's schematic is shown in Figure 2.3.

In Figure 2.3, the fixed field stands for a magnetic field which is developed by stationary permanent magnets or a stationary electromagnet and armature stands for a rotating circuit which current $i(t)$ flows through the magnetic field and feels a force. The resulting torque turns the rotating member of the motor, rotor.

A conductor moving at right angles to a magnetic field generates voltage at the terminals of the conductor equal to $e = Bl_c v$, where e is the voltage, B is the magnetic field flux density, l_c is the length of the conductor, and v is the velocity of the conductor normal to the magnetic field. Since the current-carrying armature is rotating in a magnetic field, its voltage is proportional to speed and named as back electromotive force. Thus, it is formulated by

$$v_b(t) = K_b \frac{d\theta_m(t)}{dt} \tag{2.30}$$

where K_b is the back electromotive force constant and $d\theta_m(t)/d(t) = \omega(t)$ is the angular velocity of the motor. Taking the Laplace transform of Equation (2.30) gives

$$V_b(s) = K_b s\theta_m(s). \tag{2.31}$$

The relation $v_b(t)$ between the armature current $i(t)$ and the applied armature voltage $e(t)$ can be shown by writing a loop equation around the Laplace transformed armature circuit:

$$RI(s) + LsI(s) + V_b(s) = E(s) \tag{2.32}$$

where L and R are the rotor circuit inductance and the rotor circuit resistance, respectively.

The torque developed by the motor is proportional to the armature current:

$$T_m(s) = K_t I(s) \tag{2.33}$$

where T_m is the torque, and K_t is the torque constant, which depends on the motor and magnetic field characteristics.

Rearranging Equation (2.33) yields

$$I(s) = \frac{1}{K_t} T_m(s). \tag{2.34}$$

Substituting Equation (2.31) and Equation (2.34) into Equation (2.32) gives

$$\frac{(R + Ls) T_m(s)}{K_t} + K_b s \theta_m(s) = E(s). \tag{2.35}$$

The torque developed by the motor also can be written as follows:

$$T_m(s) = \left(J_m s^2 + Ds\right) \theta_m(s) \tag{2.36}$$

where D is the viscous damping and J_m is the inertia of the motor.

Substituting Equation (2.36) in Equation (2.35) yields

$$\frac{(R+Ls)(J_m s^2 + Ds)\theta_m(s)}{K_t} + K_b s\theta_m(s) = E(s). \tag{2.37}$$

Equation (2.37) can be rewritten as

$$\frac{\theta_m(s)}{E(s)} = \frac{K_t}{(R+Ls)(J_m s^2 + Ds) + K_b K_t s}. \tag{2.38}$$

Equation (2.38) is the transfer function of the DC motor between input (voltage) and output (angular position).

Noting that

$$\omega(s) = \frac{d\theta_m}{dt} = s\theta_m(s),$$

$$\theta_m(s) = \frac{\omega(s)}{s}$$

and substituting $\frac{\omega(s)}{s}$ instead of $\theta_m(s)$ in Equation (2.38) and Equation (2.35) yields, respectively:

$$\frac{\omega(s)}{E(s)} = \frac{K_t}{(R+Ls)(J_m s + D) + K_b K_t}, \tag{2.39}$$

$$\frac{(R+Ls)T_m(s)}{K_t} + K_b\omega(s) = E(s). \tag{2.40}$$

In order to obtain torque developed by the motor and to get rid of angular velocity, substituting $\omega(s)$ from Equation (2.39) into Equation (2.40) yields

$$\frac{(R+Ls)T_m(s)}{K_t}+K_b\left(\frac{K_t}{(R+Ls)(J_ms+D)+K_bK_t}\right)E(s)=E(s). \qquad (2.41)$$

Collecting $E(s)$ terms on the right-hand-side in Equation (2.41) yields

$$\frac{R+Ls}{K_t}T_m(s)=E(s)-\frac{K_bK_t}{(R+Ls)(J_ms+D)+K_bK_t}E(s). \qquad (2.42)$$

Rearranging Equation (2.42) yields

$$\frac{R+Ls}{K_t}T_m(s)=\left(1-\frac{K_bK_t}{(R+Ls)(J_ms+D)+K_bK_t}\right)E(s). \qquad (2.43)$$

Equation (2.43) can be rewritten as

$$T_m(s)=\frac{K_t}{R+Ls}\left(1-\frac{K_bK_t}{(R+Ls)(J_ms+D)+K_bK_t}\right)E(s). \qquad (2.44)$$

Equation (2.44) is the motor torque equation without angular velocity $\omega(s)$ in the equation.

Let the force equation induced by the motor torque:

$$F(s)=\frac{n_1}{r}T_m(s) \qquad (2.45)$$

where r and n_1 are radius of pulley and gear ratio, respectively. The torque in Equation (2.45) can be rewritten as

$$T_m(s) = F(s)\frac{r}{n_1}. \tag{2.46}$$

Substituting Equation (2.46) in Equation (2.44) yields

$$F(s) = \left(\frac{n_1}{r}\right)\frac{K_t}{R+Ls}\left(1 - \frac{K_b K_t}{(R+Ls)(J_m s + D) + K_b K_t}\right)E(s). \tag{2.47}$$

In place of force F in the inverted pendulum equations of motion, DC motor armature voltage $E(s)$ can be used as the input. Towards this end, rearranging Equation (2.40) yields

$$T_m(s) = -\frac{K_b K_t}{R+Ls}\omega(s) + \frac{K_t}{R+Ls}E(s). \tag{2.48}$$

Letting translational velocity – angular velocity equation as

$$\omega(t) = \left(\frac{n_2}{r}\right)\frac{dx(t)}{dt} \tag{2.49}$$

where n_2 is gear ratio and taking Laplace transform of both sides of the Equation (2.49) yields

$$\omega(s) = \left(\frac{n_2}{r}\right)sx(s). \tag{2.50}$$

Using Equation (2.48) and Equation (2.46), the force can be written as follows:

$$F(s) = -\left(\frac{n_1}{r}\right)\frac{K_b K_t}{R + Ls}\omega(s) + \left(\frac{n_1}{r}\right)\frac{K_t}{R + Ls}E(s). \tag{2.51}$$

Substituting Equation (2.50) into Equation (2.51), one has

$$F(s) = -\left(\frac{n_1}{r}\right)\left(\frac{n_2}{r}\right)\frac{K_b K_t}{R + Ls}sx(s) + \left(\frac{n_1}{r}\right)\frac{K_t}{R + Ls}E(s). \tag{2.52}$$

Motor inductance L has a limited effect on the DC motor system, hence it is possible to take $L = 0$ for transfer function (Ata, 2014). For simplification, substituting $L = 0$ in Equation (2.52) yields

$$F(s) = -\left(\frac{n_1}{r}\right)\left(\frac{n_2}{r}\right)\frac{K_b K_t}{R}sx(s) + \left(\frac{n_1}{r}\right)\frac{K_t}{R}E(s). \tag{2.53}$$

Taking the inverse Laplace transform of Equation (2.53) gives a differential equation whose inputs are motor armature voltage $e(t)$ and translational velocity of the cart $\dot{x}(t)$, and output is the force $F(t)$ applied on the cart.

$$F(t) = -\left(\frac{n_1}{r}\right)\left(\frac{n_2}{r}\right)\frac{K_b K_t}{R}\dot{x}(t) + \left(\frac{n_1}{r}\right)\frac{K_t}{R}e(t). \tag{2.54}$$

Therefore, with Equation (2.54) electromechanical signal conversation from voltage to force is achieved.

2.4. Inverted Pendulum on a Cart System with DC Motor

Equation (2.26) through Equation (2.29) can be rearranged by substituting Equation (2.54) into them

$$\dot{x}_1 = x_2 \tag{2.55}$$

$$\dot{x}_2 = \frac{\phi x_2 + \varphi \cos(x_3)\sin(x_3) + \gamma \sin(x_3) x_4{}^2 + \eta \cos(x_3) x_4 + \lambda u}{\psi + \rho \cos^2(x_3)} \tag{2.56}$$

$$\dot{x}_3 = x_4 \tag{2.57}$$

$$\dot{x}_4 = \frac{\mu x_2 \cos(x_3) + \vartheta \sin(x_3) + \sigma x_4 + \rho \cos(x_3)\sin(x_3) x_4{}^2}{\psi + \rho \cos^2(x_3)} + \frac{\varsigma \cos(x_3) u}{\psi + \rho \cos^2(x_3)} \tag{2.58}$$

where

$$\phi = -\left(J_p + ml^2\right)\left(b + \left(\frac{n_1}{r}\right)\left(\frac{n_2}{r}\right)\left(\frac{K_b K_t}{R}\right)\right),$$

$$\varphi = m^2 l^2 g\ ,$$

$$\gamma = -\left(J_p + ml^2\right) ml\ ,$$

$$\eta = -mld\ ,$$

$$\lambda = \left(J_p + ml^2\right)\left(\left(\frac{n_1}{r}\right)\left(\frac{K_t}{R}\right)\right),$$

$$\mu = -ml\left(b + \left(\frac{n_1}{r}\right)\left(\frac{n_2}{r}\right)\left(\frac{K_b K_t}{R}\right)\right),$$

$$\vartheta = \left(M + m\right) mgl\ ,$$

$$\rho = -m^2 l^2\ ,$$

$$\sigma = -(M+m)d\,,$$

$$\varsigma = ml\left(\left(\frac{n_1}{r}\right)\left(\frac{K_t}{R}\right)\right),$$

$$\psi = \left(J_p + ml^2\right)\left(M+m\right),$$

and

$$u = e(t)\,.$$

Considering parametric uncertainties and external disturbances the state equations of the inverted pendulum on a cart system presented in Equation (2.55) to Equation (2.58) can be written as follows:

$$\begin{aligned}
\dot{x}_1 &= x_2 \\
\dot{x}_2 &= \frac{\delta_1\left(\phi x_2 + \varphi\cos\left(x_3\right)\sin\left(x_3\right) + \gamma\sin\left(x_3\right){x_4}^2 + \eta\cos\left(x_3\right)x_4\right)}{\psi + \rho\cos^2\left(x_3\right)} \\
&\quad + \frac{\lambda u}{\psi + \rho\cos^2\left(x_3\right)} + \xi_1(t) \\
\dot{x}_3 &= x_4 \\
\dot{x}_4 &= \frac{\delta_2\left(\mu x_2\cos\left(x_3\right) + \vartheta\sin\left(x_3\right) + \sigma x_4 + \rho\cos\left(x_3\right)\sin\left(x_3\right){x_4}^2\right)}{\psi + \rho\cos^2\left(x_3\right)} \\
&\quad + \frac{\varsigma\cos\left(x_3\right)u}{\psi + \rho\cos^2\left(x_3\right)} + \xi_2(t)
\end{aligned} \tag{2.59}$$

where δ_1 and δ_2 stand for the parametric uncertainties as constants; $\xi_1(t)$ and $\xi_2(t)$ the total amounts of external disturbances and unmatched uncertainties. $\xi_1(t)$ and $\xi_2(t)$ are assumed to bounded as $\left|\xi_1(t)\right| < \xi_{1\max}$ and $\left|\xi_2(t)\right| < \xi_{2\max}$.

3. DESIGN METHODS

3.1. Sliding Mode Control

The SMC is a special type of VSC method which is insensitive to the matched uncertainties and disturbances (Utkin, 1977). Accordingly, the SMC has been a widely used technique for handling nonlinear systems with undetermined dynamics and disturbances (Utkin, 1977; Utkin, 1992).

The objective of the SMC is to enforce the sliding modes in a pre-defined surface known as sliding surface in the state space of a given system using a discontinuous control.

The conventional SMC occurs in two phases; reaching phase and sliding phase. In the reaching phase, the system states are forced from an initial condition to a pre-defined sliding surface. The reaching phase is followed by the sliding phase. In this phase the system states are restricted to stay on the sliding surface and slides on the surface to an equilibrium. The reaching phase and the sliding phase are shown in Figure 3.1 where e and $\dot{e}$ denote the tracking error of a given system and its derivative respectively.

Correspond to these two phases, a conventional sliding mode controller consists of two control laws. The first control law is switching control which drives the system state trajectory to the pre-defined sliding surface. In the literature a signum function sign() is employed to create a discontinuous switching control law. The sign () function shown in Figure 3.2 can be defined as

$$sign(s) = \begin{cases} -1 & if \quad s < 0 \\ 0 & if \quad s = 0 \\ 1 & if \quad s > 0 \end{cases}$$

The second control law equivalent control is used when the system is in the sliding phase.

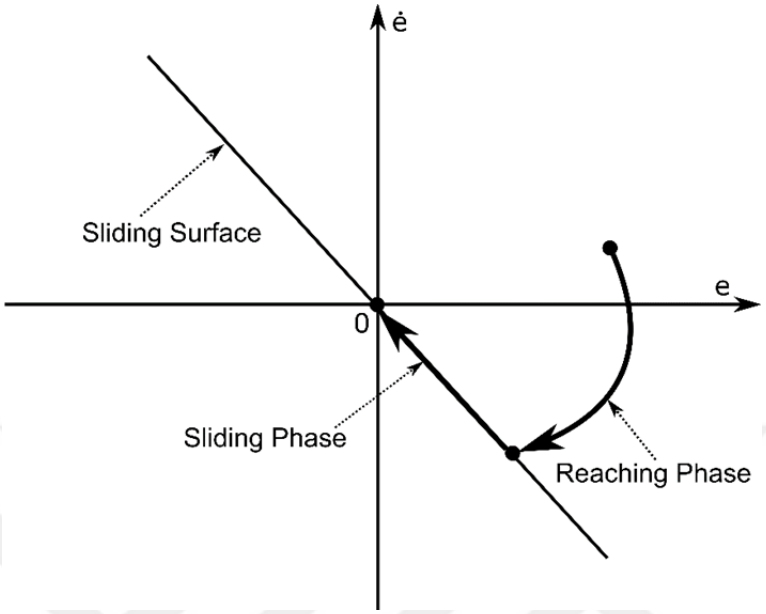

Figure 3.1. Reaching and sliding phases of the SMC

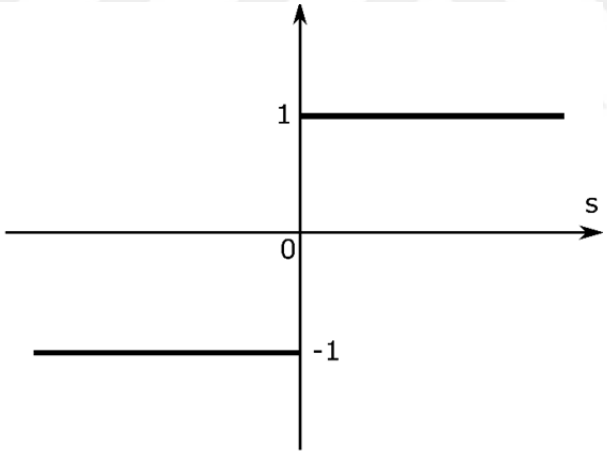

Figure 3.2. Signum function

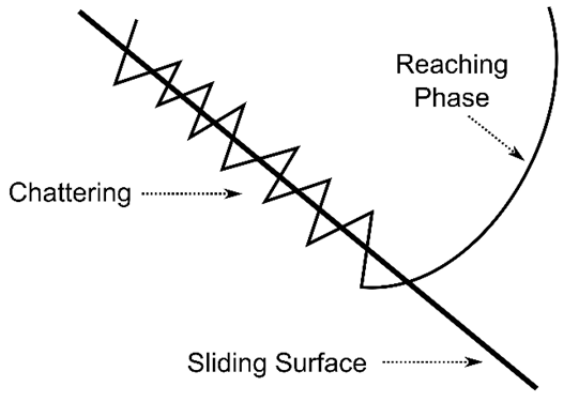

Figure 3.3. Chattering phenomenon in the SMC approach

Despite of its advantages, the SMC technique has a main drawback called chattering phenomenon which refers to finite frequency, finite amplitude oscillations of the control input. Hence, the chattering phenomenon can lead to unacceptable control accuracy.

There are two essential causes to lead chattering. First, the limited switching frequency can lead chattering because the ideal SMC approach requires infinite switching frequency (Young et al., 1999). Second, unmodelled dynamics of the system come from actuators and sensors can cause a high frequency oscillation on the sliding surface (Yu and Kaynak, 2009) as shown in Figure 3.3

Avoiding the chattering has been a challenging problem in the SMC approach. There have been various efficient methods to minimize the potential chattering. Boundary layer solution is one of the most used methods to overcome the chattering (Slotine and Li, 1991). The boundary layer approach is based on the use of a continuous approximation of the signum function in the switching control law.

Commonly a saturation function has been used instead of signum function. The saturation function shown in Figure 3.4 is defined by

$$sat\left(s/\Delta\right)=\begin{cases}\text{sign (s/}\Delta\text{)} & \text{if} \quad |s/\Delta|\geq 1\\ \text{s/}\Delta & \text{if} \quad |s/\Delta|<1\end{cases}$$

where Δ denotes a boundary level as shown in Figure 3.5.

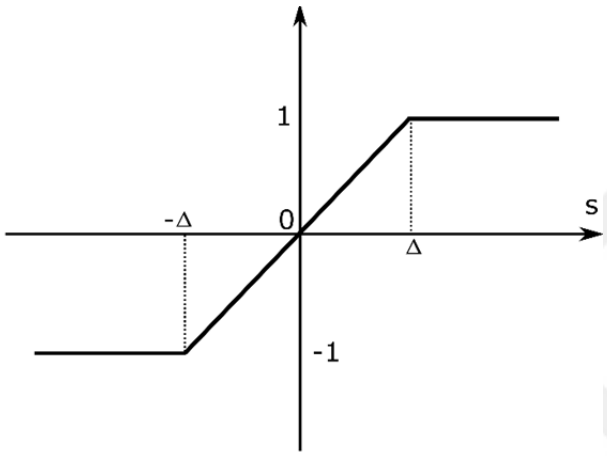

Figure 3.4. Saturation function

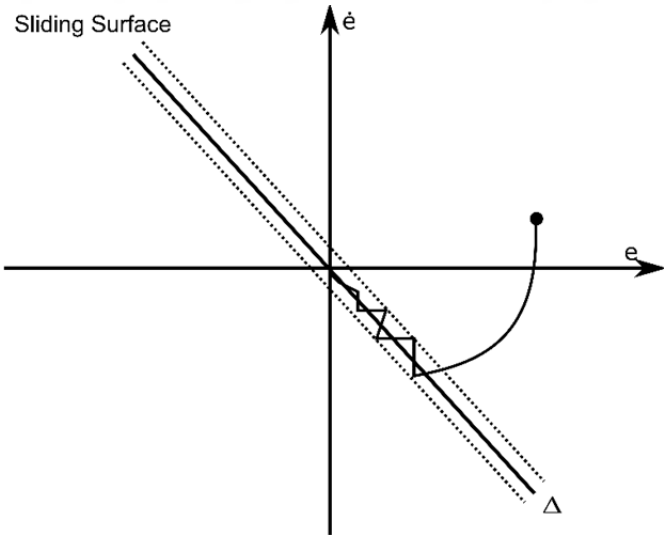

Figure 3.5. Sliding surface with the boundary layer approach

A sliding mode controller for a single input single output system can be designed as follows. Dynamical equations of a general single input single output non-linear system can be described by

$$\begin{aligned} \dot{x}_1(t) &= x_2(t) \\ \dot{x}_2(t) &= \delta f(x) + g(x)u(t) + \xi(t) \\ y(t) &= x_1(t) \end{aligned} \tag{3.1}$$

where $f(x)$ and $g(x)$ are nonlinear functions, $x = \begin{bmatrix} x_1 & x_2 \end{bmatrix}^T$ is the state vector; δ is the parametric uncertainty; $\xi(t)$ is the total amounts of external disturbances and unmatched uncertainties ; $y(t)$ is the output; and $u(t)$ is the control input. $\xi(t)$ is assumed to be bounded as $|\xi(t)| \le \xi_{\max}$ where $\xi_{\max}$ is a positive constant. In order to design a sliding mode controller for this system, a sliding surface can be defined as

$$s(t) = k_1 e(t) + \dot{e}(t) \tag{3.2}$$

using the tracking error

$$e(t) = y(t) - y_d(t), \tag{3.3}$$

where k_1 is a real positive constant and $y_d(t)$ is the desired output.

Considering a Lyapunov function

$$V(s) = \frac{1}{2} s^2(t) \tag{3.4}$$

and differentiating $V(s)$ yield

$$\begin{aligned}\dot{V}(s) &= s(t)\dot{s}(t)\\ &= s(t)\left(k_1\dot{e}(t)+\ddot{e}(t)\right)\\ &= s(t)\left(k_1\dot{e}(t)+\ddot{y}(t)-\ddot{y}_d(t)\right)\\ &= s(t)\left(k_1\dot{e}(t)+\dot{x}_2-\ddot{y}_d(t)\right)\\ &= s(t)\left(k_1\dot{e}(t)+\delta f(x)+g(x)u(t)+\xi(t)-\ddot{y}_d(t)\right).\end{aligned} \tag{3.5}$$

$\dot{V}(s)$ in Equation (3.5) will be negative definite if the control law is defined as

$$u(t)=u_{eq}(t)+u_{sw}(t) \tag{3.6}$$

with

$$u_{eq}(t)=\frac{1}{g(x)}\left(-k_1\dot{e}(t)-\delta f(x)+\ddot{y}_d(t)\right), \tag{3.7}$$

$$u_{sw}(t)=-\frac{1}{g(x)}K\text{sign}\left(s(t)\right), \tag{3.8}$$

and

$$sign\left(s(t)\right)=\begin{cases}1, & s(t)>0\\ 0, & s(t)=0\\ -1, & s(t)<0\end{cases} \tag{3.9}$$

where $K>\xi_{\max}\geq\left|\xi(t)\right|$.

Substituting Equation (3.6) into Equation (3.5) yields

$$\begin{aligned}\dot{V}(s) &= s(t)\left[k_1\dot{e}(t)+\delta f(x)-\ddot{y}_d(t)+g(x)\left(u_{eq}(t)+u_{sw}(t)\right)+\xi(t)\right]\\ &= s(t)\left[k_1\dot{e}(t)+\delta f(x)-\ddot{y}_d(t)\right.\\ &\quad \left.+g(x)\frac{1}{g(x)}\left(-k_1\dot{e}(t)-\delta f(x)+\ddot{y}_d(t)\right)+g(x)u_{sw}(t)+\xi(t)\right]\\ &= s(t)\left[g(x)u_{sw}(t)+\xi(t)\right]\\ &\le -Ks(t)\operatorname{sign}(s(t))+\xi_{\max}s(t)\\ &\le -|s(t)|\left(K-\xi_{\max}\right)\\ &< 0.\end{aligned} \tag{3.10}$$

where $K > \xi_{\max} \ge |\xi(t)|$.

According to the Lyapunov theorem, due to the fact that $\dot{V}(s)$ is negative definite, the system trajectory will be driven to sliding surface and remain in there until the origin is reached asymptotically.

Using $\operatorname{sign}(s(t))$ function will lead the chattering. A boundary level with width Δ can be defined and $\operatorname{sign}(s(t))$ function can be replaced with a saturation function in Equation (3.8) to overcome this problem as follows:

$$u_{sw}(t) = -\frac{1}{g(x)}K\operatorname{sat}(s(t)/\Delta) \tag{3.11}$$

with

$$\operatorname{sat}(\Gamma) = \begin{cases}\operatorname{sign}(\Gamma), & |\Gamma| \ge 1\\ \Gamma, & |\Gamma| < 1\end{cases} \tag{3.12}$$

where $\Delta > 0$.

3.2. Decoupled Sliding Mode Control

The SMC design can be applied to systems presented in the canonical form. Nevertheless, the dynamic representation of the inverted pendulum on a cart system presented in Equation (2.59) has a form shown below rather than the canonical form

$$\begin{aligned}
\dot{x}_1(t) &= x_2(t) \\
\dot{x}_2(t) &= \delta_1 f_1(x) + g_1(x)u(t) + \xi_1(t) \\
\dot{x}_3(t) &= x_4(t) \\
\dot{x}_4(t) &= \delta_2 f_2(x) + g_2(x)u(t) + \xi_2(t)
\end{aligned} \tag{3.13}$$

where $x = \left[x_1, x_2, x_3, x_4\right]^T$ is the state vector; $f_1(x)$, $g_1(x)$, $f_2(x)$ and $g_2(x)$ are nonlinear functions; $u(t)$ is the control input; δ_1 and δ_2 are the parametric uncertainties as constants; and $\xi_1(t)$ and $\xi_2(t)$ are the total amounts of external disturbances and unmatched uncertainties. $\xi_1(t)$ and $\xi_2(t)$ are assumed to be bounded as $\left|\xi_1(t)\right| \le \xi_{1\max}$ and $\left|\xi_2(t)\right| \le \xi_{2\max}$ where $\xi_{1\max}$ and $\xi_{2\max}$ are positive constants.

The decoupled control idea can be used to design a controller to control both the displacement and the angle in the inverted pendulum on a cart system. The main idea behind the decoupled sliding mode control is to decouple the whole system into two subsystems and define a sliding surface for each subsystem. The control objective of a sliding mode controller is to drive the sliding surface to zero, hence using an intermediate variable to transfer value from a sliding surface to the other can lead to control both subsystems simultaneously. To design a decoupled sliding mode controller for this system two different sliding surfaces can be defined as follows (Lo and Kuo, 1998; Coban and Ata, 2017):

$$s_{S1}(t) = k_1 e_1(t) + \dot{e}_1(t) \tag{3.14}$$

$$s_{S2}(t) = k_2 e_2(t) + \dot{e}_2(t) \tag{3.15}$$

using the tracking errors

$$e_1(t) = y_1(t) - y_{d1}(t) \tag{3.16}$$

and

$$e_2(t) = y_2(t) - y_{d2}(t) \tag{3.17}$$

where k_1 and k_2 are real positive constants, and $e_1(t)$ and $e_2(t)$ are tracking errors for the cart displacement and pendulum angle, respectively. $s_{S2}(t)$ in Equation (3.15) can be transformed to a decoupled sliding surface as

$$s_{S2}(t) = k_2 \left(e_2(t) - z_S(t) \right) + \dot{e}_2(t) \tag{3.18}$$

with $z_S(t)$ is a value transferred from $s_{S1}(t)$ and defined as

$$z_S(t) = \text{sat}\left(\frac{s_{S1}(t)}{\Delta_{Sz}} \right) z_{Su}, \qquad 0 < z_{Su} < 1 \tag{3.19}$$

where z_{Su} is the upper bound of $z_S(t)$ and Δ_{Sz} is the boundary level as constants. z_{Su}, the upper bound of the intermediate variable z_S guarantees that $s_{S2}(t)$ will be limited. After the sliding surface $s_{S1}(t)$ becomes zero, $s_{S2}(t)$ will be driven to zero too, thanks to z_S.

Considering a Lyapunov function

$$V_S(s_{S2}) = \frac{1}{2} {s_{S2}}^2(t) \tag{3.20}$$

and differentiating $V_S(s_{S2})$ yield

$$\begin{aligned}
\dot{V}_S(s_{S2}) &= s_{S2}(t)\dot{s}_{S2}(t) \\
&= s_{S2}(t)\left(k_2\left(\dot{e}_2(t) - \dot{z}_S(t)\right) + \ddot{e}_2(t)\right) \\
&= s_{S2}(t)\left(k_2\left(\dot{e}_2(t) - \dot{z}_S(t)\right) + \ddot{y}_2(t) - \ddot{y}_{d2}(t)\right) \\
&= s_{S2}(t)\left(k_2\left(\dot{e}_2(t) - \dot{z}_S(t)\right) + \dot{x}_4 - \ddot{y}_{d2}(t)\right) \\
&= s_{S2}(t)\Big[k_2\left(\dot{e}_2(t) - \dot{z}_S(t)\right) \\
&\quad + \delta_2 f_2(x) + g_2(x)u(t) + \xi_2(t) - \ddot{y}_{d2}(t)\Big].
\end{aligned} \tag{3.21}$$

$\dot{V}_S(s_{S2})$ in Equation (3.21) will be negative definite if the control law for $u(t)$ in Equation (3.21) is defined as

$$u_S(t) = u_{Seq}(t) + u_{Ssw}(t) \tag{3.22}$$

with

$$u_{Seq}(t) = \frac{1}{g_2(x)}\left[-k_2\left(\dot{e}_2(t) - \dot{z}_S(t)\right) - \delta_2 f_2(x) + \ddot{y}_{d2}(t)\right], \tag{3.23}$$

$$u_{Ssw}(t) = -\frac{1}{g_2(x)} K_S \operatorname{sign}\left(s_{S2}(t)\right), \tag{3.24}$$

where $K_S > \xi_{2\max} \geq \left|\xi_2(t)\right|$.

Substituting Equation (3.22) into Equation (3.21) yields

$$\begin{aligned}\dot{V}_S(s_{S2}) &= s_{S2}(t)\big[k_2\left(\dot{e}_2(t)-\dot{z}_S(t)\right)\\ &\quad +\delta_2 f_2(x)+g_2(x)\left(u_{Seq}(t)+u_{Ssw}(t)\right)+\xi_2(t)-\ddot{y}_{d2}(t)\big]\\ &= s_{S2}(t)\big[k_2\left(\dot{e}_2(t)-\dot{z}_S(t)\right)+\delta_2 f_2(x)-\ddot{y}_{d2}(t)\\ &\quad +g_2(x)\frac{1}{g_2(x)}\left(-k_2\left(\dot{e}_2(t)-\dot{z}_S(t)\right)-\delta_2 f_2(x)+\ddot{y}_{d2}(t)\right)\\ &\quad +g_2(x)u_{Ssw}(t)+\xi(t)\big]\\ &= s_{S2}(t)\big[g_2(x)u_{Ssw}(t)+\xi_2(t)\big]\\ &= -K_S s_{S2}(t)\operatorname{sign}\left(s_{S2}(t)\right)+s_{S2}(t)\xi_2(t)\\ &\le -K_S\left|s_{S2}(t)\right|+s_{S2}(t)\xi_{2\max}\\ &\le -\left|s_{S2}(t)\right|\left(K_S-\xi_{2\max}\right)\\ &< 0.\end{aligned} \tag{3.25}$$

where $K_S > \xi_{2\max} \ge \left|\xi_2(t)\right|$.

According to the Lyapunov theorem, due to the fact that $\dot{V}_S(s)$ is negative definite, the system trajectory will be driven to sliding surface and remain in there until the origin is reached asymptotically.

Therewith, a decoupled sliding mode controller for an underactuated system can be presented as in Equation (3.22).

3.3. Backstepping

The sliding mode control can handle any kind of matched uncertainties; however, it has a deficiency to handle parametric uncertainties. In order to manage this drawback, both the backstepping control and SMC techniques can be combined. Backstepping is a nonlinear stabilization technique of “adding an integrator” (Freeman and Kokotović, 1996) which is mainly used to deal with the

robust control of the nonlinear systems with parametric uncertainties and the nonlinear functions assumed to be known (Yao and Tomizuka, 2001).

The backstepping design method is described by Khalil as follows (Khalil, 2002). Consider a system

$$\dot{\alpha}(t) = f(\alpha(t)) + g(\alpha(t))\beta(t) \tag{3.26}$$

$$\dot{\beta}(t) = u(t) \tag{3.27}$$

where $f(\alpha(t))$ and $g(\alpha(t))$ are known functions, $[\alpha^T, \beta]^T$ is the state vector and $u(t)$ is the control input. Equation (3.26) can be stabilized by a state feedback control law $\beta(t) = \chi(\alpha(t))$ with $\chi(0) = 0$ as

$$\dot{\alpha}(t) = f(\alpha(t)) + g(\alpha(t))\chi(\alpha(t)). \tag{3.28}$$

Hence, the origin of Equation (3.28) is asymptotically stable. Considering a Lyapunov function $V(\alpha(t))$ will satisfies the inequality

$$\frac{\partial V(\alpha(t))}{\partial \alpha(t)}\left(f(\alpha(t)) + g(\alpha(t))\chi(\alpha(t))\right) \le -W(\alpha(t)) \tag{3.29}$$

where $W(\alpha(t))$ is positive definite.

Adding and subtracting $g(\alpha(t))\chi(\alpha(t))$ on Equation (3.26), the system equations Equation (3.26) and Equation (3.27) can be rewritten as

$$\dot{\alpha} = \left(f\left(\alpha(t)\right) + g\left(\alpha(t)\right)\chi\left(\alpha(t)\right)\right) + g\left(\alpha(t)\right)\left(\beta(t) - \chi\left(\alpha(t)\right)\right). \quad (3.30)$$

$$\dot{\beta}(t) = u(t) \quad (3.31)$$

Changing of variables $z_b(t) = \beta(t) - \chi\left(\alpha(t)\right)$ and substituting it into system equations Equation (3.30) and Equation (3.31) yields

$$\dot{\alpha}(t) = \left(f\left(\alpha(t)\right) + g\left(\alpha(t)\right)\chi\left(\alpha(t)\right)\right) + g\left(\alpha(t)\right)z_b(t) \quad (3.32)$$

$$\dot{z}_b(t) = u(t) - \dot{\chi}\left(\alpha(t)\right). \quad (3.33)$$

Since $f\left(\alpha(t)\right)$, $g\left(\alpha(t)\right)$ and $\chi\left(\alpha(t)\right)$ are known, the derivative of $\chi\left(\alpha(t)\right)$ with respect of time can be defined as

$$\frac{d\chi\left(\alpha(t)\right)}{dt} = \frac{\partial\chi\left(\alpha(t)\right)}{\partial\alpha(t)}\left(f\left(\alpha(t)\right) + g\left(\alpha(t)\right)\beta(t)\right). \quad (3.34)$$

Taking $v_b(t) = u(t) - \dot{\chi}(t)$ in the system in Equation (3.32) and Equation (3.33) results in

$$\dot{\alpha}(t) = \left(f\left(\alpha(t)\right) + g\left(\alpha(t)\right)\chi\left(\alpha(t)\right)\right) + g\left(\alpha(t)\right)z_b(t) \quad (3.35)$$

$$\dot{z}_b(t) = v_b(t) \quad (3.36)$$

where the first component of Equation (3.35) $f\left(\alpha(t)\right) + g\left(\alpha(t)\right)\chi\left(\alpha(t)\right)$ has asymptotically stable origin when the input is zero. Hence, $v_b(t)$ can be designed to stabilize the overall system. Considering a Lyapunov function

$$V_c\left(\alpha(t),\beta(t)\right)=V\left(\alpha(t)\right)+\frac{1}{2}z_b{}^2(t) \tag{3.37}$$

and differentiating it with respect to time and using Equation (3.35) and Equation (3.36) results in

$$\begin{aligned}\dot{V}_c &= \frac{\partial V\left(\alpha(t)\right)}{\partial \alpha(t)}\left(f\left(\alpha(t)\right)+g\left(\alpha(t)\right)\chi\left(\alpha(t)\right)\right)\\ &\quad+\frac{\partial V\left(\alpha(t)\right)}{\partial \alpha(t)}g\left(\alpha(t)\right)z_b(t)+z_b(t)v_b(t)\\ &\le -W\left(\alpha(t)\right)+\frac{\partial V\left(\alpha(t)\right)}{\partial \alpha(t)}g\left(\alpha(t)\right)z_b(t)+z_b(t)v_b(t).\end{aligned} \tag{3.38}$$

Choosing

$$v_b(t)=-\frac{\partial V\left(\alpha(t)\right)}{\partial \alpha(t)}g\left(\alpha(t)\right)-k_b z_b(t) \tag{3.39}$$

where $k_b>0$ yields

$$\dot{V}_c \le -W\left(\alpha(t)\right)-k_b z_b{}^2(t). \tag{3.40}$$

Since $\dot{V}_c$ is negative definite, the origin on $\alpha=0$ and $z_b=0$ will be asymptotically stable. Since $\chi(0)=0$, it is also concluded that the origin on $\alpha=0$ and $\beta=0$ will be asymptotically stable.

Consequently, substituting $v_b(t)$, $z_b(t)$, and $\dot{\chi}\left(\alpha(t)\right)$ into Equation (3.33), the backstepping control law can be written as

$$\begin{aligned} u(t) &= \dot{z}_b(t) + \dot{\chi}(\alpha(t)) \\ &= v_b(t) + \dot{\chi}(\alpha(t)) \\ &= -\frac{\partial V(\alpha(t))}{\partial \alpha(t)} g(\alpha(t)) - k_b z_b(t) + \dot{\chi}(\alpha(t)) \\ &= -\frac{\partial V(\alpha(t))}{\partial \alpha(t)} g(\alpha(t)) - k_b(\beta(t) - \chi(\alpha(t))) + \dot{\chi}(\alpha(t)) \\ &= -\frac{\partial V(\alpha(t))}{\partial \alpha(t)} g(\alpha(t)) - k_b(\beta(t) - \chi(\alpha(t))) \\ &\quad + \frac{\partial \chi(\alpha(t))}{\partial \alpha(t)}(f(\alpha(t)) + g(\alpha(t))\beta(t)). \end{aligned} \tag{3.41}$$

3.4. Backstepping Sliding Mode Control

The steps of the backstepping sliding mode control (BSMC) can be designed as follows. Consider a general single input single output nonlinear system described in Equation (3.1) and let the tracking error $e(t)$ be defined as in Equation (3.3). The derivative of the error can be presented as

$$\begin{aligned} \dot{e}(t) &= \dot{x}_1(t) - \dot{y}_d(t) \\ &= x_2(t) - \dot{y}_d(t). \end{aligned} \tag{3.42}$$

Consider a Lyapunov function

$$V_{B1}(e) = \frac{1}{2} e^2(t) \tag{3.43}$$

which is positive definite by the definition. Time derivate of $V_{B1}(e)$ is obtained as follows:

$$\begin{aligned}\dot{V}_{B1}(e) &= e(t)\dot{e}(t) \\ &= e(t)\left(x_2(t) - \dot{y}_d\left(t\right)\right).\end{aligned} \tag{3.44}$$

Letting

$$x_2(t) = s_B(t) - b_1 e(t) + \dot{y}_d\left(t\right)$$

as a virtual control and rearranging the Equation (3.41) yields

$$\dot{V}_{B1}(e) = e(t)s_B(t) - b_1 e^2(t), \qquad b_1 > 0 \tag{3.45}$$

where the sliding variable $s_B(t) = x_2(t) + b_1 e(t) - \dot{y}_d\left(t\right)$. $\dot{V}_{B1}(e) = -b_1 e^2\left(t\right) < 0$ for $s_B = 0$, therefore, $\dot{V}_{B1}(e)$ is negative definite. To design a backstepping controller the next step is required.

Selecting the second Lyapunov function as

$$V_{B2}(e) = V_{B1}(e) + \frac{1}{2} s_B{}^2(t) \tag{3.46}$$

and with the help of Equation (3.1) time derivative of the Lyapunov function in Equation (3.43) yields

$$\begin{aligned}\dot{V}_{B2}(e) &= \dot{V}_{B1}(e) + s_B(t)\dot{s}_B(t) \\ &= \dot{V}_{B1}(e) + s_B(t)\left(\delta f(x) + g(x)u_B(t) + \xi(t) + b_1\dot{e}(t) - \ddot{y}_d\left(t\right)\right).\end{aligned} \tag{3.47}$$

In order to realize that $\dot{V}_{B2}(e)$ is negative definite, the backstepping controller law can be designed as follows:

$$u_{Beq}(t) = \frac{1}{g(x)}\left(-\delta f(x) - e(t) - b_1\dot{e}(t) + \ddot{y}_d(t) - b_2 s(t)\right) \tag{3.48}$$

where b_1 and b_2 are positive constants. Hence, $\dot{V}_{B2}(e)$ becomes

$$\dot{V}_{B2}(e) = -b_1 e^2(t) - b_2 s_B{}^2(t) + \xi(t) s_B(t)\,. \tag{3.49}$$

To guarantee the stability of the system a switching control law can be defined as follows:

$$u_{Bsw}(t) = -\frac{1}{g(x)} B\,\mathrm{sign}(s_B(t))\,. \tag{3.50}$$

where B is a positive constant.

Putting the control laws in Equation (3.48) and Equation. (3.50) together gives the robust control law known as backstepping sliding mode control which can be defined as

$$u_B(t) = \frac{1}{g(x)}\left(-\delta f(x) - e(t) - b_1\dot{e}(t) + \ddot{y}_d - b_2 s(t) - B\,\mathrm{sign}\left(s_B(t)\right)\right). \tag{3.51}$$

With the help of Equation (3.51), the time derivative of the Lyapunov function in Equation (3.47) can be rewritten as

$$\begin{aligned}\dot{V}_{B2}(e) &= -b_1 e^2(t) - b_2 s_B{}^2(t) + \xi(t) s_B(t) - B\left|s_B(t)\right| \\ &\le -b_1 e^2(t) - b_2 s_B{}^2(t) - \left|s_B(t)\right|\left(B - \xi_{\max}\right) \\ &< 0\end{aligned} \tag{3.52}$$

where $B \geq \xi_{\max} \geq \left|\xi(t)\right|$. Since $\dot{V}_{B2}(e)$ is negative definite, the system trajectory will be driven to sliding surface and remain in there until the origin is reached asymptotically. Consequently, the stability of the overall system is guaranteed.

3.5. Decoupled Backstepping Sliding Mode Control

The BSMC technique can be applied to systems presented in the canonical form as in SMC. However, using the presented BSMC method, a decoupled backstepping sliding mode controller can be designed for an underactuated system as in Equation (3.14). To this end, two different tracking errors can be defined as

$$e_1(t) = x_1(t) - y_{d1}(t) \tag{3.53}$$

$$e_2(t) = x_3(t) - y_{d2}(t) \tag{3.54}$$

and time-derivating them result in

$$\begin{aligned} \dot{e}_1(t) &= \dot{x}_1(t) - \dot{y}_{d1}(t) \\ &= x_2(t) - \dot{y}_{d1}(t) \end{aligned} \tag{3.55}$$

$$\begin{aligned} \dot{e}_2(t) &= \dot{x}_3(t) - \dot{y}_{d2}(t) \\ &= x_4(t) - \dot{y}_{d2}(t). \end{aligned} \tag{3.56}$$

Considering a Lyapunov function candidate

$$V_{D1}(e) = \frac{1}{2} e_2^{\,2}(t) \tag{3.57}$$

and differentiating it with respect to time results in

$$\begin{aligned}\dot{V}_{D1}(e) &= e_2(t)\dot{e}_2(t) \\ &= e_2(t)\left(x_4(t) - y_{d2}(t)\right).\end{aligned} \tag{3.58}$$

In this step of the DBSMC design, two different sliding surfaces can be chosen unlike the BSMC

$$s_{D1}(t) = c_1 e_1(t) + \dot{e}_1(t) \tag{3.59}$$

$$s_{D2}(t) = c_2 e_2(t) + \dot{e}_2(t). \tag{3.60}$$

where c_1 and c_2 are real positive constants.

Letting

$$x_4(t) = s_{D2}(t) - c_2 e_2(t) + \dot{y}_{d2}(t) \tag{3.61}$$

from s_{D2} in Equation (3.60) and substituting it into Equation (3.58), one has

$$\dot{V}_{D1}(e) = e_2(t) s_{D2}(t) - c_2 {e_2}^2. \tag{3.62}$$

$\dot{V}_{D1}(e) = -c_2 {e_2}^2(t)$ will be negative definite, if only $s_{D2}(t) = 0$. Therefore, in order to ensure the stability of the DBSMC, the Lyapunov function for the next step can be chosen as follows:

$$V_{D2}(e) = V_{D1}(e) + \frac{1}{2} {s_{D2}}^2(t). \tag{3.63}$$

Using Equation (3.13), the time derivative of the Equation (3.63) is

$$\begin{aligned}\dot{V}_{D2}(e) &= \dot{V}_{D1}(e) + s_{D2}(t)\dot{s}_{D2}(t) \\ &= e_2(t)s_{D2}(t) - c_2 e_2^{\,2}(t) \\ &+ s_{D2}(t)\left(\delta_2 f_2(x) + g_2(x)u_D(t)\right) \\ &+ s_{D2}(t)\left(\xi_2(t) + c_2\dot{e}_2(t) - \ddot{y}_{d2}(t)\right)\end{aligned} \tag{3.64}$$

In order to ensure $\dot{V}_{D2}(e)$ is negative definite, the decoupled backstepping control law can be chosen as

$$\begin{aligned}u_{Deq}(t) &= \frac{1}{g_2(x)}\left(-\delta_2 f_2(x) - e_2(t) - c_2\dot{e}_2(t)\right) \\ &+ \frac{1}{g_2(x)}\left(\ddot{y}_{d2}(t) - c_3 s_{D2}(t)\right)\end{aligned} \tag{3.65}$$

where c_3 is a real positive constant. To ensure the stability of the system a switching control law can be defined as follows:

$$u_{Dsw}(t) = -\frac{1}{g_2(x)}C\,\mathrm{sign}\left(s_{D2}(t)\right) \tag{3.66}$$

where C is a real positive constant.

The control law $u_D(t)$ can be defined as putting the control laws in Equation (3.65) and Equation (3.66) together

$$u_D(t) = u_{Deq}(t) + u_{Dsw}(t) \tag{3.67}$$

Substitution of Equation (3.67) into Equation (3.64) results in

$$\begin{aligned}\dot{V}_{D2}(e) &= -c_2 {e_2}^2(t) - c_3 {s_{D2}}^2(t) + \xi_2(t) s_{D2}(t) - C\left|s_{D2}(t)\right| \\ &\le -c_2 {e_2}^2(t) - c_3 {s_{D2}}^2(t) - \left|s_{D2}(t)\right|\left(C - \xi_{2\max}\right) \\ &< 0\end{aligned} \tag{3.68}$$

The time derivative of the Lyapunov function $\dot{V}_{D2}$ will be negative definite where $C \ge \xi_{2\max} \ge \left|\xi_2(t)\right|$.

To create a decoupled controller a virtual sliding surface s_d can be considered as

$$s_d(t) = c_2(e_2(t) - z_D) + \dot{e}_2(t) \tag{3.69}$$

with z_D is a value transferred from s_{D1} and defined as

$$z_D(t) = \text{sat}\left(s_{D1}(t)/\Delta_{Dz}\right) z_{Du}, \quad 0 < z_{Du} < 1 \tag{3.70}$$

where z_{Du} is the upper bound of the $z_D(t)$ and guarantees that $s_d(t)$ will be limited.

Consequently, substituting $s_d(t)$ in Equation (3.69) into the Equation (3.67) for $s_{D2}(t)$ gives the DBSMC law for a general underactuated system as presented in Equation (3.13)

$$\begin{aligned}u_D(t) = &\frac{1}{g_2(x)}\left(-\delta_2 f_2(x) - e_2(t) - c_2\dot{e}_2(t)\right) \\ &+ \frac{1}{g_2(x)}\left(\ddot{y}_{d2}(t) - c_3 s_d(t) - C\text{sign}(s_d(t))\right).\end{aligned} \tag{3.71}$$

4. RESULTS AND DISCUSSIONS

4.1. Controller Design

The steps of the controller designs for the inverted pendulum on a cart system using both the DSMC and the DBSMC methods are presented in the following subsections.

4.1.1. The DSMC Design for the Inverted Pendulum on a Cart System

Using the inverted pendulum on a cart model introduced in Equation (2.59) and the decoupled sliding mode controller presented in Equation (3.22), a decoupled sliding mode controller for the inverted pendulum on a cart system can be designed as follows:

Tracking errors $e_1(t)$ and $e_2(t)$ can be defined as the error of cart displacement and the errors of the pendulum angle, respectively. Using tracking errors, the sliding surfaces can be defined as

$$s_{DS1}(t) = k_{DS1}\left(x_1(t) - y_{d1}(t)\right) + \left(x_2(t) - \dot{y}_{d1}(t)\right) \tag{4.1}$$

$$s_{DS2}(t) = k_{DS2}\left(x_3(t) - y_{d2}(t) - z_{DS}(t)\right) + \left(x_4(t) - \dot{y}_{d2}(t)\right) \tag{4.2}$$

where

$$z_{DS}(t) = sat\left(\frac{s_{DS1}(t)}{\Delta_{DSz}}\right) z_{DSu}, \qquad 0 < z_{DSu} < 1. \tag{4.3}$$

Hence the control law for the decoupled sliding mode controller for the inverted pendulum on a cart can be defined as

$$u_{DS}(t)=\frac{1}{g_2(x)}\left[-\delta_2 f_2(x)-k_{DS2}\left(x_4(t)-\dot{y}_{d2}(t)-\dot{z}_{DS}(t)\right)\right] + \frac{1}{g_2(x)}\left(-K_{DS}\,\mathrm{sign}\left(s_{DS2}(t)\right)\right) \tag{4.4}$$

where $K_{DS} > \xi_{2\max} \geq \left|\xi_2(t)\right|$,

$$f_2(x)=\frac{\mu x_2 \cos(x_3)+\vartheta \sin(x_3)+\sigma x_4+\rho \cos(x_3)\sin(x_3){x_4}^2}{\psi+\rho\cos^2(x_3)}$$

and

$$g_2(x)=\frac{\varsigma\cos(x_3)}{\psi+\rho\cos^2(x_3)}$$

with

$$\mu=-ml\left(b+\left(\frac{n_1}{r}\right)\left(\frac{n_2}{r}\right)\left(\frac{K_b K_t}{R}\right)\right),$$

$$\vartheta=(M+m)mgl,$$

$$\rho=-m^2l^2,$$

$$\sigma=-(M+m)d,$$

$$\varsigma=ml\left(\left(\frac{n_1}{r}\right)\left(\frac{K_t}{R}\right)\right),$$

and,

$$\psi = \left(J_p + ml^2\right)\left(M + m\right).$$

The decoupled sliding mode controller for the inverted pendulum on a cart in Equation (4.4) can be rewritten using the saturation function to avoid the chattering as

$$\begin{aligned} u_{DS}(t) = & \frac{1}{g_2(x)}\left[-\delta_2 f_2(x) - k_{DS2}\left(x_4(t) - \dot{y}_{d2}(t) - z_{DS}(t)\right)\right] \\ & + \frac{1}{g_2(x)}\left(-K_{DS}\, sat\left(s_{DS2}(t)/\Delta_{DSs}\right)\right). \end{aligned} \tag{4.5}$$

4.1.2. The DBSMC Design for Inverted Pendulum on a Cart System

Using the inverted pendulum on a cart model introduced in Equation (2.59) and the decoupled backstepping sliding mode controller presented in Equation (3.71), a decoupled backstepping sliding mode controller for the inverted pendulum on a cart system can be designed as follows

Tracking errors e_1 and e_2 can be defined as the error of cart displacement and the error of the pendulum angle, respectively. Using tracking errors, the sliding surfaces can be defined as

$$s_{DB1}(t) = c_{DB1}\left(x_1(t) - y_{d1}(t)\right) + \left(x_2(t) - \dot{y}_{d1}(t)\right) \tag{4.6}$$

$$s_{DB2}(t) = c_{DB2}\left(x_3(t) - y_{d2}(t)\right) + \left(x_4(t) - \dot{y}_{d2}(t)\right) \tag{4.7}$$

and the virtual sliding surface can be considered as

$$s_{DB}(t) = c_{DB2}\left(x_3(t) - y_{d2}(t) - z_{DB}(t)\right) + \left(x_4(t) - \dot{y}_{d2}(t)\right) \tag{4.8}$$

where

$$z_{DB}(t) = sat\left(\frac{s_{DB1}(t)}{\Delta_{DBz}}\right) z_{DBu}, \qquad 0 < z_{DBu} < 1. \tag{4.9}$$

Hence the control law for the decoupled backstepping sliding mode controller for the inverted pendulum on a cart can be defined as

$$\begin{aligned} u_{DB}(t) = & \frac{1}{g_2(x)}\left[-\delta_2 f_2(x) - \left(x_3(t) - y_{d2}(t)\right) - c_{DB2}\left(x_4(t) - \dot{y}_{d2}(t)\right)\right] \\ & + \frac{1}{g_2(x)}\left(\ddot{y}_{d2}(t) - c_{DB3} s_{DB}(t) - C_{DB}\,\mathrm{sign}(s_{DB}(t))\right). \end{aligned} \tag{4.10}$$

where $C_{DB} > \xi_{2\max} \geq \left|\xi_2(t)\right|$,

$$f_2(x) = \frac{\mu x_2 \cos(x_3) + \vartheta \sin(x_3) + \sigma x_4 + \rho \cos(x_3)\sin(x_3) {x_4}^2}{\psi + \rho \cos^2(x_3)}$$

and

$$g_2(x) = \frac{\varsigma \cos(x_3)}{\psi + \rho \cos^2(x_3)}$$

with

$$\mu = -ml\left(b + \left(\frac{n_1}{r}\right)\left(\frac{n_2}{r}\right)\left(\frac{K_b K_t}{R}\right)\right),$$

$$\vartheta = (M+m)mgl,$$

$$\rho = -m^2 l^2,$$

$$\sigma = -(M+m)d\ ,$$

$$\varsigma = ml\left(\left(\frac{n_1}{r}\right)\left(\frac{K_t}{R}\right)\right),$$

and,

$$\psi = \left(J_p + ml^2\right)\left(M+m\right).$$

The decoupled backstepping sliding mode controller for the inverted pendulum on a cart in Equation (4.10) can be rewritten using the saturation function to avoid the chattering as

$$\begin{aligned} u_{DB}(t) = \frac{1}{g_2(x)}\Big[-\delta_2 f_2(x) - \left(x_3(t) - y_{d2}(t)\right) - c_{DB2}\left(x_4(t) - \dot{y}_{d2}(t)\right)\Big] \\ + \frac{1}{g_2(x)}\left(\ddot{y}_{d2}(t) - c_{DB3}s_{DB}(t) - C_{DB}\,\mathrm{sat}\left(s_{DB}(t)/\Delta_{DBs}\right)\right). \end{aligned} \tag{4.11}$$

4.2. Simulation Results

The simulation setup, simulation results, and comparison results are presented in the following subsections.

4.2.1. Simulation Setup

The inverted pendulum on a cart system model described in Equation (2.59) is simulated using MATLAB and Simulink software. The inverted pendulum and DC motor parameters used in simulations are given in Table 4.1 and Table 4.2 respectively. The decoupled sliding mode controller introduced in Equation (4.5) and the decoupled backstepping sliding mode controller introduced in Equation (4.11) are modeled to control simulated system. Block diagrams of the

decoupled sliding mode controller and the decoupled backstepping sliding mode controller are shown in Figure 4.1 and Figure 4.2, respectively. Also, the controller parameters chosen by trial and error are given in Table 4.3. For all simulations, simulation time and step size are chosen as *T=10 sec* and *h=0.001 sec*, respectively.

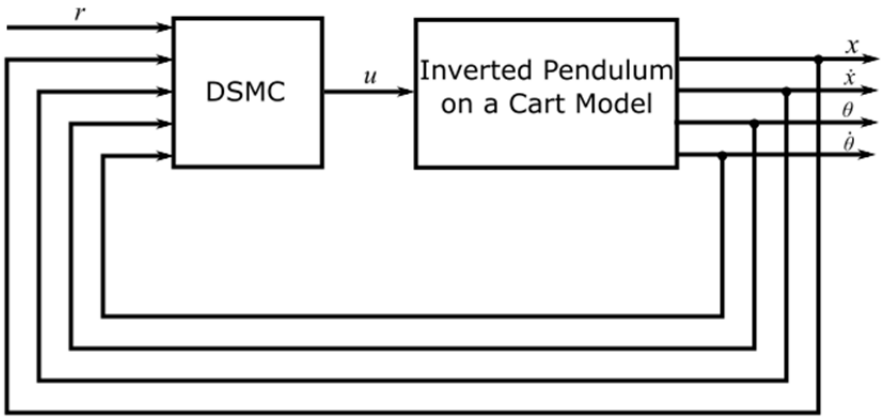

Figure 4.1. Block diagram of the decoupled sliding mode controller simulation

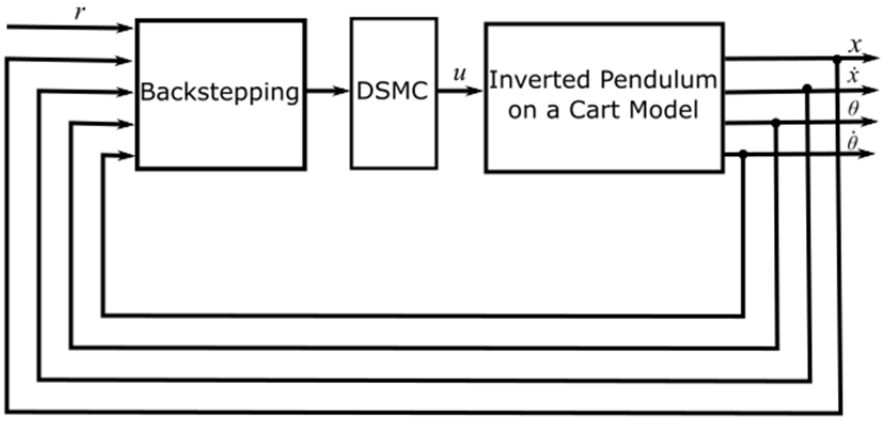

Figure 4.2. Block diagram of the decoupled backstepping sliding mode controller simulation

Table 4.1. Parameters of the inverted pendulum on a cart system (Feedback Instruments, 2006)

Parameter	Value
m	0.2 kg
l	0.3 m
M	2.3 kg
g	9.81 m/s^2
J_p	0.009 kgm^2
b	0.005 Ns/m
d	0.0005 Nms/rad

Table 4.2. Parameters of the DC motor (Feedback Instruments, 2006)

Parameter	Value
R	2.5 Ω
r	0.0314 m
K_t	0.05
K_b	0.05
n_1	18.84
n_2	0.986

Table 4.3. Parameters of the controllers

Parameter	Value
k_{DS1} , c_{DB1}	1
k_{DS2} , c_{DB2}	40
c_{DB3}	10
K_{DS} , C_{DB}	30
z_{DSu} , z_{DBu}	0.97
Δ_{DSz} , Δ_{DBz}	5
Δ_{DSs} , Δ_{DBs}	6

4.2.2. The DSMC Simulation Results

This simulation is carried out to investigate the stability and the performance of the decoupled sliding mode controller for the inverted pendulum on a cart system with parametric uncertainty $\delta_2 = 1$. The goals of this simulation are to show the changes on the position of the cart x, pendulum angel θ, and the control signal u based on initial conditions of $\begin{bmatrix} x_0 & \dot{x}_0 & \theta_0 & \dot{\theta}_0 \end{bmatrix}$ and the reference signal r.

In this simulation test, for reference signal $r = 0.1$ and initial conditions $\begin{bmatrix} x_0 & \dot{x}_0 & \theta_0 & \dot{\theta}_0 \end{bmatrix} = \begin{bmatrix} 0 & 0 & 0.1 & 0 \end{bmatrix}$, cart position, pendulum angel, and the control signal are plotted and shown in Figure 4.3, Figure 4.4, and Figure 4.5, respectively.

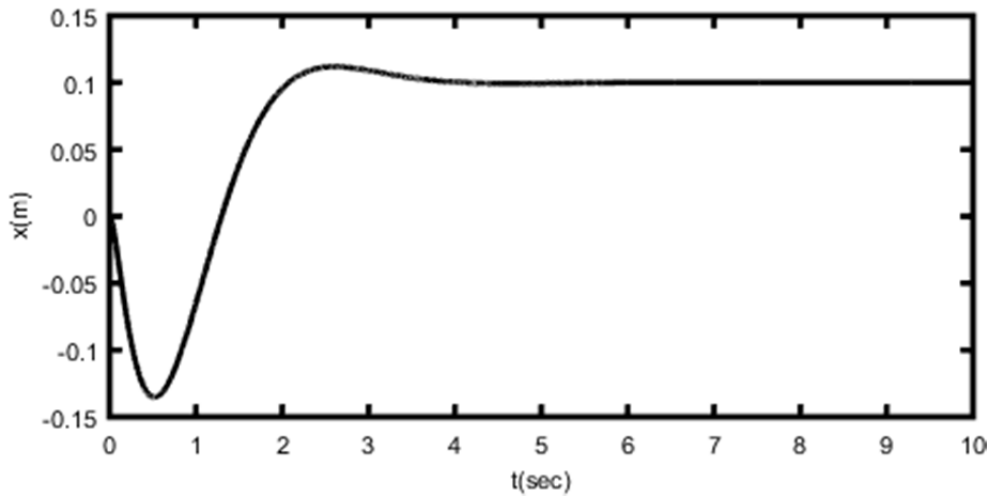

Figure 4.3. Cart position x for $r = 0.1$ and $\begin{bmatrix} x_0 & \dot{x}_0 & \theta_0 & \dot{\theta}_0 \end{bmatrix} = \begin{bmatrix} 0 & 0 & 0.1 & 0 \end{bmatrix}$ on the DSMC simulation

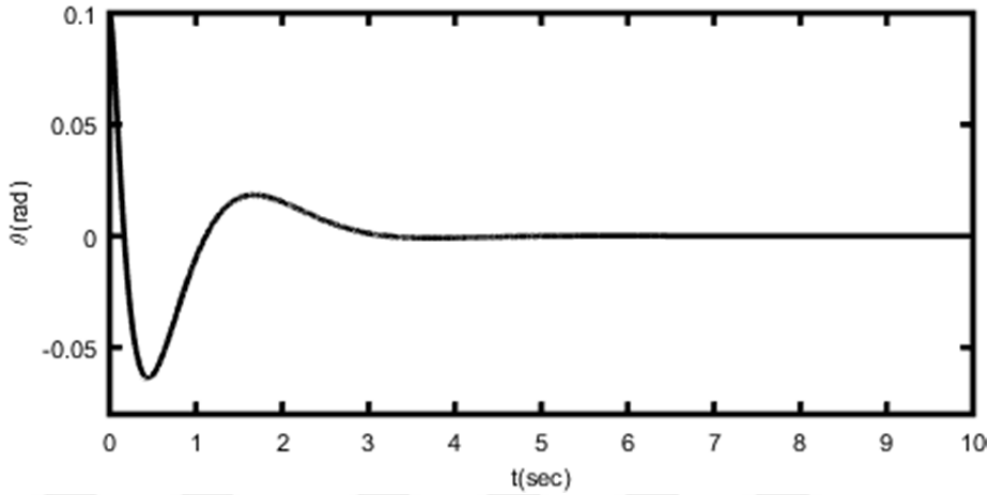

Figure 4.4. Pendulum angle θ for $r = 0.1$ and $\begin{bmatrix} x_0 & \dot{x}_0 & \theta_0 & \dot{\theta}_0 \end{bmatrix} = \begin{bmatrix} 0 & 0 & 0.1 & 0 \end{bmatrix}$ on the DSMC simulation

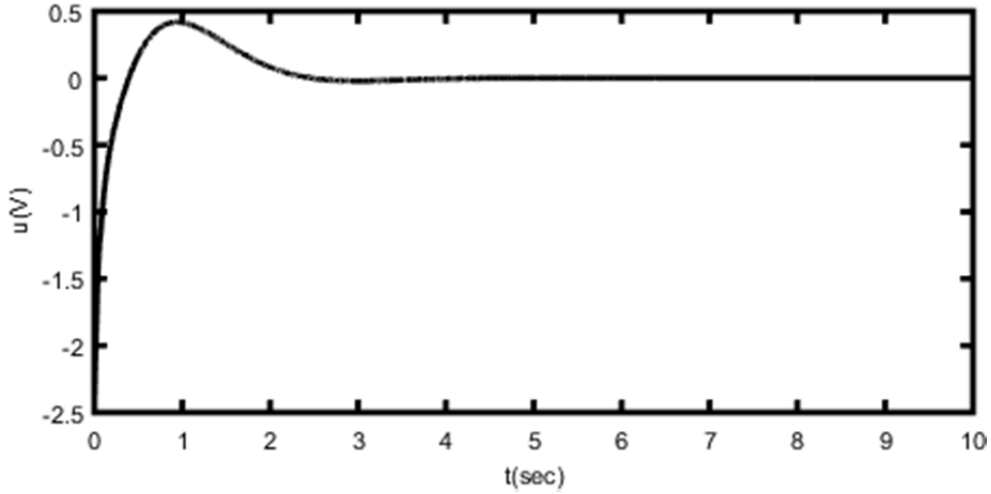

Figure 4.5. Control signal u for $r = 0.1$ and $\begin{bmatrix} x_0 & \dot{x}_0 & \theta_0 & \dot{\theta}_0 \end{bmatrix} = \begin{bmatrix} 0 & 0 & 0.1 & 0 \end{bmatrix}$ on the DSMC simulation

The decoupled sliding mode controller managed to keep the pendulum in upright position ($\theta = 0$ *rad*), while bringing the cart from the initial position *0 m* to desired position *0.1 m* as shown in Figure 4.3. The settling time of the position is 3.3885 *sec* with 11.81 percent overshoot and 135.18 percent undershoot.

The pendulum angle came to -0.065 *rad* from the initial position and then move to 0.02 *rad* in about 1.7 *sec*, after that it has settled to desired position 0 *rad* in 2.8932 *sec* as shown in Figure 4.4.

The control signal *u* started from -2.5 *V* and came to 0.4 *V* in about 1 *sec* then it has reached 0 *V* in about 3 *sec* as shown in Figure 4.5. Also, it met the physical constraint which the control signal must be in the range of -2.5 *V* and +2.5 *V*.

The main objective of the controller is to force the system trajectory to zero in a finite time and keep them at that point. Considering the errors $e_1(t)$ for the position and $e_2(t)$ for the pendulum angle, the errors versus their first-time derivatives are illustrated for position and angle in Figure 4.6 and Figure 4.7, respectively.

Since the sliding surfaces of the decoupled sliding mode controller are based on the error and its time derivative, it is expected that the sliding surfaces also converges to the zero. Considering the first sliding surface as s_1, the value derived from s_1 as z and the second sliding surface as s_2; the sliding surfaces of the controller versus time are shown in Figure 4.8, Figure 4.9, and Figure 4.10 for s_1, z, and s_2, respectively.

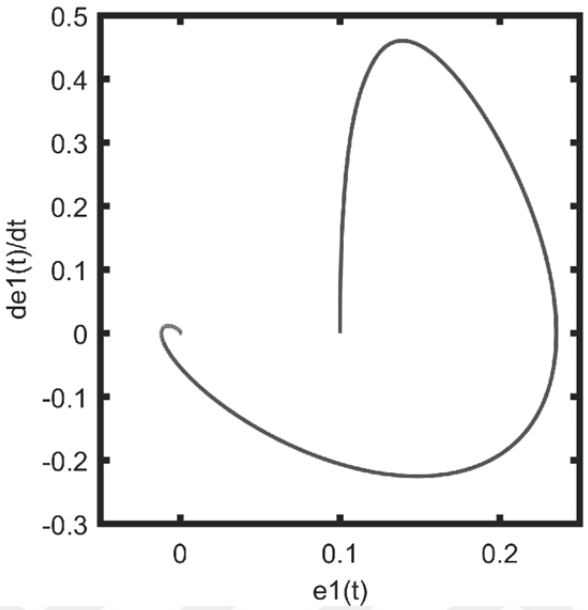

Figure 4.6. Motion of system trajectories for position on the DSMC simulation

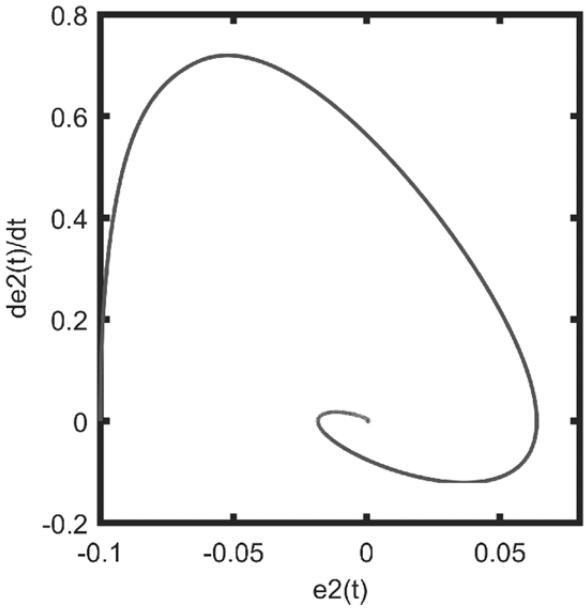

Figure 4.7. Motion of system trajectories for pendulum angle on the DSMC simulation

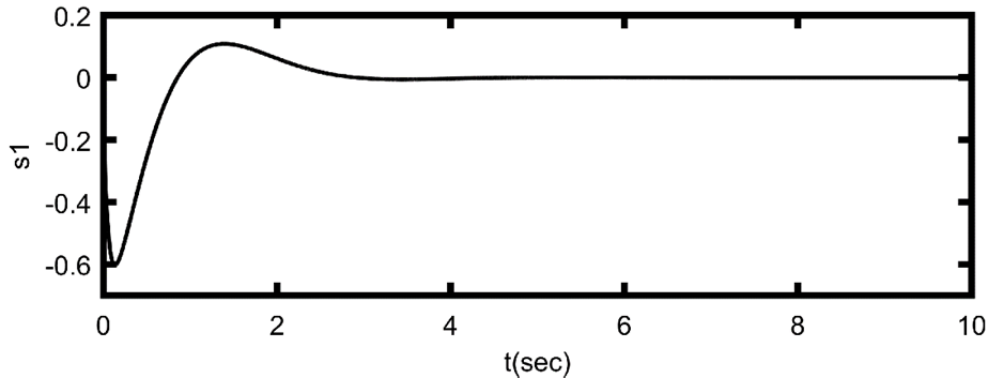

Figure 4.8. Motion of the first sliding surface on the DSMC simulation

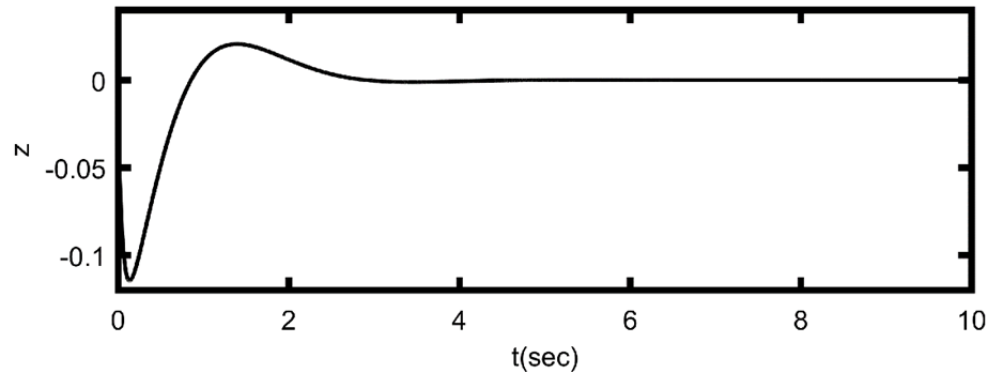

Figure 4.9. Motion of the *z* on the DSMC simulation

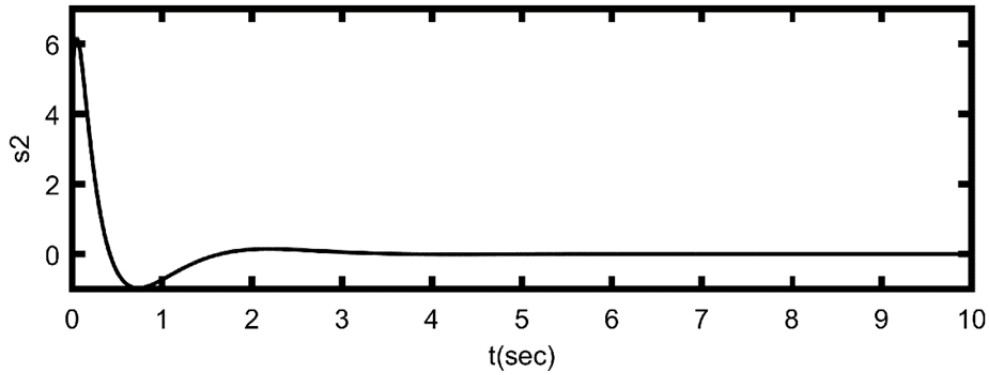

Figure 4.10. Motion of the second sliding surface on the DSMC simulation

4.2.3. The DBSMC Simulation Results

This simulation is carried out to investigate the stability and the performance of the proposed decoupled backstepping sliding mode controller for the inverted pendulum on a cart system with parametric uncertainty $\delta_2 = 1$. The goals of this simulation are to show the changes on the position of the cart x, pendulum angel θ, and the control signal u based on initial conditions of $\begin{bmatrix} x_0 & \dot{x}_0 & \theta_0 & \dot{\theta}_0 \end{bmatrix}$ and the reference signal r.

In this simulation test, for reference signal $r = 0.1$ and initial conditions $\begin{bmatrix} x_0 & \dot{x}_0 & \theta_0 & \dot{\theta}_0 \end{bmatrix} = \begin{bmatrix} 0 & 0 & 0.1 & 0 \end{bmatrix}$, cart position, pendulum angel, and the control signal are plotted and shown in Figure 4.11, Figure 4.12, and Figure 4.13, respectively.

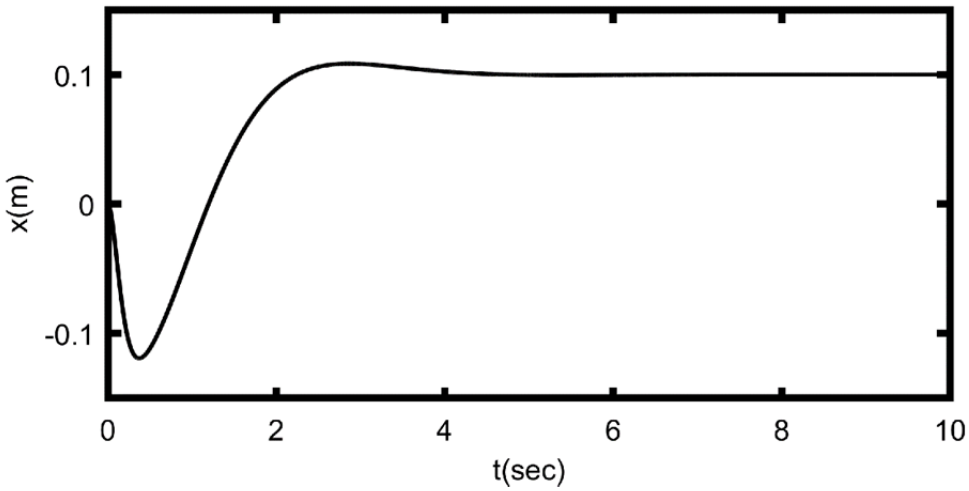

Figure 4.11. Cart position x for $r = 0.1$ and $\begin{bmatrix} x_0 & \dot{x}_0 & \theta_0 & \dot{\theta}_0 \end{bmatrix} = \begin{bmatrix} 0 & 0 & 0.1 & 0 \end{bmatrix}$ on the DBSMC simulation

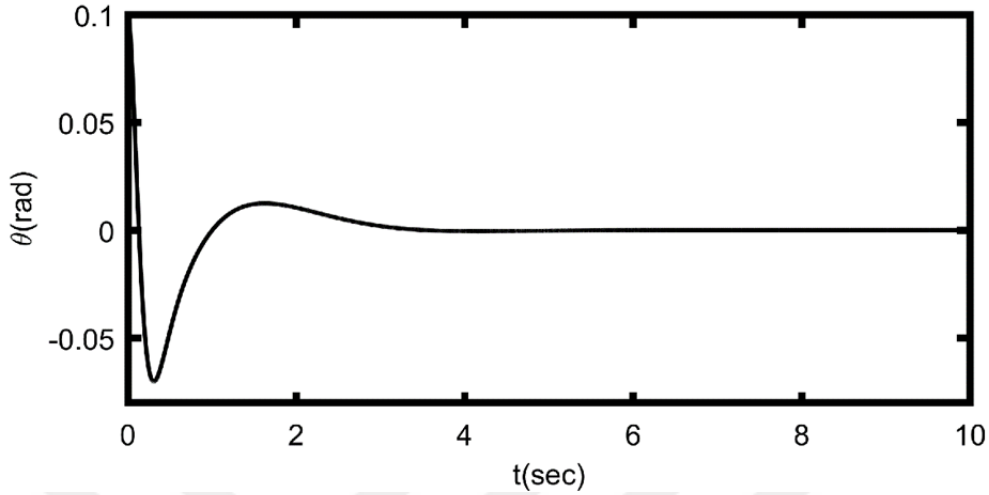

Figure 4.12. Pendulum angle θ for $r = 0.1$ and $\begin{bmatrix} x_0 & \dot{x}_0 & \theta_0 & \dot{\theta}_0 \end{bmatrix} = \begin{bmatrix} 0 & 0 & 0.1 & 0 \end{bmatrix}$ on the DBSMC simulation

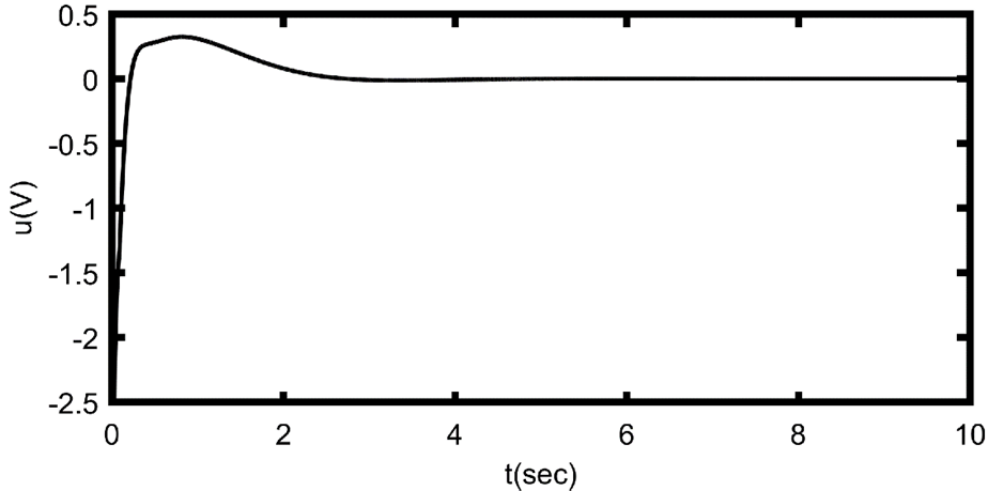

Figure 4.13. Control signal u for $r = 0.1$ and $\begin{bmatrix} x_0 & \dot{x}_0 & \theta_0 & \dot{\theta}_0 \end{bmatrix} = \begin{bmatrix} 0 & 0 & 0.1 & 0 \end{bmatrix}$ on the DBSMC simulation

The decoupled backstepping sliding mode controller managed to keep the pendulum in upright position ($\theta = 0$ *rad*), while bringing the cart from the initial position *0 m* to desired position *0.1 m* as shown in Figure 4.11. The settling time of

the position is 3.6533 *sec* with 8.50 percent overshoot and 119.53 percent undershoot.

The pendulum angle came to -0.07 *rad* from the initial position and then move to 0.01 *rad* in about 1.6 *sec*, after that it has settled to desired position 0 *rad* in 2.9832 *sec* as shown in Figure 4.12.

The control signal *u* started from -2.5 *V* and came to 0.3 *V* in about 1 *sec* then it has reached 0 *V* in about 3 *sec* as shown in Figure 4.13. Also, it met the physical constraint which the control signal must be in the range of -2.5 *V* and +2.5 *V*.

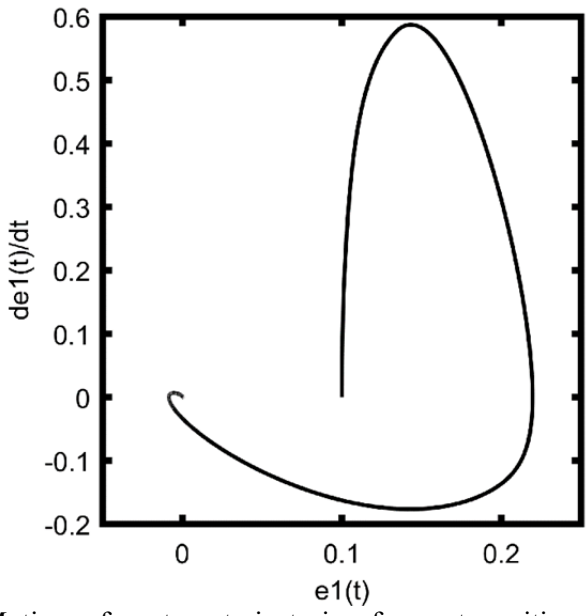

Figure 4.14. Motion of system trajectories for cart position on the DBSMC simulation

The main objective of the controller is to force the system trajectory to zero in a finite time and keep them at that point. Considering the errors $e_1(t)$ for the position and $e_2(t)$ for the pendulum angle, the errors versus their first-time

derivatives are illustrated for position and angle in Figure 4.14 and Figure 4.15, respectively.

Since the sliding surfaces of the decoupled backstepping sliding mode controller are based on the error and its time derivative, it is expected that the sliding surfaces also converges to the zero. Considering the first sliding surface as s_1, the value derived from s_1 as z and the second sliding surface as s_2; the sliding surfaces of the controller versus time are shown in Figure 4.16, Figure 4.17, and Figure 4.18 for s_1, z, and s_2, respectively.

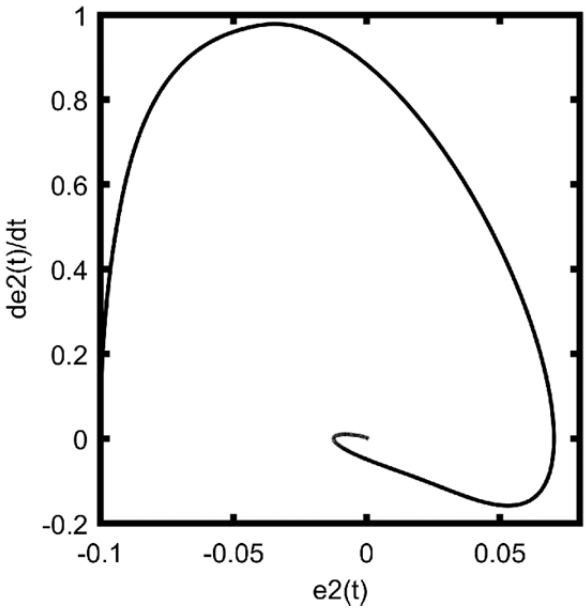

Figure 4.15. Motion of system trajectories for pendulum angle on the DBSMC simulation

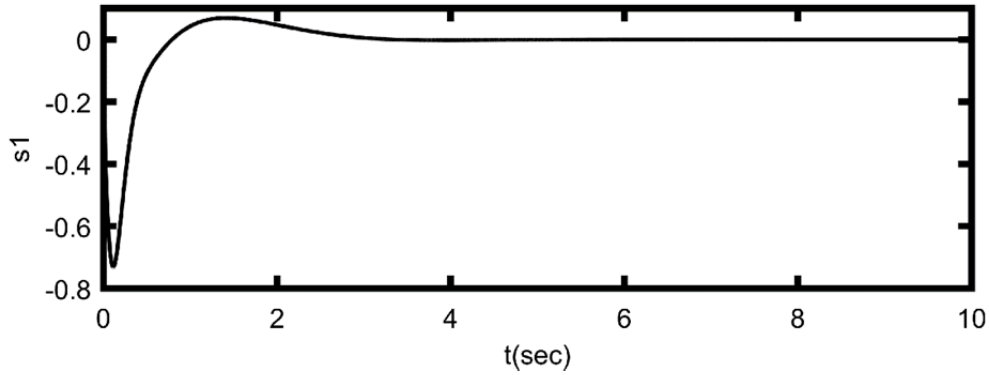

Figure 4.16. Motion of the first sliding surface on the DBSMC simulation

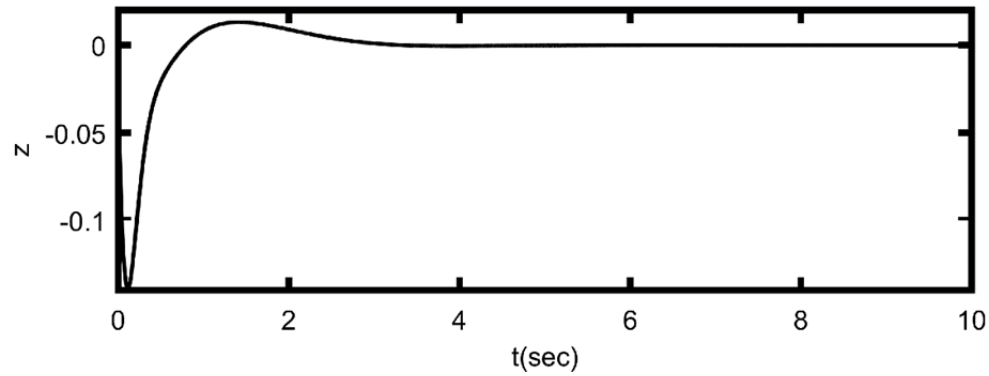

Figure 4.17. Motion of the *z* on the DBSMC simulation

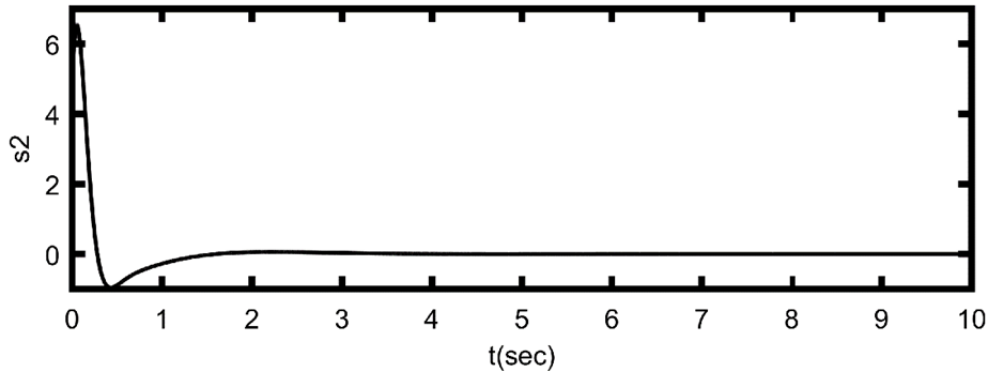

Figure 4.18. Motion of the second sliding surface on the DBSMC simulation

4.2.4. Comparison Results for Simulation

The DSMC and the proposed DBSMC methods are compared in four different simulation tests to investigate their performance on the inverted pendulum on a cart system.

In the first test, for reference signal $r = 0.3$ and initial conditions $\begin{bmatrix} x_0 & \dot{x}_0 & \theta_0 & \dot{\theta}_0 \end{bmatrix} = \begin{bmatrix} 0 & 0 & 0.1 & 0 \end{bmatrix}$ with parametric uncertainty $\delta_2 = 1$, cart position x, pendulum angel θ, and the control signal u for both DSMC and DBSMC are plotted and shown in Figure 4.19, Figure 4.20, and Figure 4.21, respectively.

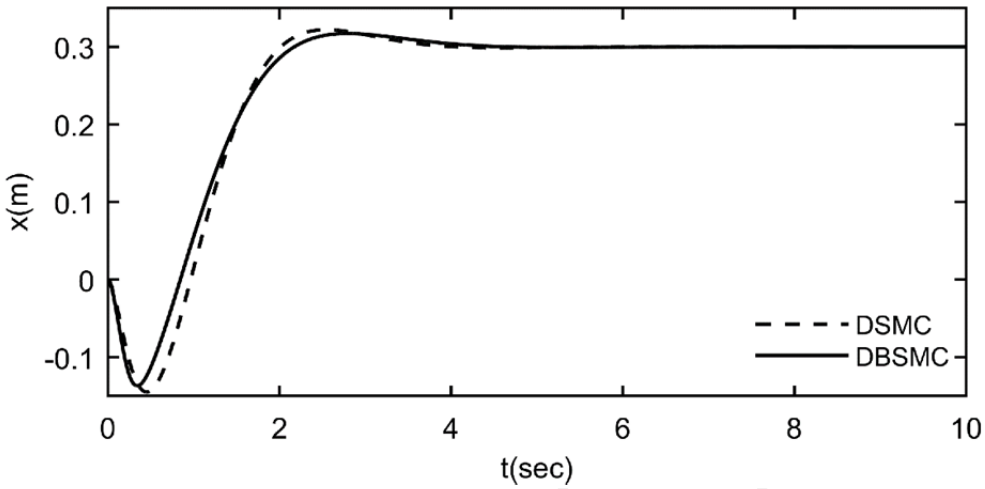

Figure 4.19. Cart position x for $r = 0.3$ and $\begin{bmatrix} x_0 & \dot{x}_0 & \theta_0 & \dot{\theta}_0 \end{bmatrix} = \begin{bmatrix} 0 & 0 & 0.1 & 0 \end{bmatrix}$ with $\delta_2 = 1$ on comparison simulation

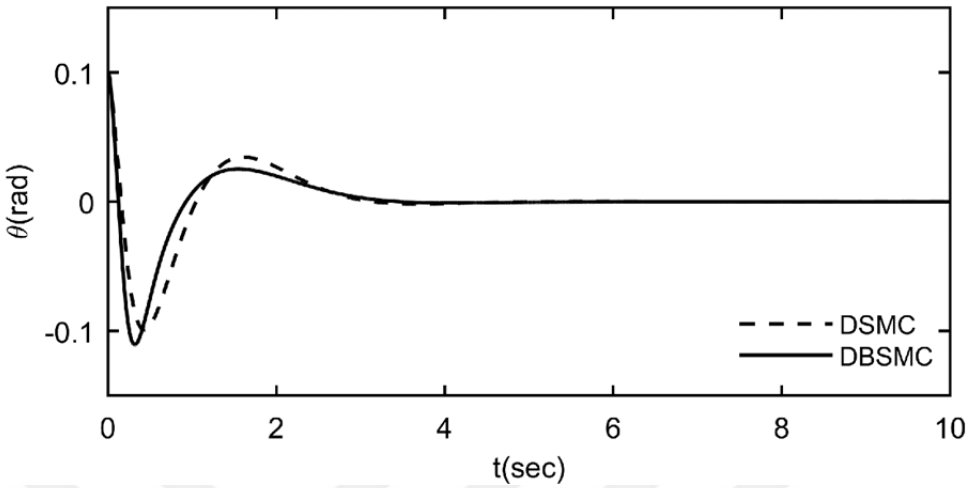

Figure 4.20. Pendulum angle θ for $r = 0.3$ and $\begin{bmatrix} x_0 & \dot{x}_0 & \theta_0 & \dot{\theta}_0 \end{bmatrix} = \begin{bmatrix} 0 & 0 & 0.1 & 0 \end{bmatrix}$ with $\delta_2 = 1$ on comparison simulation

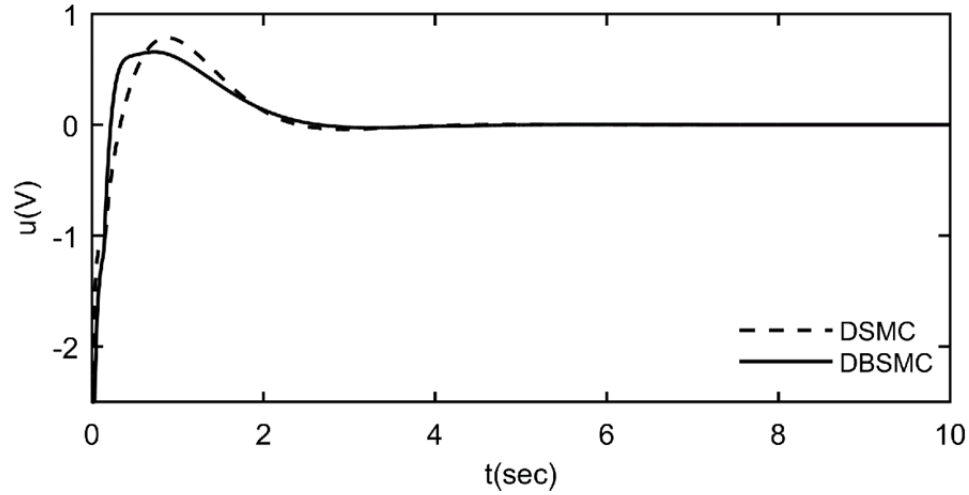

Figure 4.21. Control signal u for $r = 0.3$ and $\begin{bmatrix} x_0 & \dot{x}_0 & \theta_0 & \dot{\theta}_0 \end{bmatrix} = \begin{bmatrix} 0 & 0 & 0.1 & 0 \end{bmatrix}$ with $\delta_2 = 1$ on comparison simulation

Although the DSMC has a slightly faster settling time than the DBSMC, the proposed method decreases overshoot and undershoot as shown in Figure 4.19. The settling time on the position for DSMC is 3.3246 *sec* with 7.38 percent

overshoot and 48.36 percent undershoot and the settling time on the position for DBSMC is 3.4929 *sec* with 5.75 percent overshoot and 45.71 percent undershoot. Both the DSMC and DBSMC manage to bring the pendulum upright position in 2.9 *sec* as shown in Figure 4.20. The control signal u started from -2.5 V on both controllers then settled 0 in 2.2 sec on DSMC and, 2.3 sec on DBSMC, however, the DBSMC created a smoother control signal than DSMC as shown in Figure 4.21.

The performance of the controllers can also be measured by the performance indices which use the tracking error with the evaluation time, generally. Some of the error-based performance indices are formulated as follows:

Integral Absolute Error (IAE):

$$\int_0^T |e(t)| dt \tag{4.12}$$

Integral Squared Error (ISE):

$$\int_0^T e^2(t) dt \tag{4.13}$$

Integral Time Absolute Error (ITAE):

$$\int_0^T t|e(t)| dt \tag{4.14}$$

Integral Time Squared Error (ITSE):

$$\int_0^T te^2(t) dt \,. \tag{4.15}$$

The performances of the DSMC and the DBSMC based on performance indices for reference signal $r = 0.3$ and initial conditions $\begin{bmatrix} x_0 & \dot{x}_0 & \theta_0 & \dot{\theta}_0 \end{bmatrix} = \begin{bmatrix} 0 & 0 & 0.1 & 0 \end{bmatrix}$ with parametric uncertainty $\delta_2 = 1$ are given in Table 4.4 and Table 4.5.

Table 4.4. DSMC and DBSMC simulation performance indices for $r = 0.3$ and $\begin{bmatrix} x_0 & \dot{x}_0 & \theta_0 & \dot{\theta}_0 \end{bmatrix} = \begin{bmatrix} 0 & 0 & 0.1 & 0 \end{bmatrix}$ with $\delta_2 = 1$

	IAE		**ISE**	
Tracking Error	**DSMC**	**DBSMC**	**DSMC**	**DBSMC**
Cart Position	523.65	495.18	170.78	151.64
Pendulum Angle	101.01	86.92	5.58	4.8
Control Signal	1189.02	1178.91	865.43	941.61

Table 4.5. DSMC and DBSMC simulation performance indices for $r = 0.3$ and $\begin{bmatrix} x_0 & \dot{x}_0 & \theta_0 & \dot{\theta}_0 \end{bmatrix} = \begin{bmatrix} 0 & 0 & 0.1 & 0 \end{bmatrix}$ with $\delta_2 = 1$

	ITAE		**ITSE**	
Tracking Error	**DSMC**	**DBSMC**	**DSMC**	**DBSMC**
Cart Position	410467	391571	99313	82496
Pendulum Angle	105322	85305	3692	2466
Control Signal	1122332	1020884	539543	416449

The magnitudes of the performance indices are generally smaller in the DBSMC rather than the DSMC as shown in Table 4.4 and Table 4.5. Consequently, the DBSMC produced a more accurate control input than the DSMC.

In the second test, the initial condition of the pendulum angle is started from 0.3 *rad* to create a more challenging control problem. In this test, for

reference signal $r = 0.3$ and initial conditions $\begin{bmatrix} x_0 & \dot{x}_0 & \theta_0 & \dot{\theta}_0 \end{bmatrix} = \begin{bmatrix} 0 & 0 & 0.3 & 0 \end{bmatrix}$ with parametric uncertainty $\delta_2 = 1$, cart position x, pendulum angel θ, and the control signal u for both DSMC and DBSMC are plotted and shown in Figure 4.22, Figure 4.23, and Figure 4.24, respectively.

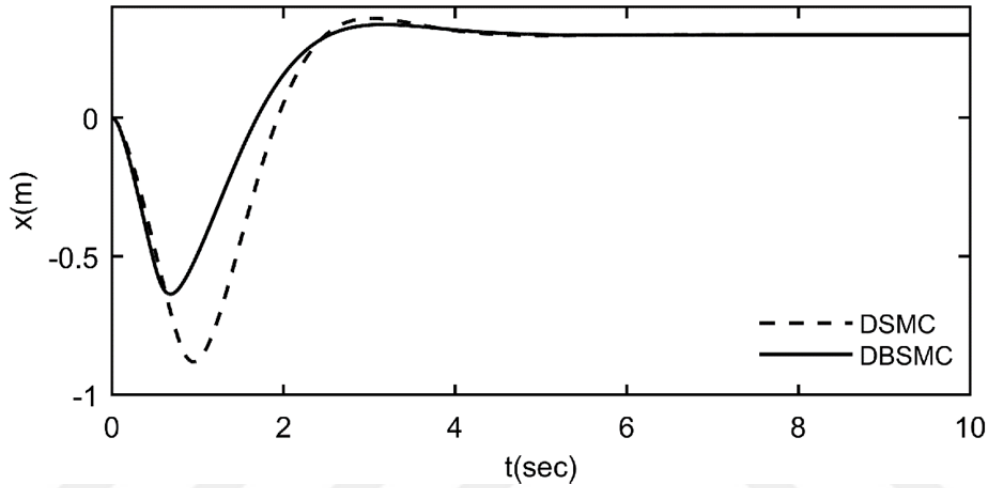

Figure 4.22. Cart position x for $r = 0.3$ and $\begin{bmatrix} x_0 & \dot{x}_0 & \theta_0 & \dot{\theta}_0 \end{bmatrix} = \begin{bmatrix} 0 & 0 & 0.3 & 0 \end{bmatrix}$ with $\delta_2 = 1$ on comparison simulation

Although the DSMC is 0.1 *sec* faster on settling time than the DBSMC, the proposed method decreases overshoot and undershoot as shown in Figure 4.22. The settling time on the position for DSMC is 3.8056 *sec* with 19.63 percent overshoot and 293.77 percent undershoot and the settling time on the position for DBSMC is 3.9531 *sec* with 12.14 percent overshoot and 212.32 percent undershoot. Both the DSMC and DBSMC manage to bring the pendulum upright position in 3.4 *sec* as shown in Figure 4.23. The control signal *u* started from -2.5 *V* on both controllers then settled 0 in 4.12 *sec* on DSMC and, 3.88 *sec* on DBSMC. The DBSMC created a smoother control signal than DSMC as shown in Figure 4.24.

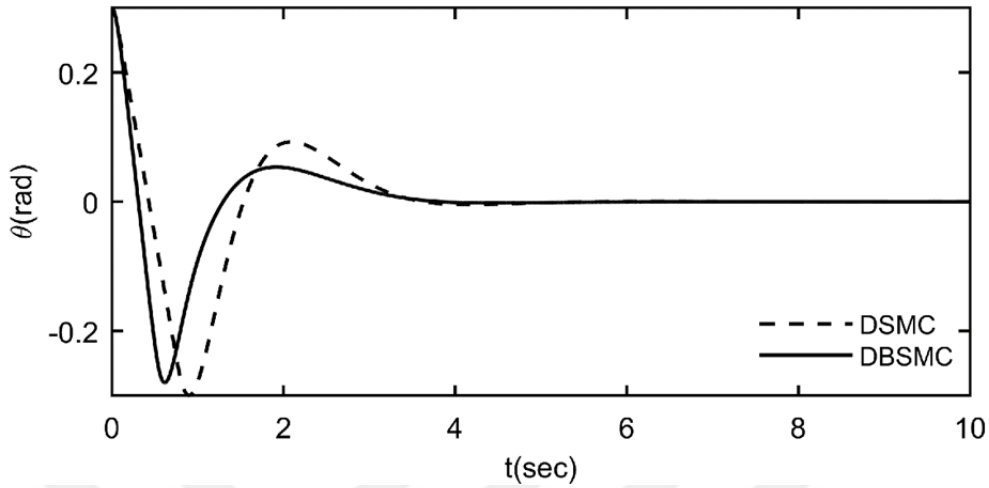

Figure 4.23. Pendulum angle θ for $r = 0.3$ and $\begin{bmatrix} x_0 & \dot{x}_0 & \theta_0 & \dot{\theta}_0 \end{bmatrix} = \begin{bmatrix} 0 & 0 & 0.3 & 0 \end{bmatrix}$ with $\delta_2 = 1$ on comparison simulation

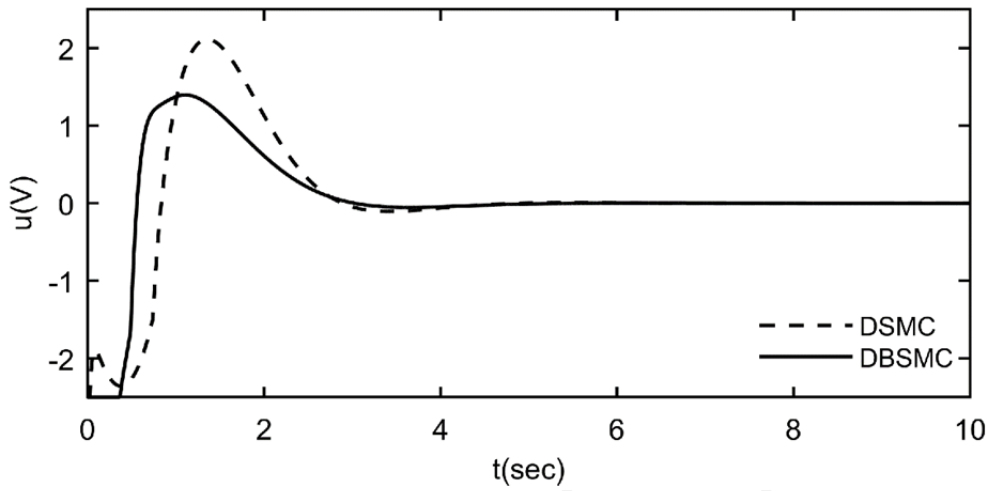

Figure 4.24. Control signal u for $r = 0.3$ and $\begin{bmatrix} x_0 & \dot{x}_0 & \theta_0 & \dot{\theta}_0 \end{bmatrix} = \begin{bmatrix} 0 & 0 & 0.3 & 0 \end{bmatrix}$ with $\delta_2 = 1$ on comparison simulation

The performances of the DSMC and the DBSMC based on performance indices for reference signal $r = 0.3$ and initial conditions

$\begin{bmatrix} x_0 & \dot{x}_0 & \theta_0 & \dot{\theta}_0 \end{bmatrix} = \begin{bmatrix} 0 & 0 & 0.3 & 0 \end{bmatrix}$ with parametric uncertainty $\delta_2 = 1$ on comparison simulation are given in Table 4.6 and Table 4.7.

Table 4.6. DSMC and DBSMC simulation performance indices for $r = 0.3$ and $\begin{bmatrix} x_0 & \dot{x}_0 & \theta_0 & \dot{\theta}_0 \end{bmatrix} = \begin{bmatrix} 0 & 0 & 0.3 & 0 \end{bmatrix}$ with $\delta_2 = 1$

	IAE		**ISE**	
Tracking Error	**DSMC**	**DBSMC**	**DSMC**	**DBSMC**
Cart Position	1622.30	1228.88	1322.05	783.19
Pendulum Angle	357.83	262.994	61.78	42.0811
Control Signal	4049.38	3116.48	7080.96	4814.25

Table 4.7. DSMC and DBSMC simulation performance indices for $r = 0.3$ and $\begin{bmatrix} x_0 & \dot{x}_0 & \theta_0 & \dot{\theta}_0 \end{bmatrix} = \begin{bmatrix} 0 & 0 & 0.3 & 0 \end{bmatrix}$ with $\delta_2 = 1$

	ITAE		**ITSE**	
Tracking Error	**DSMC**	**DBSMC**	**DSMC**	**DBSMC**
Cart Position	1827784	1258751	1321328	652371
Pendulum Angle	440350	268507	54715	25127
Control Signal	4694616	3117558	6683092	3119900

The magnitudes of all performance indices are smaller in the DBSMC rather than the DSMC as shown in Table 4.6 and Table 4.7. Consequently, the DBSMC produced a more accurate control input than the DSMC.

In the third test, for reference signal $r = 0.3$ and initial conditions $\begin{bmatrix} x_0 & \dot{x}_0 & \theta_0 & \dot{\theta}_0 \end{bmatrix} = \begin{bmatrix} 0 & 0 & 0.1 & 0 \end{bmatrix}$ with parametric uncertainties parametric uncertainty $\delta_2 = 0.8$, cart position, pendulum angel, and the control signal for both DSMC and DBSMC are plotted and shown in Figure 4.25, Figure 4.26, and Figure 4.27, respectively.

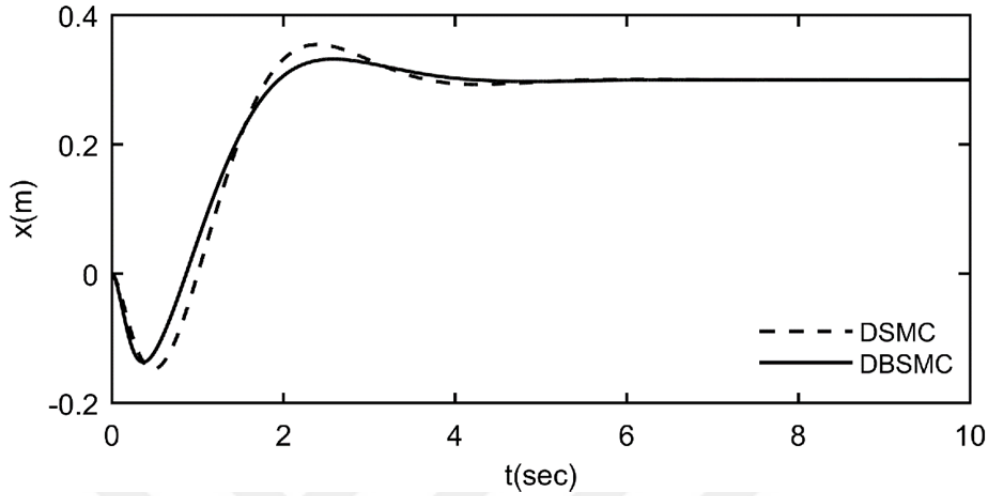

Figure 4.25. Cart position x for $r = 0.3$ and $\begin{bmatrix} x_0 & \dot{x}_0 & \theta_0 & \dot{\theta}_0 \end{bmatrix} = \begin{bmatrix} 0 & 0 & 0.1 & 0 \end{bmatrix}$ with $\delta_2 = 0.8$ on comparison simulation

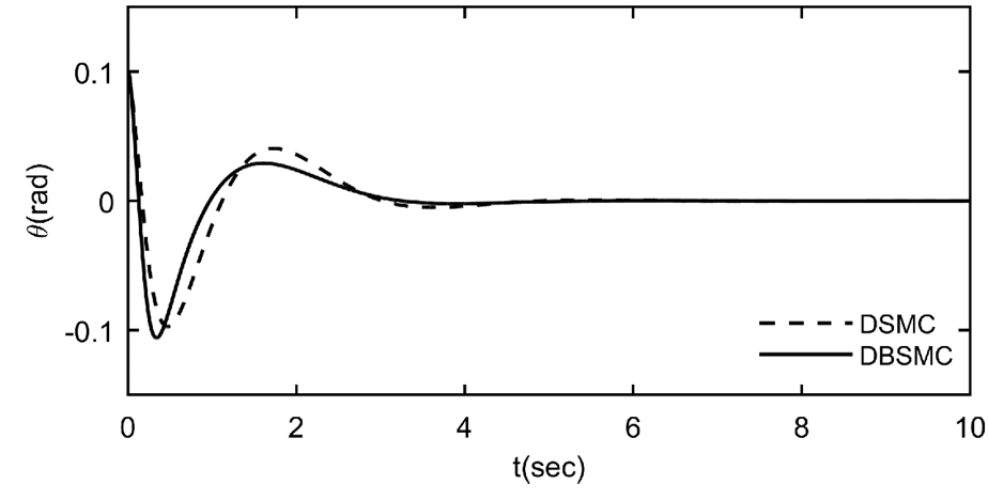

Figure 4.26. Pendulum angle θ for $r = 0.3$ and $\begin{bmatrix} x_0 & \dot{x}_0 & \theta_0 & \dot{\theta}_0 \end{bmatrix} = \begin{bmatrix} 0 & 0 & 0.1 & 0 \end{bmatrix}$ with $\delta_2 = 0.8$ on comparison simulation

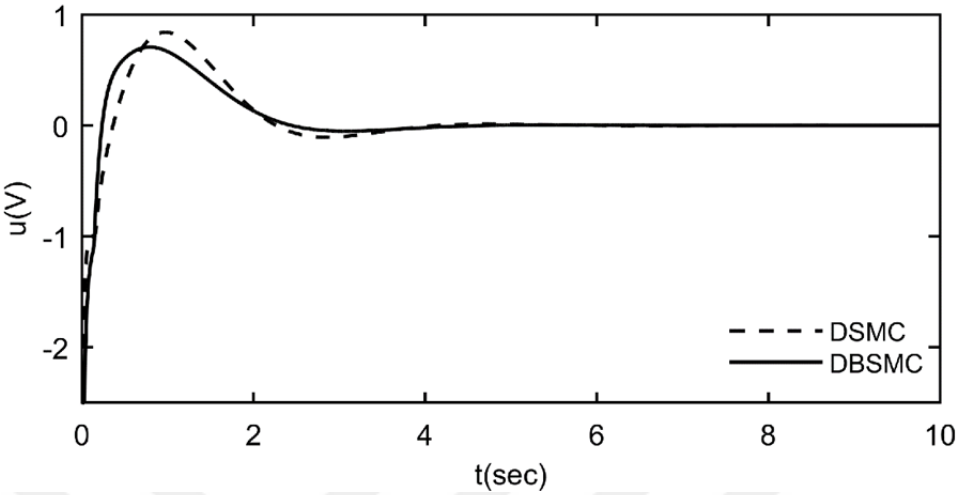

Figure 4.27. Control signal u for $r = 0.3$ and $\begin{bmatrix} x_0 & \dot{x}_0 & \theta_0 & \dot{\theta}_0 \end{bmatrix} = \begin{bmatrix} 0 & 0 & 0.1 & 0 \end{bmatrix}$ with $\delta_2 = 0.8$ on comparison simulation

Although the DSMC has 0.2 *sec* faster settling time than the DBSMC, the proposed method decreases overshoot and undershoot as shown in Figure 4.25. The settling time on the position for DSMC is 3.4210 *sec* with 18.25 percent overshoot and 49.22 percent undershoot and the settling time on the position for DBSMC is 3.6488 *sec* with 10.70 percent overshoot and 45.65 percent undershoot. The DBSMC manage to bring the pendulum upright position faster than the DSMC as shown in Figure 4.26. The settling time on the pendulum angle for DSMC is 4.3818 *sec* and the settling time on the pendulum angle for DBSMC is 3.0421 *sec.* The control signal *u* started from -2.5 *V* on both controllers then settled 0 in 3.5448 *sec* on DSMC and, 3.19 *sec* on DBSMC. The DBSMC created a smoother control signal than DSMC as shown in Figure 4.27.

The performances of the DSMC and the DBSMC based on performance indices for reference signal $r = 0.3$ and initial conditions $\begin{bmatrix} x_0 & \dot{x}_0 & \theta_0 & \dot{\theta}_0 \end{bmatrix} = \begin{bmatrix} 0 & 0 & 0.3 & 0 \end{bmatrix}$ with parametric uncertainty $\delta_2 = 0.8$ are given in Table 4.8 and Table 4.9.

Table 4.8. DSMC and DBSMC simulation performance indices for $r = 0.3$ and $\begin{bmatrix} x_0 & \dot{x}_0 & \theta_0 & \dot{\theta}_0 \end{bmatrix} = \begin{bmatrix} 0 & 0 & 0.1 & 0 \end{bmatrix}$ with $\delta_2 = 0.8$

	IAE		ISE	
Tracking Error	**DSMC**	**DBSMC**	**DSMC**	**DBSMC**
Cart Position	565	507	177	154
Pendulum Angle	115	94	6	5
Control Signal	1337	1225	939	947

Table 4.9. DSMC and DBSMC simulation performance indices for $r = 0.3$ and $\begin{bmatrix} x_0 & \dot{x}_0 & \theta_0 & \dot{\theta}_0 \end{bmatrix} = \begin{bmatrix} 0 & 0 & 0.1 & 0 \end{bmatrix}$ with $\delta_2 = 0.8$

	ITAE		ITSE	
Tracking Error	**DSMC**	**DBSMC**	**DSMC**	**DBSMC**
Cart Position	521808	429018	108547	84689
Pendulum Angle	141698	100820	4848	2962
Control Signal	1513456	1168022	691147	478374

The magnitudes of the performance indices are generally smaller in the DBSMC rather than the DSMC as shown in Table 4.8 and Table 4.9. Consequently, the DBSMC produced a more accurate control input than the DSMC.

In the last simulation test, for reference signal $r = 0.3$ and initial conditions $\begin{bmatrix} x_0 & \dot{x}_0 & \theta_0 & \dot{\theta}_0 \end{bmatrix} = \begin{bmatrix} 0 & 0 & 0.3 & 0 \end{bmatrix}$ with parametric uncertainty $\delta_2 = 0.8$, cart position, pendulum angel, and the control signal for both DSMC and DBSMC are plotted and shown in Figure 4.28, Figure 4.29, and Figure 4.30, respectively.

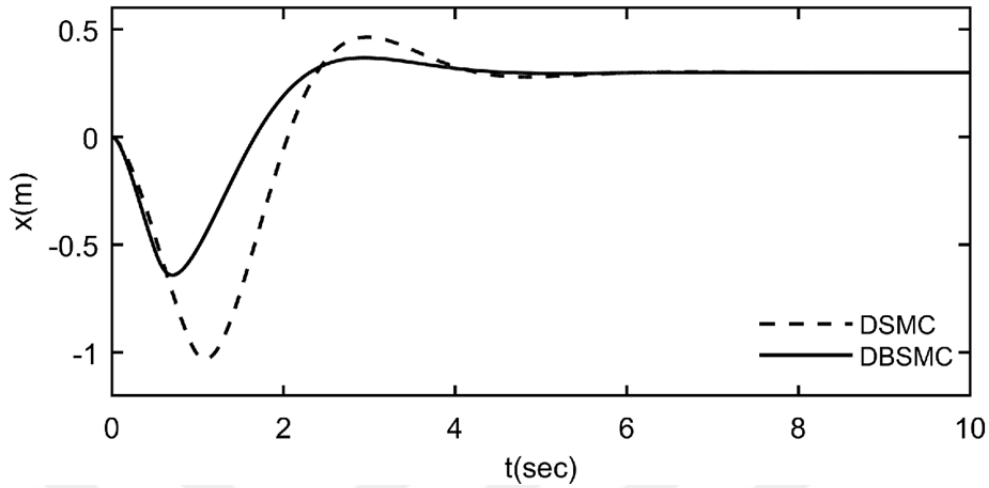

Figure 4.28. Cart position x for $r = 0.3$ and $\begin{bmatrix} x_0 & \dot{x}_0 & \theta_0 & \dot{\theta}_0 \end{bmatrix} = \begin{bmatrix} 0 & 0 & 0.3 & 0 \end{bmatrix}$ with $\delta_2 = 0.8$ on comparison simulation

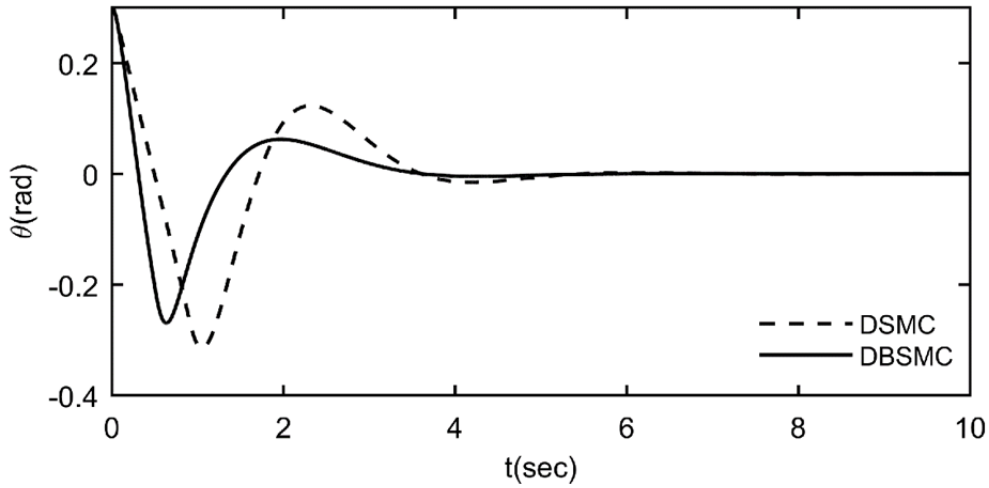

Figure 4.29. Pendulum angle θ for $r = 0.3$ and $\begin{bmatrix} x_0 & \dot{x}_0 & \theta_0 & \dot{\theta}_0 \end{bmatrix} = \begin{bmatrix} 0 & 0 & 0.3 & 0 \end{bmatrix}$ with $\delta_2 = 0.8$ on comparison simulation

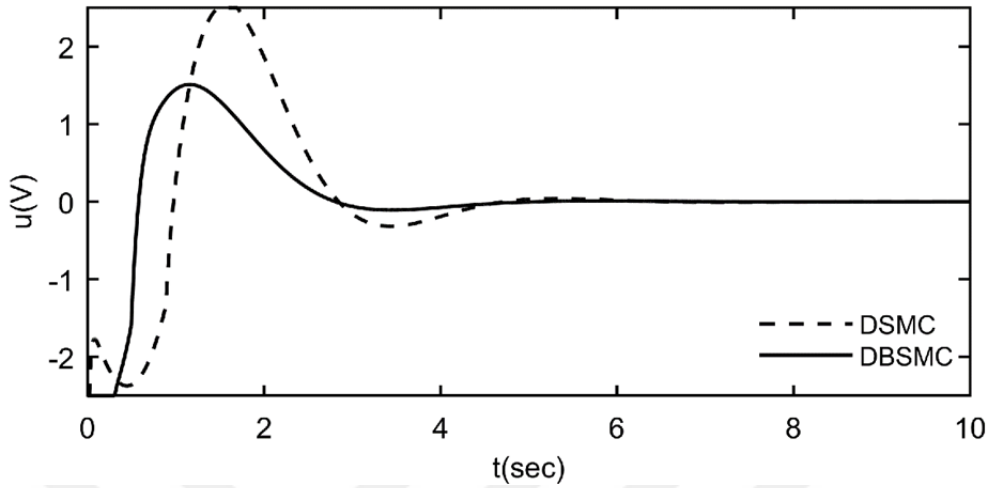

Figure 4.30. Control signal u for $r = 0.3$ and $\begin{bmatrix} x_0 & \dot{x}_0 & \theta_0 & \dot{\theta}_0 \end{bmatrix} = \begin{bmatrix} 0 & 0 & 0.3 & 0 \end{bmatrix}$ with $\delta_2 = 0.8$ on comparison simulation

Both the DSMC and DBSMC manage to bring the cart to the desired position in 4. *sec*, however, the proposed method decreases overshoot and undershoot as shown in Figure 4.28. The settling time on the position for DSMC is 4.00 *sec* with 54.77 percent overshoot and 343 percent undershoot and the settling time on the position for DBSMC is 4.00 *sec* with 22.73 percent overshoot and 213.63 percent undershoot.

The DBSMC manage to bring the pendulum upright position faster than the DSMC as shown in Figure 4.29. The settling time on the pendulum angle for DSMC is 4.94 *sec* and the settling time on the pendulum angle for DBSMC is 3.35 *sec.*

The control signal *u* started from -2.5 *V* on both controllers then settled 0 in 4.46 *sec* on DSMC and, 4.26 *sec* on DBSMC. The DBSMC created a smoother control signal than DSMC as shown in Figure 4.30.

The performances of the DSMC and the DBSMC based on performance indices for reference signal $r = 0.3$ and initial conditions

$\begin{bmatrix} x_0 & \dot{x}_0 & \theta_0 & \dot{\theta}_0 \end{bmatrix} = \begin{bmatrix} 0 & 0 & 0.3 & 0 \end{bmatrix}$ with parametric uncertainty $\delta_2 = 0.8$ are given in Table 4.10 and Table 4.11.

Table 4.10. DSMC and DBSMC simulation performance indices for $r = 0.3$ and $\begin{bmatrix} x_0 & \dot{x}_0 & \theta_0 & \dot{\theta}_0 \end{bmatrix} = \begin{bmatrix} 0 & 0 & 0.3 & 0 \end{bmatrix}$ with $\delta_2 = 0.8$

	IAE		ISE	
Tracking Error	**DSMC**	**DBSMC**	**DSMC**	**DBSMC**
Cart Position	1997	1254	1760	764
Pendulum Angle	439	280	77	43
Control Signal	5045	3238	9395	4966

Table 4.11. DSMC and DBSMC simulation performance indices for $r = 0.3$ and $\begin{bmatrix} x_0 & \dot{x}_0 & \theta_0 & \dot{\theta}_0 \end{bmatrix} = \begin{bmatrix} 0 & 0 & 0.3 & 0 \end{bmatrix}$ with $\delta_2 = 0.8$

	ITAE		ITSE	
Tracking Error	**DSMC**	**DBSMC**	**DSMC**	**DBSMC**
Cart Position	2655254	1346246	1965345	667655
Pendulum Angle	658715	308456	85345	28070
Control Signal	7125421	3480784	10907339	3487018

The magnitudes of all performance indices are smaller in the DBSMC rather than the DSMC as shown in Table 4.10 and Table 4.11. Consequently, the DBSMC produced a more accurate control input than the DSMC.

In the first simulation test, the conventional DSMC and the DBSMC methods compared for reference signal $r = 0.3$ and initial conditions $\begin{bmatrix} x_0 & \dot{x}_0 & \theta_0 & \dot{\theta}_0 \end{bmatrix} = \begin{bmatrix} 0 & 0 & 0.1 & 0 \end{bmatrix}$. After that to simulate a more challenging problem the DSMC and the DBSMC methods compared for reference signal $r = 0.3$ and initial conditions $\begin{bmatrix} x_0 & \dot{x}_0 & \theta_0 & \dot{\theta}_0 \end{bmatrix} = \begin{bmatrix} 0 & 0 & 0.3 & 0 \end{bmatrix}$. In these tests

simulated with parametric uncertainty $\delta_2 = 1$. In the third and fourth tests, first and second simulation tests are recreated with parametric uncertainty $\delta_2 = 0.8$. Overall, the simulation results have shown that the proposed DBSM method is more efficient than the conventional DSMC method.

4.3. Experimental Results

Satisfactory performance has obtained during the simulation tests, however, applying the proposed control method to a real plant will provide a clearer view about the performance. The experimental setup and results of experimental tests are presented in the following subsections.

4.3.1. Experimental Setup

Experiments have performed on Feedback's 33-200 digital pendulum mechanical unit which consists of a cart driven inverted pendulum and a belt with DC motor on adjustable feet as shown in Figure 4.31. The PC with PCI 1711 Advantech card serves as the main control unit. The control signal is transferred to the Digital Pendulum Controller (DPC), which drives the DC motor. The cart position and the pendulum angle encoder signals are transferred to the DPC and then to the PC.

In order to evaluate the performance of the proposed DBSMC, the DSMC and the DBSMC are applied to the inverted pendulum on a cart system having the parameters given in Table 4.1 and Table 4.2. Block diagrams of the DSMC and the DBSMC are shown in Figure 4.32 and Figure 4.33, respectively.

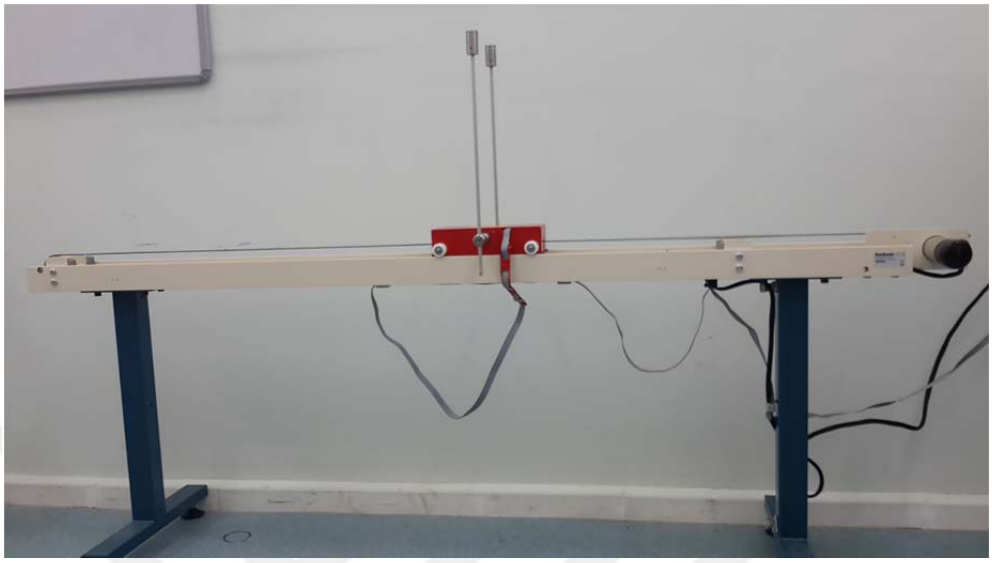

Figure 4.31. The inverted pendulum on a cart system

The experimental setup has two physical constraints. The first one is the cart position which is physically bounded by the rail length which is 0.8 m. Since it is assumed that the initial cart position is in the middle of the rail, the position of the cart should be limited to $|x| \leq 0.4$ m. Therefore, the controllers are designed to limit the maximum displacement of the cart to ±0.35 m. The second constraint is the bound of the control signal which must be in the range of −2.5 V and +2.5 V. The DSMC and the DBSMC parameters which are chosen by trial and error method with considering these constraints are given in Table 4.3.

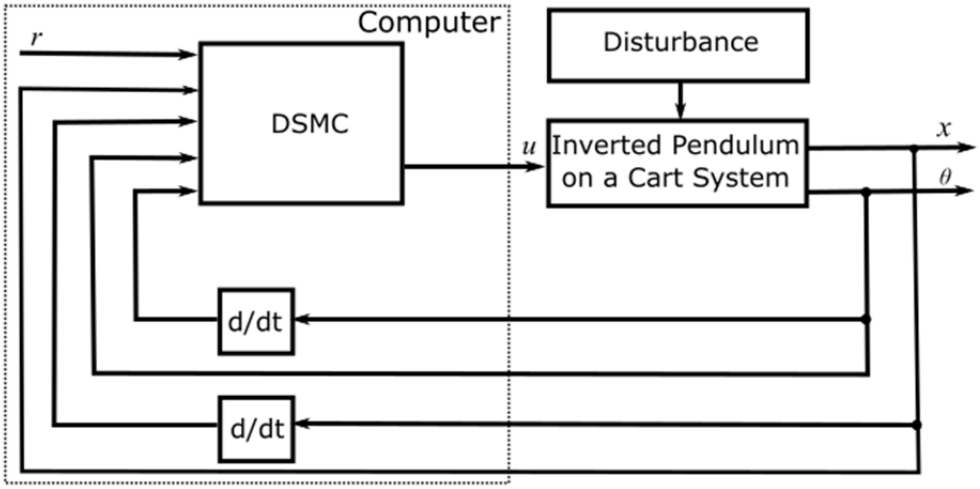

Figure 4.32. Block diagram of the DSMC

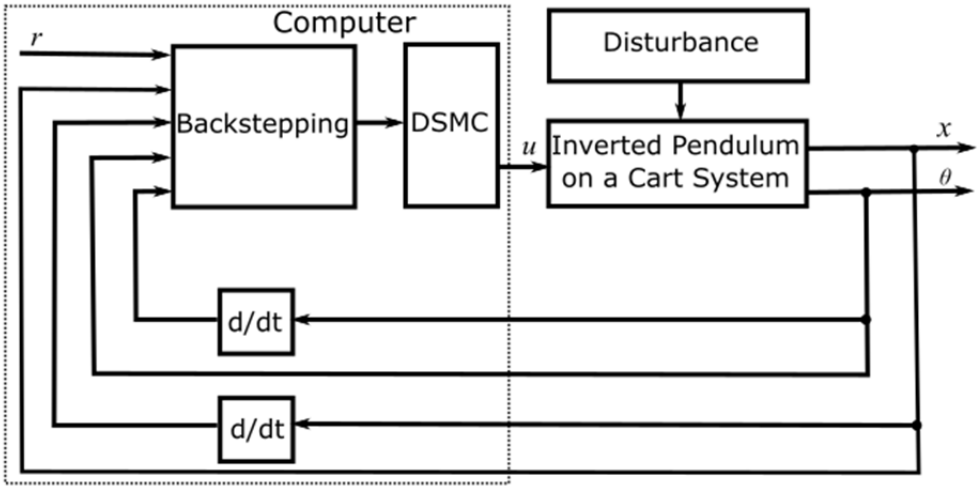

Figure 4.33. Block diagram of the DBSMC

4.3.2. Experimental Comparison Results

In the first experiment, both the DSMC and the DBSMC are applied to the inverted pendulum on a cart system with the parametric uncertainty $\delta_2 = 1$. Thus, the control methods are tested on own parametric uncertainties of the system without any additional parametric uncertainty. The test results of the cart position, pendulum angle and control signal for reference signal $r = 0.3$ and initial

conditions $\begin{bmatrix} x_0 & \dot{x}_0 & \theta_0 & \dot{\theta}_0 \end{bmatrix} = \begin{bmatrix} 0 & 0 & 0.1 & 0 \end{bmatrix}$ plotted and shown in Figure 4.34, Figure 4.35 and Figure 4.36, respectively.

The settling time of position is 4.45 sec for the DSMC and 4.14 sec for the DBSMC; the overshoot and undershoot are 4.2 percent and 7.8 percent for the DSMC and 4.14 percent and 5.8 percent for the DBSMC, respectively. Both the DSMC and the DBSMC manage to bring the cart from the initial position to the desired position as shown in Figure 4.34. However, the DBSMC has a better performance to stabilize the position.

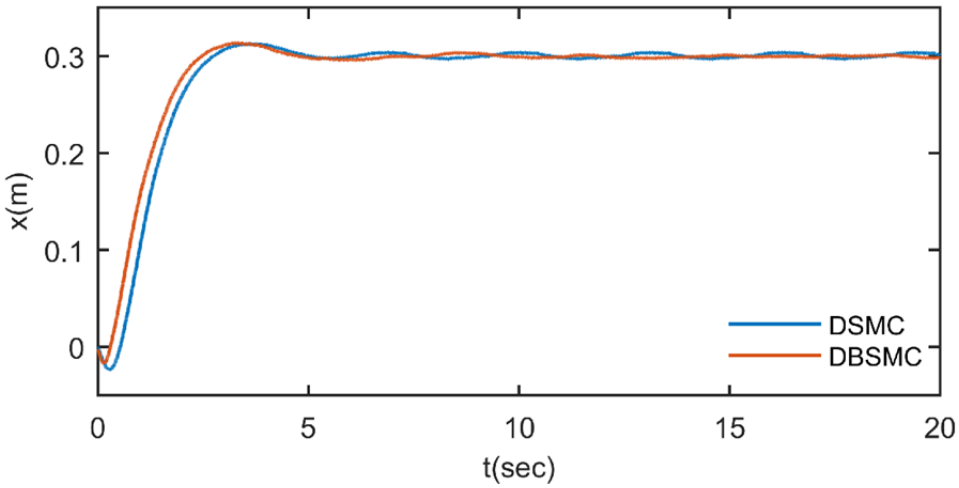

Figure 4.34. Cart position x for $r = 0.3$ and $\begin{bmatrix} x_0 & \dot{x}_0 & \theta_0 & \dot{\theta}_0 \end{bmatrix} = \begin{bmatrix} 0 & 0 & 0.1 & 0 \end{bmatrix}$ with $\delta_2 = 1$

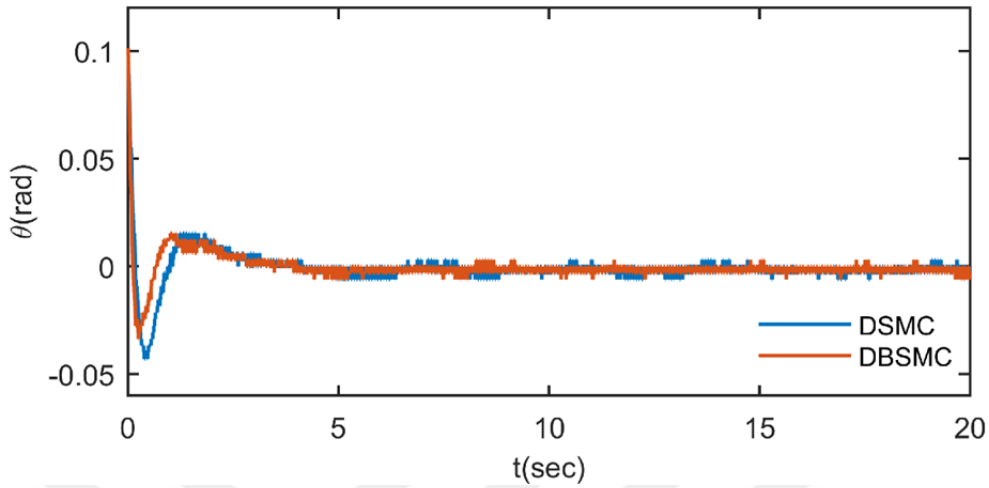

Figure 4.35. Pendulum angle θ for $r = 0.3$ and $\begin{bmatrix} x_0 & \dot{x}_0 & \theta_0 & \dot{\theta}_0 \end{bmatrix} = \begin{bmatrix} 0 & 0 & 0.1 & 0 \end{bmatrix}$ with $\delta_2 = 1$

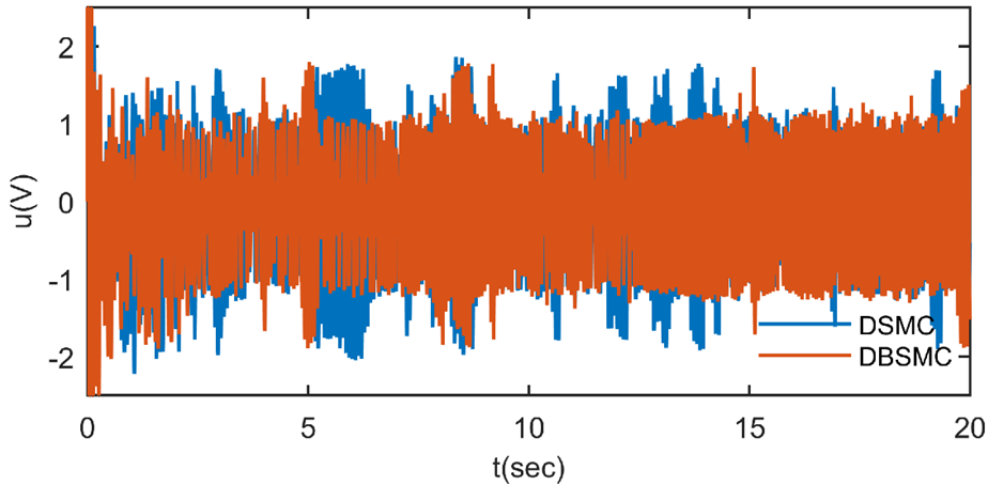

Figure 4.36. Control signal u for $r = 0.3$ and $\begin{bmatrix} x_0 & \dot{x}_0 & \theta_0 & \dot{\theta}_0 \end{bmatrix} = \begin{bmatrix} 0 & 0 & 0.1 & 0 \end{bmatrix}$ with $\delta_2 = 1$

Figure 4.35 clearly shows that both controllers are able to keep the pendulum on the upright position. The chattering in the control signal is slightly lower in the DBSMC as compared the DSMC as shown in Figure 4.36.

The performances of the DSMC and the DBSMC based on performance indices for reference signal $r = 0.3$ and initial conditions $\begin{bmatrix} x_0 & \dot{x}_0 & \theta_0 & \dot{\theta}_0 \end{bmatrix} = \begin{bmatrix} 0 & 0 & 0.1 & 0 \end{bmatrix}$ with the parametric uncertainty $\delta_2 = 1$ are given in Table 4.12 and Table 4.13.

Table 4.12. DSMC and DBSMC experiment performance indices for $r = 0.3$ and $\begin{bmatrix} x_0 & \dot{x}_0 & \theta_0 & \dot{\theta}_0 \end{bmatrix} = \begin{bmatrix} 0 & 0 & 0.1 & 0 \end{bmatrix}$ with $\delta_2 = 1$

	IAE		**ISE**	
Tracking Error	**DSMC**	**DBSMC**	**DSMC**	**DBSMC**
Cart Position	449	364	96	71
Pendulum Angle	75.61	63	1.38	0.87
Control Signal	15185	14791	15472	13971

Table 4.13. DSMC and DBSMC experiment performance indices for $r = 0.3$ and $\begin{bmatrix} x_0 & \dot{x}_0 & \theta_0 & \dot{\theta}_0 \end{bmatrix} = \begin{bmatrix} 0 & 0 & 0.1 & 0 \end{bmatrix}$ with $\delta_2 = 1$

	ITAE		**ITSE**	
Tracking Error	**DSMC**	**DBSMC**	**DSMC**	**DBSMC**
Cart Position	736437	479734	55228	34471
Pendulum Angle	414072	373195	1887	1424
Control Signal	142322735	146402953	134474143	130869680

The magnitudes of the performance indices are generally smaller in the DBSMC rather than the DSMC as shown in Table 4.12 and Table 4.13. Consequently, the DBSMC produced a more accurate control input than the DSMC.

In the second experiment, both the DSMC and the DBSMC are applied to the inverted pendulum on a cart system with the parametric uncertainty $\delta_2 = 1$. The

initial condition of the pendulum angle is changed to 0.3 rad to create a more challenging situation. The test results of the cart position, pendulum angle and control signal for reference signal $r = 0.3$ and initial conditions $\begin{bmatrix} x_0 & \dot{x}_0 & \theta_0 & \dot{\theta}_0 \end{bmatrix} = \begin{bmatrix} 0 & 0 & 0.3 & 0 \end{bmatrix}$ plotted and shown in Figure 4.37, Figure 4.38 and Figure 4.39, respectively.

The settling time of position is 8.02 sec for the DSMC and 4.18 sec for the DBSMC; the overshoot and undershoot are 5.11 percent and 28.58 percent for the DSMC and 3.59 percent and 7.9 percent for the DBSMC, respectively. Both the DSMC and the DBSMC manage to bring the cart from the initial position to the desired position as shown in Figure 4.37. However, the DBSMC has a better performance to stabilize the position.

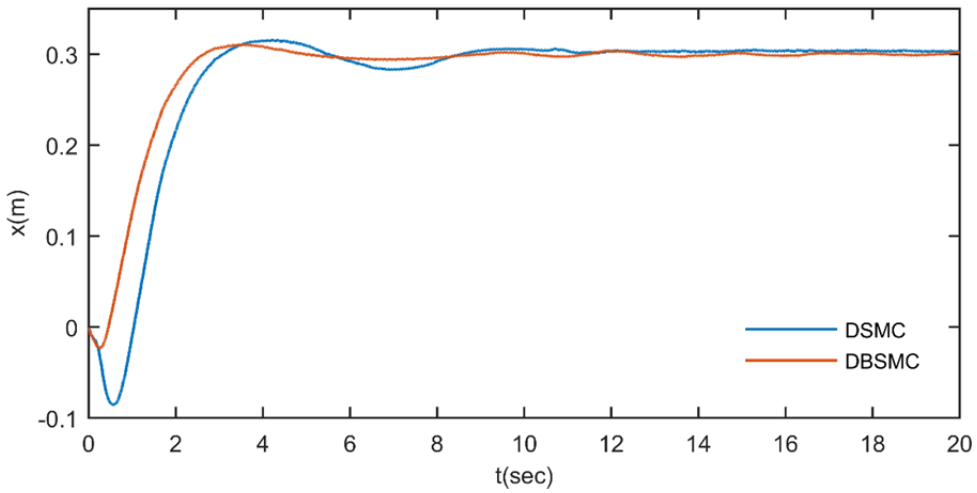

Figure 4.37. Cart position x for $r = 0.3$ and $\begin{bmatrix} x_0 & \dot{x}_0 & \theta_0 & \dot{\theta}_0 \end{bmatrix} = \begin{bmatrix} 0 & 0 & 0.3 & 0 \end{bmatrix}$ with $\delta_2 = 1$

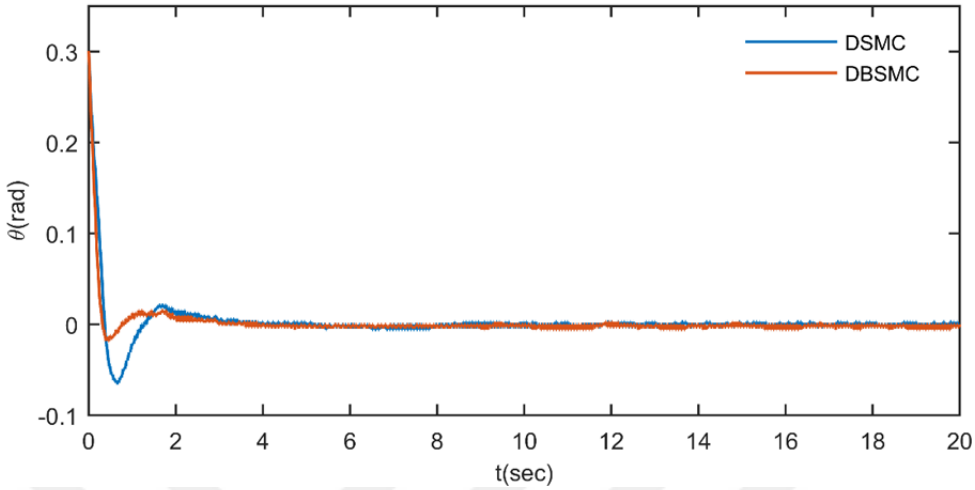

Figure 4.38. Pendulum angle θ for $r = 0.3$ and $\begin{bmatrix} x_0 & \dot{x}_0 & \theta_0 & \dot{\theta}_0 \end{bmatrix} = \begin{bmatrix} 0 & 0 & 0.3 & 0 \end{bmatrix}$ with $\delta_2 = 1$

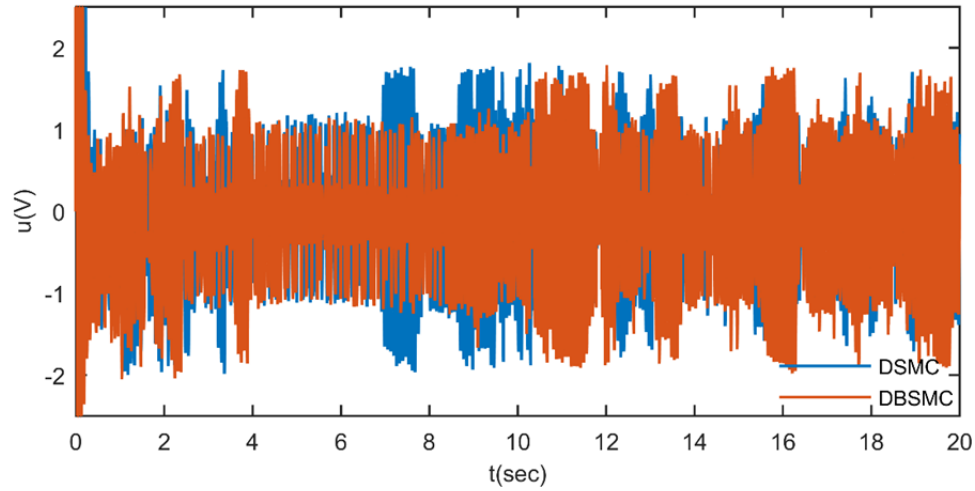

Figure 4.39. Control signal u for $r = 0.3$ and $\begin{bmatrix} x_0 & \dot{x}_0 & \theta_0 & \dot{\theta}_0 \end{bmatrix} = \begin{bmatrix} 0 & 0 & 0.3 & 0 \end{bmatrix}$ with $\delta_2 = 1$

Both controllers are able to keep the pendulum on the upright position as shown in figure 4.38. However, the DBSMC has a better performance to stabilize

the pendulum angle. The chattering in the control signal is slightly lower in the DSMC as compared the DBSMC as shown in Figure 4.39.

The performances of the DSMC and the DBSMC based on performance indices for reference signal $r = 0.3$ and initial conditions $\begin{bmatrix} x_0 & \dot{x}_0 & \theta_0 & \dot{\theta}_0 \end{bmatrix} = \begin{bmatrix} 0 & 0 & 0.1 & 0 \end{bmatrix}$ with the parametric uncertainty $\delta_2 = 1$ are given in Table 4.14 and Table 4.15.

Table 4.14. DSMC and DBSMC experiment performance indices for $r = 0.3$ and $\begin{bmatrix} x_0 & \dot{x}_0 & \theta_0 & \dot{\theta}_0 \end{bmatrix} = \begin{bmatrix} 0 & 0 & 0.3 & 0 \end{bmatrix}$ $\delta_2 = 1$

	IAE		ISE	
Tracking Error	**DSMC**	**DBSMC**	**DSMC**	**DBSMC**
Cart Position	664	417	163	87
Pendulum Angle	126	96	12	7
Control Signal	14236	15749	14132	16262

Table 4.15. DSMC and DBSMC experiment performance indices for $r = 0.3$ and $\begin{bmatrix} x_0 & \dot{x}_0 & \theta_0 & \dot{\theta}_0 \end{bmatrix} = \begin{bmatrix} 0 & 0 & 0.3 & 0 \end{bmatrix}$ $\delta_2 = 1$

	ITAE		ITSE	
Tracking Error	**DSMC**	**DBSMC**	**DSMC**	**DBSMC**
Cart Position	1410546	616975	123828	46374
Pendulum Angle	287436	450702	3214	2346
Control Signal	131990884	161302423	120905810	165443692

The magnitudes of the performance indices are generally smaller in the DBSMC rather than the DSMC as shown in Table 4.14 and Table 4.15. Consequently, the DBSMC produced a more accurate control input than the DSMC.

In the third experiment, both the DSMC and the DBSMC are applied to the inverted pendulum on a cart system with the parametric uncertainty $\delta_2 = 0.8$. The test results of the cart position, pendulum angle and control signal for reference signal $r = 0.3$ and initial conditions $\begin{bmatrix} x_0 & \dot{x}_0 & \theta_0 & \dot{\theta}_0 \end{bmatrix} = \begin{bmatrix} 0 & 0 & 0.1 & 0 \end{bmatrix}$ plotted and shown in Figure 4.40, Figure 4.41 and Figure 4.42, respectively.

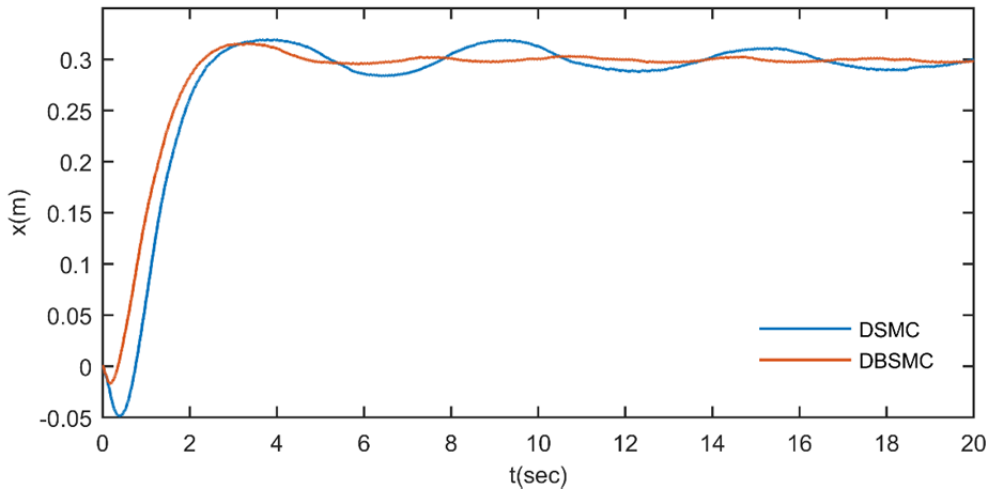

Figure 4.40. Cart position x for $r = 0.3$ and $\begin{bmatrix} x_0 & \dot{x}_0 & \theta_0 & \dot{\theta}_0 \end{bmatrix} = \begin{bmatrix} 0 & 0 & 0.1 & 0 \end{bmatrix}$ with $\delta_2 = 0.8$

Although the DSMC is able to bring and keep the pendulum at the upright position, it fails to stabilize the cart at the desired position as shown in Figure 4.40 and Figure 4.41. On the other hand, the DBSMC manages to handle parametric uncertainty and control the cart position successfully with 4.4 *sec* settling time with 5.24 percent overshoot and 5.76 percent undershoot. Besides, the DBSMC yields slightly lower chattering in the control signal compared to the DSMC as shown in Figure 4.42.

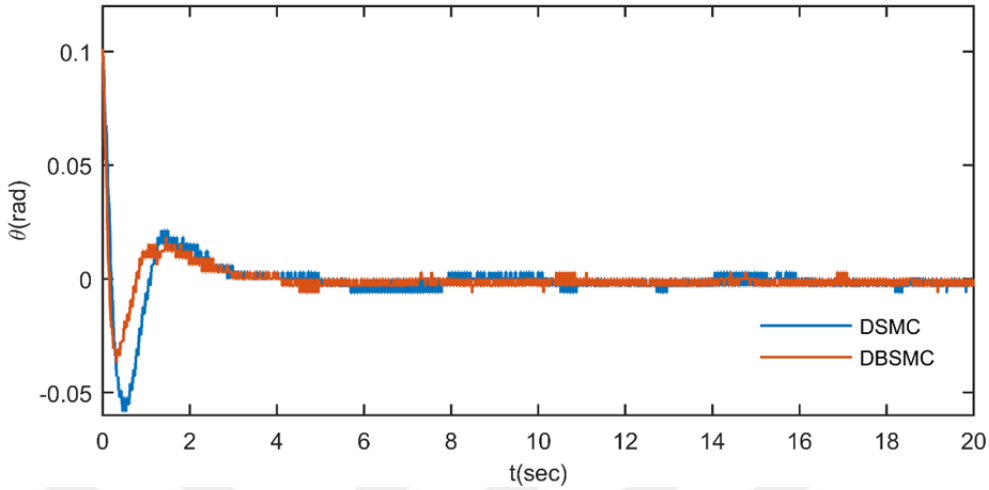

Figure 4.41. Pendulum angle θ for $r = 0.3$ and $\begin{bmatrix} x_0 & \dot{x}_0 & \theta_0 & \dot{\theta}_0 \end{bmatrix} = \begin{bmatrix} 0 & 0 & 0.1 & 0 \end{bmatrix}$ with $\delta_2 = 0.8$

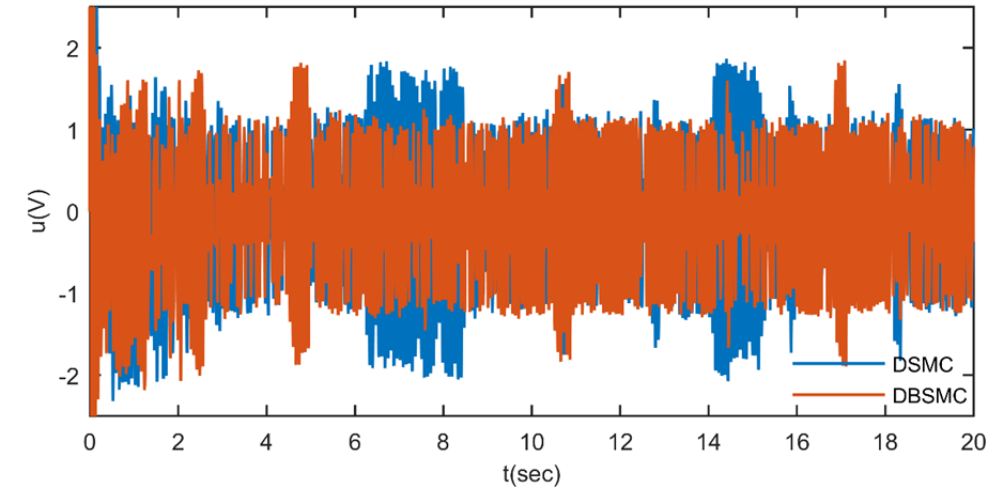

Figure 4.42. Control signal u for $r = 0.3$ and $\begin{bmatrix} x_0 & \dot{x}_0 & \theta_0 & \dot{\theta}_0 \end{bmatrix} = \begin{bmatrix} 0 & 0 & 0.1 & 0 \end{bmatrix}$ with $\delta_2 = 0.8$

Although the DSMC fails in the third experiment, the fourth experiment is carried to investigate the performance of the DBSMC in a more challenging situation. In the fourth experiment, both the DSMC and the DBSMC are applied to

the inverted pendulum on a cart system with the parametric uncertainty $\delta_2 = 0.8$. The initial condition of the pendulum angle is changed to 0.3 rad to create a more challenging situation. The test results of the cart position, pendulum angle and control signal for reference signal $r = 0.3$ and initial conditions $\begin{bmatrix} x_0 & \dot{x}_0 & \theta_0 & \dot{\theta}_0 \end{bmatrix} = \begin{bmatrix} 0 & 0 & 0.3 & 0 \end{bmatrix}$ plotted and shown in Figure 4.43, Figure 4.44 and Figure 4.45, respectively.

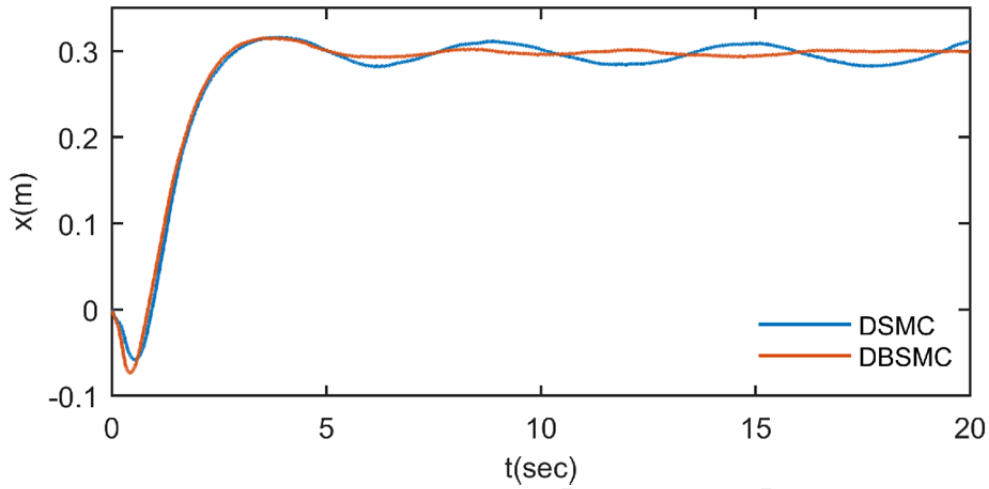

Figure 4.43. Cart position x for $r = 0.3$ and $\begin{bmatrix} x_0 & \dot{x}_0 & \theta_0 & \dot{\theta}_0 \end{bmatrix} = \begin{bmatrix} 0 & 0 & 0.3 & 0 \end{bmatrix}$ with $\delta_2 = 0.8$

Although the DSMC is able to bring and keep the pendulum at the upright position, it fails to stabilize the cart at the desired position as shown in Figure 4.43 and Figure 4.44. On the other hand, the DBSMC manages to handle parametric uncertainty and control the cart position successfully with 4.59 *sec* settling time with 5.04 percent overshoot and 24.5 percent undershoot. Besides, the DBSMC yields slightly lower chattering in the control signal compared to the DSMC as shown in Figure 4.45.

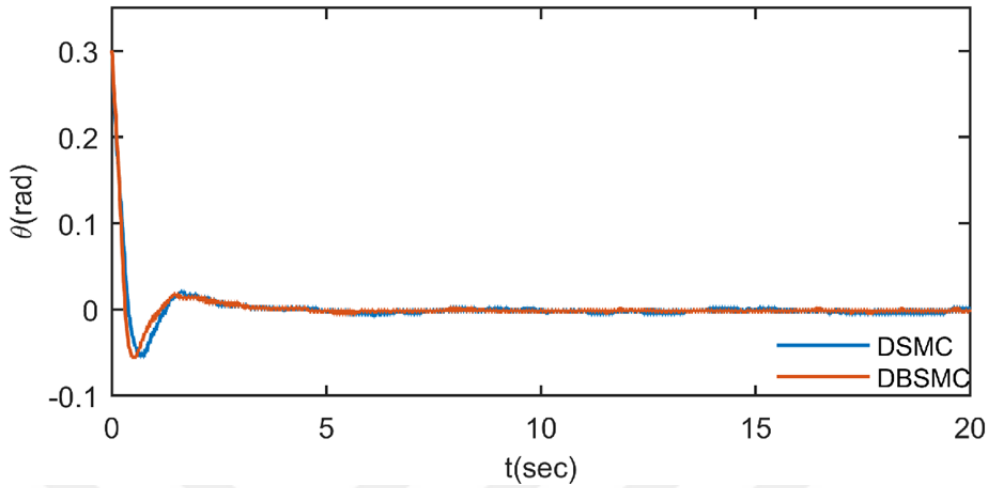

Figure 4.44. Pendulum angle θ for $r = 0.3$ and $\begin{bmatrix} x_0 & \dot{x}_0 & \theta_0 & \dot{\theta}_0 \end{bmatrix} = \begin{bmatrix} 0 & 0 & 0.3 & 0 \end{bmatrix}$ with $\delta_2 = 0.8$

In the first experiment, conventional DSMC and the DBSMC methods compared for reference signal $r = 0.3$ and initial conditions $\begin{bmatrix} x_0 & \dot{x}_0 & \theta_0 & \dot{\theta}_0 \end{bmatrix} = \begin{bmatrix} 0 & 0 & 0.1 & 0 \end{bmatrix}$. After that to create a more challenging problem the DSMC and the DBSMC methods compared for reference signal $r = 0.3$ and initial conditions $\begin{bmatrix} x_0 & \dot{x}_0 & \theta_0 & \dot{\theta}_0 \end{bmatrix} = \begin{bmatrix} 0 & 0 & 0.3 & 0 \end{bmatrix}$. These experiments carried with parametric uncertainty $\delta_2 = 1$. In the third and fourth tests, first two experiments are recreated with parametric uncertainty $\delta_2 = 0.8$. These experiments show that the DBSMC manages to handle parametric uncertainty and control the cart position successfully where the DSMC fails. Overall, the experimental results have shown that the proposed DBSM method is more efficient than the conventional DSMC method.

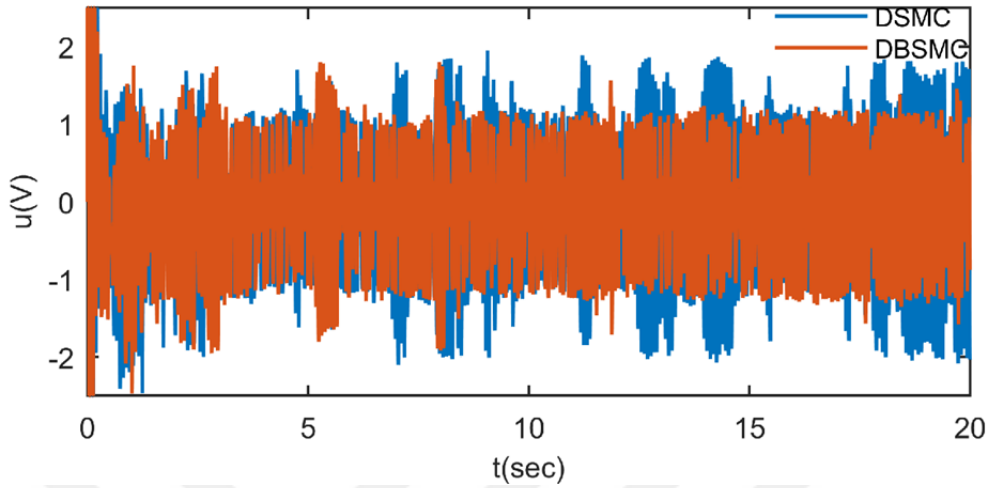

Figure 4.45. Control signal u for $r = 0.3$ and $\begin{bmatrix} x_0 & \dot{x}_0 & \theta_0 & \dot{\theta}_0 \end{bmatrix} = \begin{bmatrix} 0 & 0 & 0.3 & 0 \end{bmatrix}$ with $\delta_2 = 0.8$

5. CONCLUSION AND FUTURE WORK

In this study, a decoupled backstepping sliding mode control (DBSMC) method is proposed to control underactuated systems under uncertainties and disturbances. The proposed DBSMC keeps the advantages of the sliding mode control and overcomes the difficulties caused by the parametric uncertainties.

In order to confirm the effectiveness of the proposed DBSMC, it is applied to an inverted pendulum on a cart system as a benchmark example for underactuated systems. The complete mathematical model of the inverted pendulum on a cart system is derived from the laws of motion according to movement characteristics of the system. To create a more realistic model, the DC motor characteristics are added to the mathematical model of the inverted pendulum on a cart system.

Using the derived inverted pendulum on a cart model with DC motor, the system is simulated to investigate the stability and the performance of the proposed DBSMC for the inverted pendulum on a cart system. Simulation results show that the proposed DBSMC is managed to control the inverted pendulum on a cart system and it can be applied to real plants. Also, the simulation results prove that the proposed DBSMC produces a more accurate control input compared to the decoupled sliding mode control (DSMC).

After obtaining a satisfactory performance of the proposed DBSMC during the simulations, the proposed DBSMC is applied to a real plant to provide a clearer view of the performance. The experimental results show that the DBSMC is more effective compared to the DSMC. Also, the experimental results prove that the DBSMC provides a robust control on the systems with parametric uncertainties where the DSMC fails.

This study provides a basis for the application of the DBSMC to the underactuated systems. Future research can consider the potential of the DBSMC

method on different underactuated systems. Also, adding an adaptive scheme to the DBSMC might prove an important area for future research.

In the present study, the parameters of the proposed DBSMC are chosen by the trial and error method. Intelligent optimization techniques can be integrated into the proposed DBSMC for parameter tuning in future works.

REFERENCES

Adhikary, N. and Mahanta, C., 2013. Integral backstepping sliding mode control for underactuated systems: Swing-up and stabilization of the Cart-Pendulum System. ISA Transactions, 52:870–880.

Anderson, C. W., 1988. Learning to Control an Inverted Pendulum Using Neural Networks, 1988 IEEE American Control Conference, 2294–2298.

Åström, K. J. and Furuta, K., 2000. Swinging up a pendulum by energy control. Automatica, 36:287–295.

Ata, B., 2014. Quadratic Optimal Control of an inverted pendulum Using Artificial Bee Colony Algorithm, MSc. Thesis. Cukurova University.

Ata, B. and Coban, R., 2015. Artificial Bee Colony Algorithm Based Linear Quadratic Optimal Controller Design for a Nonlinear Inverted Pendulum. International Journal of Intelligent Systems and Applications in Engineering, 3:1.

Ata, B. and Coban, R., 2017. Linear Quadratic Optimal Control of an Inverted Pendulum on a Cart using Artificial Bee Colony Algorithm: An Experimental Study. Cukurova University Journal of the Faculty of Engineering and Architecture, 32:109–124.

Ata, B. and Coban, R., 2019. Decoupled Backstepping Sliding Mode Control of Underactuated Systems with Uncertainty: Experimental Results. Arabian Journal for Science and Engineering, 1-9.

Chang, W.D., Hwang, R.C., and Hsieh, J.G, 2002. A self-tuning PID control for a class of nonlinear systems based on the Lyapunov approach. Journal of Process Control, 12:233–242.

Coban, R., 2017a. Backstepping integral sliding mode control of an electromechanical system. Automatika, 58:266–272.

Coban, R., 2017b. Dynamical adaptive integral backstepping variable structure controller design for uncertain systems and experimental application. International Journal of Robust and Nonlinear Control, 27:4522–4540.

Coban, R. and Ata, B., 2017. Decoupled sliding mode control of an inverted pendulum on a cart: An experimental study. 2017 IEEE International Conference on Advanced Intelligent Mechatronics, 993–997.

Davison, E. J., 1990. Benchmark problems for the control system design: report of the IFAC Theory Committe.

Elhasairi, A., and Pechev, A., 2015. Humanoid Robot Balance Control Using the Spherical Inverted Pendulum Mode. Frontiers in Robotics and AI, 2:1–13.

Feedback Instruments, 2006. 33-936s Digital Pendulum Control Experiments Manual.

Freeman, R. A. and Kokotović, P., 1996. Robust Nonlinear Control Design. Birkhäuser Boston, Boston.

Furat, M. and Eker, I., 2014. Second-order integral sliding-mode control with experimental application. ISA Transactions, 53:1661–1669.

Huang, X., Ralescu, A. L., Gao, H. and Huang, H., 2018. A survey on the application of fuzzy systems for underactuated systems. Journal of Systems and Control Engineering, 233:217–244.

Hussein, I. I. and Bloch, A. M., 2008. Optimal control of underactuated nonholonomic mechanical systems. IEEE Transactions on Automatic Control, 53:668–682.

Jeong, S. H. and Takahashi, T., 2007. Wheeled Inverted PENdulum Type Assistant Robot: Inverted mobile, standing, and sitting motions. IEEE International Conference on Intelligent Robots and Systems, 1932–1937.

Khalil, H. K., 2002. Nonlinear Systems. 3th Edition. Prentice Hall, New Jersey.

Kumar, V. E. and Jerome, J., 2013. Robust LQR controller design for stabilizing and trajectory tracking of inverted pendulum. Procedia Engineering, 64:169–178.

Kuo, A. D., 2007. The six determinants of gait and the inverted pendulum analogy: A dynamic walking perspective. Human Movement Science, 26:617–656.

Lee, H. and Utkin, V. I., 2007. Chattering suppression methods in sliding mode

control systems. Annual Reviews in Control, 31:179–188.

Levant, A., 1993. Sliding order and sliding accuracy in sliding mode control. International Journal of Control, 58:1247–1263.

Levant, A., 2003. Higher-order sliding modes, differentiation and output-feedback control. International Journal of Control, 76:924–941.

Lin, C. M. and Mon, Y. J., 2005. Decoupling Control by Hierarchical Fuzzy Sliding-Mode Controller. IEEE Transactions on Control Systems Technology, 13:593–598.

Lo, J.C. and Kuo, Y.H., 1998. Decoupled fuzzy sliding-mode control. IEEE Transactions on Fuzzy Systems, 6:426–435.

Lu, C.H., Hwang, Y.R. and Shen, Y.T., 2011. Backstepping sliding mode tracking control of a vane-type air motor X–Y table motion system. ISA Transactions, 50:278–286.

Mablekos, V. E., 1980. Electric Machine Theory for Power Engineers. HarperCollins Publishers, New York.

Mahjoub, S., Mnif, F. and Derbel, N., 2015. Second-order sliding mode approaches for the control of a class of underactuated systems. International Journal of Automation and Computing, 12:134–141.

Man, W. and Lin, J.S., 2010. Nonlinear control design for a class of underactuated systems. 2010 IEEE International Conference on Control Applications, 1439–1444.

Nejadfard, A., Yazdanpanah, M. J. and Hassanzadeh, I., 2013. Friction compensation of double inverted pendulum on a cart using locally linear neuro-fuzzy model. Neural Computing and Applications, 22:337–347.

Nise, N., 2010. Control Systems Engineering. Sixth edition. John Wiley & Sons.

Olfati-Saber, R. 2001. Nonlinear Control of Underactuated Mechanical Systems with Application to Robotics and Aerospace Vehicles. PhD Thesis. Massachusetts Instıtute of Technology.

Oryschuk, P., Salerno, A, Al-Husseini, A. M. and Angeles, J., 2009. Experimental

validation of an underactuated two-wheeled mobile robot. IEEE/ASME Transactions on Mechatronics, 14:252–257.

Park, M. S. and Chwa, D., 2009. Swing-up and stabilization control of inverted-pendulum systems via coupled sliding-mode control method. IEEE Transactions on Industrial Electronics, 56:3541–3555.

Shah, I. and Rehman, F. U., 2018. Smooth Second Order Sliding Mode Control of a Class of Underactuated Mechanical Systems. IEEE Access, 6:7759–7771.

She, J., Zhang, A., Lai, X. and Wu, M., 2012. Global stabilization of 2-DOF underactuated mechanical systems—an equivalent-input-disturbance approach. Nonlinear Dynamics, 69:495–509.

Siuka, A. and Schöberl, M., 2009. Applications of energy based control methods for the inverted pendulum on a cart. Robotics and Autonomous Systems, 57:1012–1017.

Slotine, J.J. and Li, W., 1991. Applied Nonlinear Optimal Control. Prentice Hall, New Jersey.

Spong, M. W., 1987. Modeling and Control of Elastic Joint Robots. Journal of Dynamic Systems, Measurement, and Control, 109:310.

Spong, M. W., 1995. The Swing Up Control of the Acrobot. IEEE Control Systems Magazine, 15:49–55.

Spong, M. W., 1996. Energy Based Control of a Class of Underactuated Mechanical Systems. IFAC Proceedings Volumes, 29:2828–2832.

Spong, M. W., 1998. Underactuated mechanical systems. Control Problems in Robotics and Automation, Springer:135–150.

Subudhi, B., Ghosh, A. and Krishnan, T. R., 2012. Robust proportional–integral–derivative compensation of an inverted cart–pendulum system: an experimental study. IET Control Theory & Applications, 6:1145–1152.

Utkin, V., 1977. Variable structure systems with sliding modes. IEEE Transactions on Automatic Control, 22:212–222.

Utkin, V., 1992. Sliding Modes in Control and Optimization. Springer Berlin Heidelberg, Berlin, Heidelberg.

Utkin, V. and Lee H., 2006. Chattering Problem in Sliding Mode Control Systems. International Workshop on Variable Structure Systems, 346–350

Voytsekhovsky, D. and Hirschorn, R. M., 2008. Stabilization of single-input nonlinear systems using higher-order term compensating sliding mode control. International Journal of Robust and Nonlinear Control, 18:468–480.

Walsh, G. C., Montgomery, R. and Sastry, S. S., 1994. Orientation control of the dynamic satellite. Proceedings of 1994 American Control Conference , 138–142.

Wang, N. and Adeli, H., 2012. Algorithms for chattering reduction in system control. Journal of the Franklin Institute, 349:2687–2703.

Wang, Q. and Stengel, R. F., 2002. Robust control of nonlinear systems with parametric uncertainty. Automatica, 38:1591–1599.

Woods, S. A., Bauer, R. J. and Seto, M. L., 2012. Automated ballast tank control system for autonomous underwater vehicles. IEEE Journal of Oceanic Engineering, 37:727–739.

Yao, B. and Tomizuka, M., 2001. Adaptive robust control of MIMO nonlinear systems in semi-strict feedback forms. Automatica, 37:1305–1321.

Young, K. D., Utkin, V. and Özgüner, Ü., 1999. A control engineer's guide to sliding mode control. IEEE Transactions on Control Systems Technology, 7:328–342.

Yu, H. and Liu, Y., 2013. A survey of underactuated mechanical systems. IET Control Theory & Applications, 7:921–935.

Yu, X. and Kaynak, O., 2009. Sliding-mode control with soft computing: A survey. IEEE Transactions on Industrial Electronics, 56:3275–3285.

Zeng-Guang, H, An-Min, Z., Long C. and Min T., 2009. Adaptive Control of an Electrically Driven Nonholonomic Mobile Robot via Backstepping and Fuzzy Approach. IEEE Transactions on Control Systems Technology, 17:803–815.

Zhang, A., Lai, X., Wu, M. and She, J., 2017. Nonlinear stabilizing control for a class of underactuated mechanical systems with multi degree of freedoms. Nonlinear Dynamics, 89:2241–2253.

Zhang, S., An, R., and Shao, S., 2011. A New Type of Adaptive Neural Network Fuzzy Controller in the Double Inverted Pendulum System. Pages 149–157 *in* H. Deng, D. Miao, and J. Lei, editors. Artificial Intelligence and Computational Intelligence. Springer Berlin Heidelberg.

CURRICULUM VITAE

Barış ATA was born in Akşehir in 1986. He received his BSc. from Department of Computer Engineering of Kocaeli University in 2010 and MSc. from Department of Computer Engineering Cukurova University in 2014, respectively. He has been working as a research assistant in Department of Computer Engineering of Cukurova University since 2012.